Australian Government
Geoscience Australia

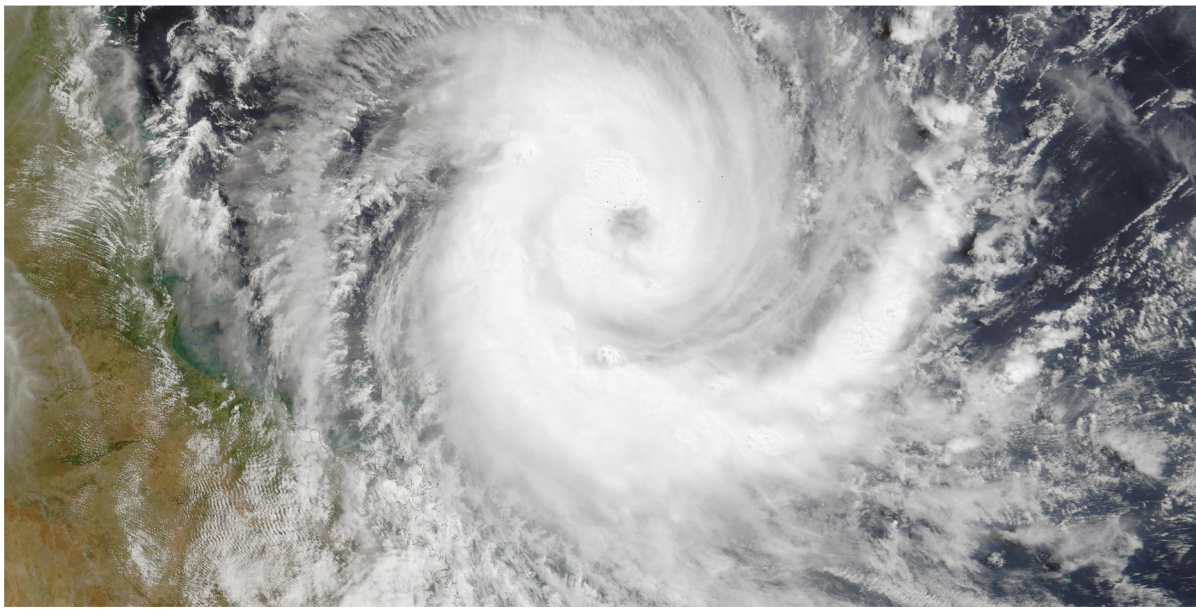

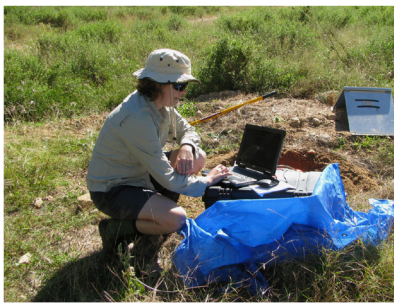

Record 2013/15 | **GeoCat** 75085

Reforming Planning Processes Trial: Rockhampton 2050

Technical Report on Current and Future Climate Hazards

D. Moore, M. Hazelwood, R. Cechet, C. Arthur, I. French, R. Dunsmore, A. Sanabria, T. Yang, and M. Woolf

Reforming Planning Processes Trial: Rockhampton 2050

Technical Report on Current and Future Climate Hazards

GEOSCIENCE AUSTRALIA
RECORD 2013/15

D. Moore, M. Hazelwood, R. Cechet, C. Arthur, I. French, R. Dunsmore, A. Sanabria, T. Yang, and M. Woolf

Australian Government
Geoscience Australia

Department of Resources, Energy and Tourism

Minister for Resources and Energy: The Hon Gary Gray AO MP
Secretary: Mr Blair Comley, PSM

Geoscience Australia
Chief Executive Officer: Dr Chris Pigram
This paper is published with the permission of the CEO, Geoscience Australia

ISSN 1448-2177 (Print)
ISSN 2201-702X (PDF)

ISBN 978-1-922201-40-9 (Print)
ISBN 978-1-922201-39-3 (PDF)

GeoCat 75085

Bibliographic reference: Moore, D., Hazelwood, M., Cechet, R.P., Arthur, W.C., French, I., Dunsmore, R., Sanabria, A., Yang, T., and Woolf, M., 2013. *Reforming Planning Processes Trial: Rockhampton 2050 Technical Report on Current and Future Climate Hazards*. Record 2013/15. Geoscience Australia: Canberra.

Current as at April 2, 2013

Thanks to those who supported this project including members of the Climate Hazards and Risk Section, the Coastal, Marine and Climate Change Group and the National Elevation Services Section at Geoscience Australia.

Thanks also to Penelope-Jane Fry (Flinders Group) and Sam Williams (Rockhampton Regional Council) and Chris Buenen (Rockhampton Regional Council) for support in completing this project.

Contents

Glossary

Term	Definition
AHD	Australian Height Datum. Vertical height datum which is approximately equal to Mean Sea Level.
Annual Exceedance Probability	The annual probability of an event occurring or being exceeded in magnitude.
ARI	Average Recurrence Interval, the average or expected period of time between exceedances of a given event magnitude. Equivalent to Return Period.
BoM	Bureau of Meteorology
cal. yrs BP	Calibrated years before present
CCAM	Cubic Conformal Atmospheric Model
CSIRO	Commonwealth Scientific and Industrial Research Organisation
DCC	Department of Climate Change
FFDI	Forest Fire Danger Index
GCM	General Circulation Model or Global Circulation Model
Generalised Extreme Value Distribution (GEV)	A family of probability distributions used to model the distribution of maxima of a series of randomly distributed variables
GFDI	Grassland Fire Danger Index
GHG	Greenhouse Gas
Grid	Regular square mesh spatial data
HAT	Highest Astronomical Tide
IPCC	Intergovernmental Panel on Climate Change
IPCC AR4	Intergovernmental Panel on Climate Change Fourth Assessment Report
LSCB	Large-Scale Coastal Behaviour
LULCC	Land-use and land-cover change
m/s	Metres per second. Convert to kilometres per hour through multiplying by a factor of 3.6
MHWS	Mean High Water Springs. The long-term mean of the heights of two successive high waters during those periods of 24 hours (approximately once a fortnight) when the range of tide is greatest, during full and new moon.(Source: Maritime Safety Queensland[1])
MLWS	Mean Low Water Springs. The long-term mean of the heights of two successive low waters over the same periods as defined for MHWS.(Source: Maritime Safety Queensland[2])

[1] http://www.msq.qld.gov.au/Tides/Notes-and-definitions.aspx

[2] http://www.msq.qld.gov.au/Tides/Notes-and-definitions.aspx

Term	Definition
MSL	Mean Sea Level
PDF	Probability Density Function
QCHG	Queensland Coastal Hazards Guideline
Raster	Regular square mesh spatial data
RCM	Regional Climate Model
Return Period (RP)	The average or expected period between exceedances of a given event magnitude. Equivalent to the Average Recurrence Interval.
RMW	Radius of Maximum Winds
SEQCARI	South East Queensland Climate Adaptation Research Initiative
SLR	Sea-Level Rise
SRES	Special Report on Emissions Scenarios (IPCC AR4)
Storm tide	Describes the increase in water level from the combined effect of astronomical tide, storm surge and wave set up.
TC	Tropical Cyclone
TCRM	Tropical Cyclone Risk Model
Topographic LiDAR	Onshore LiDAR derived elevation data or digital elevation model

Figures

This page is intentionally blank

1 Executive summary

Due to the developing understanding of the science, climate change uncertainties present significant challenges for land use planning, emergency management and risk mitigation across Australia. Even in current-climate conditions, the Rockhampton Regional Council area is subject to the impacts of natural hazards, such as bushfires, floods, and tropical cyclones (extreme winds and storm surges). All of these hazards may worsen with climate change.

The Commonwealth Government's first pass national assessment of the potential impact of climate change on coastal infrastructure (Cechet *et al.,* 2012) indicated that, of the significantly populated Queensland Local Government Areas (LGAs), the Rockhampton Regional Council has the largest area potentially inundated through the combined impacts of sea-level rise, coastal erosion and storm tide. Considering the expected population increase in Rockhampton (from under 117 000 people in 2011 to over 175 000 for 2031 under the high series prediction (Qld OESR, 2012)) even current-climate hazard will, through time, progressively expose greater numbers of people to the impact of natural disasters. A potential increase in future-climate hazard would further increase exposure. The Rockhampton Regional Council will need prudent planning to accommodate the increased population while taking into account potential changes in the hazard. The process of incorporating projected changes in hazards into planning processes offers important insights for other regional councils in Australia.

To consider future-climate hazard within council practices, the Rockhampton Regional Council received funding from the National Climate Change Adaptation Research Grants Program Project for a project under the Settlements and Infrastructure theme. This funding was provided to evaluate the ability of urban planning principles and practices to accommodate climate change and the uncertainty of climate change impacts. Within this project, the Rockhampton Regional Council engaged Geoscience Australia to undertake the modelling of natural hazards under current and future climate. This report describes the methodology and the results of the work undertaken by Geoscience Australia and constitutes the final project deliverable for the Rockhampton Regional Council.

Geoscience Australia's work within the broader project has utilised natural hazard modelling techniques to develop a series of spatial datasets describing hazards under current-climate conditions and a future-climate scenario. The following natural hazards were considered:

- tropical cyclone wind
- bushfire
- storm tide
- coastal erosion
- sea-level rise.

The future-climate scenario considered was the A2 greenhouse gas (GHG) emissions scenario (Special Report on Emissions Scenario; SRES) from the Intergovernmental Panel on Climate Change (IPCC) (Nakicenovic and Swart, 2000). By 2100, the A2 emissions scenario predicts a 'best estimate' average global surface air temperature warming of 3.4 °C (2.0-5.4 °C; IPCC, 2007) based on a number of climate models with a range of climate sensitivities (IPCC, 2001). The application of downscaling techniques to the global A2 scenario produces a mid- to high-range climate response for

the likely projected future for the study region. Current observed global emissions are tracking very close to the A2 emissions scenario projections (Peters *et al.,* 2012).

1.1 Methodology

The tropical cyclone wind hazard assessment was generated with Geoscience Australia's Tropical Cyclone Risk Model (TCRM; Arthur, In Prep). The TCRM produces a stochastic catalogue of synthetic events that are statistically similar to the input events. Firstly, current climate tropical cyclone wind hazard was modelled based on the historical record of activity in the Rockhampton area, including the impact of local terrain on damaging wind speeds. Then, to model future climate, the TCRM was trained on outputs from a downscaled General (also referred to as Global) Circulation Model (GCM) forced by the SRES A2 emissions scenario for the two decades centred around 2050 and 2090 to provide details on changes in frequency, intensity and tracks of tropical cyclones.

The bushfire hazard assessment was based on the Forest Fire Danger Index (FFDI) and the Grassland Fire Danger Index (GFDI). These indices quantify fire weather hazard. Weather observations (temperature, relative humidity and wind speed) were combined with an estimate of the fuel state to predict likely fire behaviour in the event of ignition. The spatial distribution of the weather components of the FFDI across the Rockhampton region was modelled with a high resolution numerical weather model. Future climate was based on output from three downscaled GCMs forced by the SRES A2 emissions scenario for the two decades centred around 2050 and 2090.

The storm tide (storm surge plus tide) assessment was based on modelled tide levels from a national hydrodynamic study of extreme water levels by Haigh *et al.* (2012). The potential inundation based on the modelled storm tide heights were predicted using a bath-tub methodology (Eastman, 1993). For future climate, projected sea-level rise scenario heights for 2050, 2070 and 2100 were added to the modelled current-climate storm tide heights.

The coastal erosion assessment applied the method outlined by the Queensland Coastal Hazards Guideline (QCHG; DERM, 2012a). Current-climate coastal areas prone to erosion were identified based on the analysis of coastal change identified from historical aerial photography captured from 1961 and 1964 and compared with a 2010 image. The eroding sections of coast identified represent the areal extent of coastal erosion hazard under current climate. For future climate, the erosion hazard was determined using the proscribed QCHG widths for the 100 year planning period.

The sea-level rise (SLR) hazard assessment considered the still water extent (i.e. no wave setup or run-up) of the area prone to inundation from projected sea levels. The analysis considered three scenarios; the combining of the 2012 value for Highest Astronomical Tide (HAT) with each of four sea level increases projected for 2050, 2070 and 2100. The inundated area was predicted using a bath-tub methodology (Eastman, 1993).

1.2 Key Findings

1.2.1 Current Climate

The Rockhampton region is exposed to a significant level of hazard even in current-climate conditions. Some key findings of the current-climate hazard assessment are:

- *Tropical cyclone:* Rockhampton is in a high tropical cyclone hazard region. The results of the severe cyclonic wind assessment indicate hazard levels similar to the design wind speeds from the existing building code, although they are much greater than the wind hazard estimated from the observational record at Rockhampton Airport.
  - Higher elevation locations can be expected to experience extreme wind speeds equivalent to Tropical Cyclone (TC) Category 4 and 5, or higher, on average every 20 to 25 years. This includes Mount Archer, Flat Top Range, Mount Morgan and Native Cat Range.
  - The remainder of the study region is exposed to TC Category 3 wind speeds at similar recurrence intervals, with only small areas exposed to lower hazard levels.
- *Bushfire:* Days with “Extreme” and “Catastrophic” Fire Danger ratings can be expected to occur once every fifty or one hundred years for many locations in the Rockhampton region: notably Flat Top Range and south to the Fitzroy River and Mount Archer National Park.
- *Storm tide*: Many low-lying areas were shown to be susceptible to inundation from storm tide; such as wetlands, lakes and also built-up areas. Roads shown as being exposed to storm-tide hazard include Yeppoon-Emu Park Road and Bajool-Port Alma Road.
- *Coastal erosion:* Some buildings in Yeppoon and Emu Park are within the zone identified as exposed to coastal erosion.
- *Sea-level rise*: The current climate HAT identifies significant inundation. The area exposed to inundation under a HAT event includes Yeppoon Road, the Bajool-Port Alma Road, Port Alma, the Scenic Highway, South of Yeppoon and buildings in the vicinity of Keppel Sands.

1.2.2 Future Climate

All hazards considered in this study, with the exception of tropical cyclone wind hazard, increase under simulated future-climate conditions. However, the change is not uniform across the region; some areas will experience relatively much less increase then others.

Some key findings of the future-climate hazard are:

- Tropical cyclone: There is an apparent decline in wind hazard into the future; however, due to the variability of the process modelled, uncertainties are large, and none of the changes were statistically significant
- Bushfire: The area characterised by “High” bushfire hazard increases in both magnitude and extent through 2050 to 2090. Significant areas of higher bushfire hazard include:
  - south-west of Gracemere
  - north of Rockhampton on the eastern side of the Bruce Highway
  - south of Rockhampton on the western side of the Bruce Highway.
- Storm tide: The storm tide hazard increases with the addition of sea-level rise. Exposure under current climate increases with the addition of sea-level rise, e.g. the Yeppoon-Emu Park Road

will be inundated under the 2100 future-climate scenario inundation. New areas were exposed, such as the Keppel Sands Road which is exposed to the 2100 SLR future-climate scenario.

- Coastal erosion: The 2100 simulated coastline is within 0 and 400 m landward of the existing coastline. Buildings were exposed in many cases, e.g. in Keppel Sands, Emu Park, Shoal Bay and Yeppoon.
- Sea-level rise: The sea-level rise analysis, HAT + SLR, identified that the HAT inundation on the floodplain downstream of Rockhampton is progressively exacerbated, with increasing SLR heights towards the city of Rockhampton and the Bruce Highway. The open coast appears to not be further exposed with the addition of SLR heights to HAT.

1.3 Conclusion

The results of this study provide an assessment of hazard from extreme events, under both current and future climate, that is indicative on a regional scale. Land use planning should consider how the projected future hazard level may impact on proposed development. Effective local planning could contribute to reducing the risk from some hazard types, e.g. storm surge and bushfire Hazard levels across the wider region may need to be considered when planning access roads or other infrastructure. The present study did not include flooding, or consider the correlation between hazards such as coincident cyclone, storm surge and flood hazard; both of which are important components of a full understanding of current and future hazard.

1.4 Uncertainty and Limitations

This study has been completed using currently available world best-practice methods. Climate science is a developing field and, as such, the results of this study need to be compared to future-climate research to consider the ongoing validity of the results. The future-climate simulation in this study has been based on regional climate simulations that have, in turn, been based on the global IPCC AR4 results. The IPCC Fifth Assessment Report (AR5) is due for release in September 2013. The climate impacts and adaptation research community, including such organisations as the CSIRO, provide a constantly evolving source of information relating to hazards and future-climate effects. Within this study, a single global emissions scenario was considered within the future climate; completing the same analysis for a suite of emissions scenarios would result in a range of future-climate hazard for consideration. Alternatively, Representative Concentration Pathways (RCPs) which are four greenhouse gas concentration (not emissions) trajectories, have been adopted by the IPCC for its Fifth Assessment Report (AR5) and could form the basis of further work exploring the uncertainty of future hazard.

2 Introduction

2.1 Background

Due to the developing understanding of the science of climate change, model uncertainties present significant challenges for land use planning, emergency management and risk mitigation across Australia. Even under current-climate conditions, the Rockhampton Regional Council area is subject to the impacts of natural hazards, such as bushfires, floods, and tropical cyclones (extreme winds and storm surge). All of these hazards may worsen with climate change.

The Commonwealth Government's first pass national assessment of the potential impact of climate change on coastal infrastructure (Cechet *et al.,* 2012) indicated that, of the significantly populated Queensland Local Government Areas (LGAs), the Rockhampton Regional Council has the largest area potentially inundated through the combined impacts of sea-level rise, erosion and storm tide. Considering the expected population increase in Rockhampton (from under 117 thousand people in 2011 to over 175 thousand for 2031 under the high series prediction (Qld OESR, 2012)), even current-climate hazard will, through time, progressively expose greater numbers of people to the impact of disasters. A potential future-climate increase in hazard combined with the predicted population increase in the Rockhampton region will result in an increase in exposure. Therefore, the Rockhampton Regional Council will need prudent planning to accommodate the increased population while taking into account potential changes in the hazard. The process of incorporating projected changes in hazards into the planning processes could offer important insights for other regional councils in Australia.

To consider future-climate hazard within council practices, the Rockhampton Regional Council received funding from the National Climate Change Adaptation Research Grants Program Project for a project under the Settlements and Infrastructure theme. This funding was provided to evaluate the ability of urban planning principles and practices to accommodate climate change and the uncertainty of climate change impacts. Within this project, the Rockhampton Regional Council engaged Geoscience Australia to undertake the modelling of natural hazards under current and future climate. This report describes the methodology and the results of the work undertaken by Geoscience Australia and constitutes the final contract deliverable for the Rockhampton Regional Council.

2.2 Aim

The aim of this study is to utilise natural hazard modelling techniques to develop a series of spatial datasets describing hazards under current-climate conditions and a future-climate scenario.

This study considers the following natural hazards:

- tropical cyclone wind
- bushfire
- storm tide
- coastal erosion
- sea-level rise.

Flood modelling was not within the scope of Geoscience Australia's work for this study. It is recognised that flood modelling should be included within an "all-hazards" approach; specifically as Rockhampton is prone to flood (1918, 10.11 metres peak height above gauge datum; 1954, 9.4 m; 1991, 9.3 m; and 2011, 9.15 m). Flood modelling could augment this study in the future.

The outputs of this study include:

- A description of the methodologies and discussion of results (this report)
- Hazard maps
- Hazard modelling results in digital form.

The aim of the hazard maps, supplied alongside the report, is to spatially communicate the regional hazard results. The maps should be interpreted with this report and should not be used in isolation. The hazard maps are indicative of the hazard levels at a regional scale, and are not intended for use for local planning purposes. The maps have not been designed to communicate the hazard to the general public.

The aim of the hazard modelling results, in the form of digital spatial data, is to support the Rockhampton Regional Council in evaluating the ability of existing urban planning principles and practices to accommodate climate change and the uncertainty of climate change impacts. The digital spatial data has been provided to the Rockhampton Regional Council to enable the council to further analyse or visualise the data.

2.3 Study Region

The spatial extent of this study is shown in Figure 2.1. This extent was selected as it covered the most populated area within the Rockhampton Regional Council LGA, and the area Rockhampton is likely to expand within as the population increases.

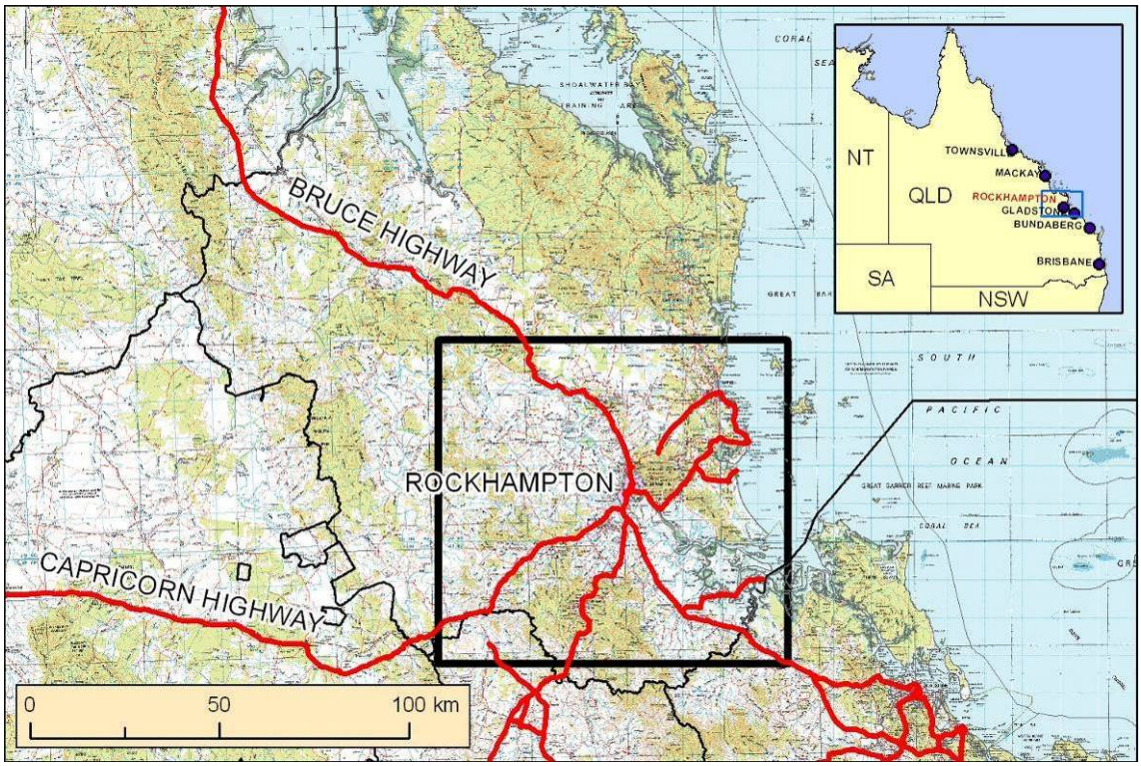

Figure 2.1. The Rockhampton study region (black outline) and primary roads (red lines).

2.4 Future Climate in Queensland

2.4.1 Future Climate Overview – Central Queensland

The DERM report "*ClimateQ: towards a greener Queensland*" (DERM, 2009) provides the scientific and policy context for climate change for Queensland. It includes eight sectoral strategies to reset and expand Queensland's policy approach for managing future greenhouse gas impacts and safeguarding Queensland's future. Appendix 3 of the report provides regional climate change summaries. Box 1 shows an excerpt from the summary of the key findings on projected climate change for Central Queensland which includes the Rockhampton region.

Box 1. Climate Change in the Central Queensland Region

Temperature

- Average annual temperature in Central Queensland has increased 0.5 °C over the last decade (from 21.6 °C to 22.1 °C).
- Projections indicate an increase of up to 4.5 °C by 2070 leading to annual temperatures well beyond those experienced over the last 50 years.
- By 2070, Rockhampton may have four times the number of days over 35 °C (increasing from an average of 16 per year to an average of 64 per year by 2070), while Barcaldine may have nearly twice the number of hot days (increasing from an average of 87 per year to an average of 163 per year by 2070).

Rainfall

- Average annual rainfall in the last decade fell by nearly 14 per cent compared with the previous 30 years. This is generally consistent with natural variability experienced over the last 110 years, which makes it difficult to detect any influence of climate change at this stage.
- Models have projected a range of rainfall changes from an annual increase of 17 per cent to a decrease of 35 per cent by 2070. The 'best estimate' of projected rainfall change show a decrease under all emissions scenarios.

Evaporation

- Projections indicate annual potential evaporation could increase 7–15 per cent by 2070.

Extreme events

- The 1-in-100-year storm tide event is projected to increase by 51 cm in Gladstone and 32 cm at Cape Clinton (near Yeppoon) if certain conditions eventuate. These conditions are a 30 cm sea-level rise, a 10 per cent increase in cyclone intensity and frequency, as well as a 130 km shift southwards in cyclone tracks.

2.5 Future-Climate Hazard Modelling

Modelling the hazards within the future climate was completed through running General Circulation Models (GCMs) for current and future climate and scaling the current-climate hazard (Tropical Cyclone (TC) wind and bushfire) or building on results from other studies (storm tide, coastal erosion and sea-level rise).

Future-climate projections, such as those in Box 1, are typically based on the outputs from GCMs. These climate models represent the physics in the atmosphere, and/or oceans, and can be 'forced' by Greenhouse Gas (GHG) emissions scenarios to project the future global climate. The results in Box 1 are based on the low (B1) and high (A1FI) emissions scenarios specified by the Intergovernmental Panel for Climate Change (IPCC) in the Special Report on Emissions Scenarios (SRES, Nakicenovic and Swart, 2000).

The future-climate scenario in this study was based on the SRES A2 GHG emissions scenario. Figure 2.2 presents the global average surface air temperatures resulting from the SRES emissions scenarios. The A2 GHG scenario predicts a mid- to high range response for the projected climate response to the emissions, resulting by 2100 in an average global warming of 3.4ºC (with a range of 2.0-5.4ºC) based on outputs from a range of GCMs (IPCC, 2007a). The A2 scenario storyline designates the global focus to remain on economic development rather than environmental sustainability. Current observed emissions are tracking the A2 emissions scenario projection (Peters *et al.,* 2012).

Global or even regional climate models are fundamental to climate science; however they tend not to effectively capture the extreme climate events that cause natural disasters. This is partly because extreme climate events typically operate on small spatial scales, often below the resolution of the models (ACE CRC, 2010). Moreover, extreme climate events are per definition rare, and creating sufficiently long GCM or Regional Climate Model (RCM) simulations to understand their behaviour is computationally still prohibitively expensive. Instead, natural disasters are often studied using a variety of modelling approaches that integrate the physics that drives the event with statistical techniques to parameterise small-scale processes. GCMs were run with current-climate GHG forcing and then compared with the results from the GCMs being forced by the A2 GHG emissions scenario (Nakicenovic and Swart, 2000). For specific hazard modelling characteristics the ratio of current to future-climate GCM results could then be applied to the current-climate hazard to model the future-climate hazard.

Geoscience Australia has developed a capability for modelling natural disasters for Australia and the Asia-Pacific region; ranging from earthquake, tsunami, storm surge and flood to extreme wind and, currently, bushfire. This capability has successfully been applied to model a range of hazards under future-climate conditions, e.g. Arthur *et al.*, 2011; Cechet *et al.,* 2011; Cechet *et al.,* 2012; Hazelwood *et al.,* 2012.

This study draws on available scientific work undertaken by other agencies studying current and future climate, including a national storm tide study. This study builds on those outputs by applying hazard modelling techniques to develop an overview of multiple climate hazards in the Rockhampton region under current and future-climate conditions.

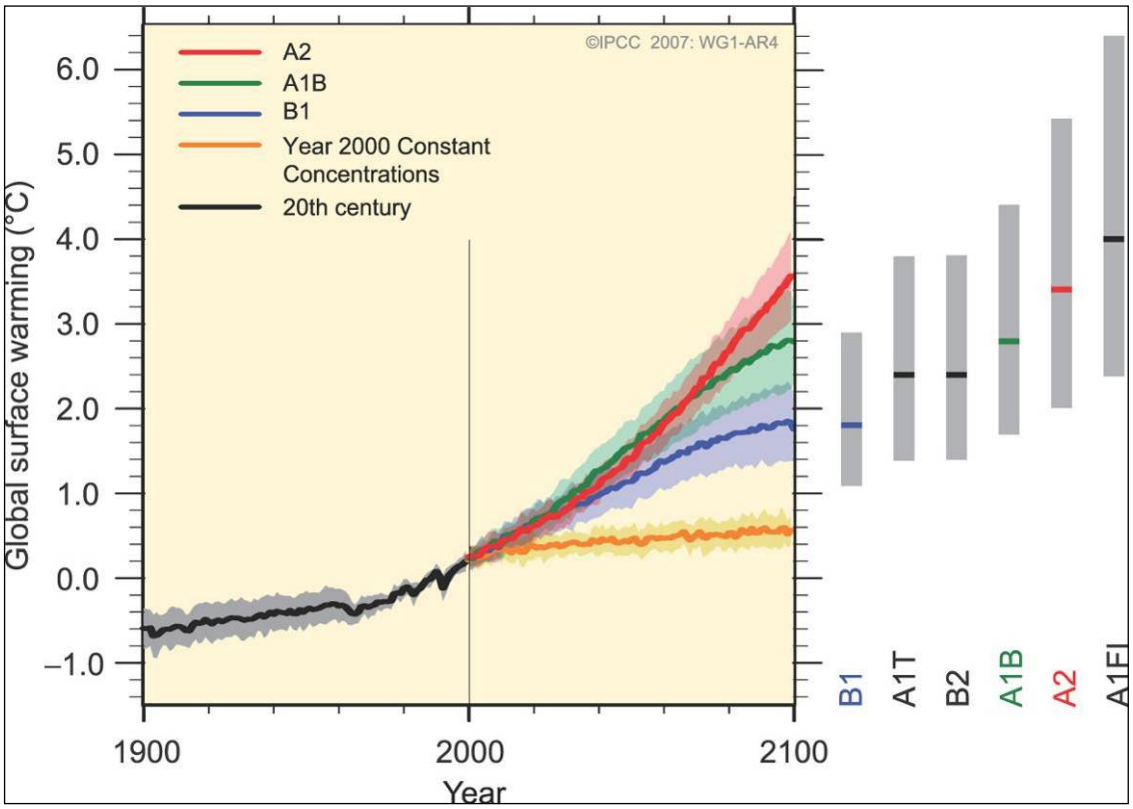

Figure 2.2. Multi-model averages and assessed ranges for surface warming (IPCC, 2007a).

Within this report, the hazard probability is specified in terms of the Average Recurrence Interval (ARI). The ARI is a measure of how often a certain severity of a hazard is experienced. For example, a 500 year ARI wind speed of 60 m/s indicates that winds of that severity, or higher, occur on average once every 500 years at that location. Note that the ARI is based on a probability calculated over a long time period; it is entirely possible that a 500 year ARI wind speed occurs twice in subsequent years, or even in a single year. Therefore, it is important that planning processes consider high ARI hazard as well as the frequent hazard levels with a low or medium ARI. The ARI is equivalent to other measures used to express probability of extreme events and natural disasters, such as the return period (RP).

2.6 Report Structure

This report consists of a summary written specifically for a non-technical audience within the Rockhampton Regional Council. The summary report comprises a synopsis of the methods and results of each of the hazards covered under current and future climate. The summary, which presents the 50 and 100 year ARI hazard, is supplemented by the technical appendices which provide additional technical detail, including discussions of the methods and results. The full results, including other ARI hazard, which should be considered as hazard may not scale linearly with probability, is given in the appendices, and a digital version of the results (hazard maps) is provided with this report.

3 Tropical Cyclone Wind

Rockhampton is in Australia's high-risk zone for tropical cyclones. This is reflected by its location in the cyclonic region in the Australian building code for wind (AS/NZS 1170.2). The last cyclone, causing major wind damage, impacted Rockhampton in 1949. The typical tropical cyclone season extends from 1 November to 30 April.

3.1 Method

Tropical cyclone hazard in this study was modelled using the TCRM, a statistical-parametric computational tool developed by Geoscience Australia for estimating the wind hazard from tropical cyclones (Arthur, In Prep). The TCRM does not model storm surge associated with tropical cyclones. The TCRM was used to generate a synthetic catalogue equivalent to 5000 years of potential events, based on the characteristics of historically observed cyclones across the region and Australia. For each event in the synthetic catalogue, the swath of damaging winds was calculated. This incorporated localised effects of topography, land cover (e.g. forests, croplands, urban areas and water bodies) and the shielding effects provided by closely-spaced buildings. Based on this, the ARI wind speeds were calculated for the study region.

To calculate current-climate TC wind hazard, TCRM was trained on the catalogue of observed events (1950-2012, Kuleshov *et al.,* 2008). To determine the cyclone hazard under the future-climate scenario, the synthetic event catalogue was generated based on the tracks detected in the GCM output, assuming the SRES A2 GHG emission scenario (Nakicenovic and Swart, 2000), for 2050 and 2100.

3.2 Results

Complete results are presented in Appendix A. Here the 50 year ARI results are presented for current climate and for 2090.

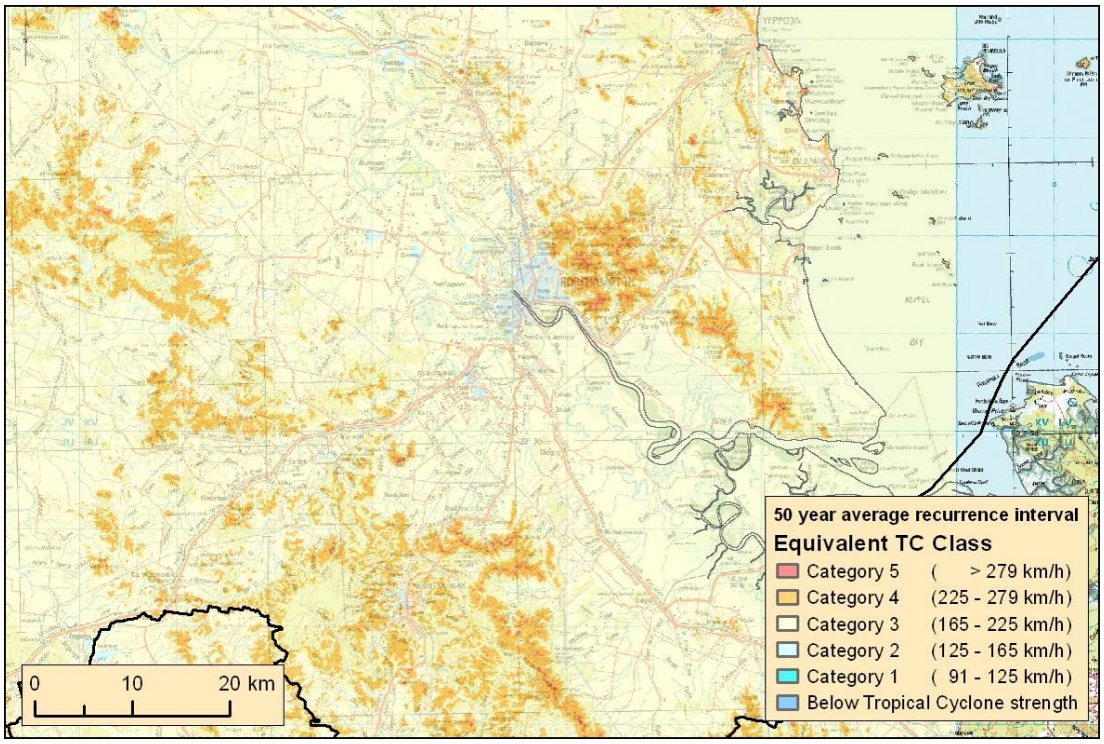

Figure 3.1 Current-climate 50 year ARI TC wind hazard[3].

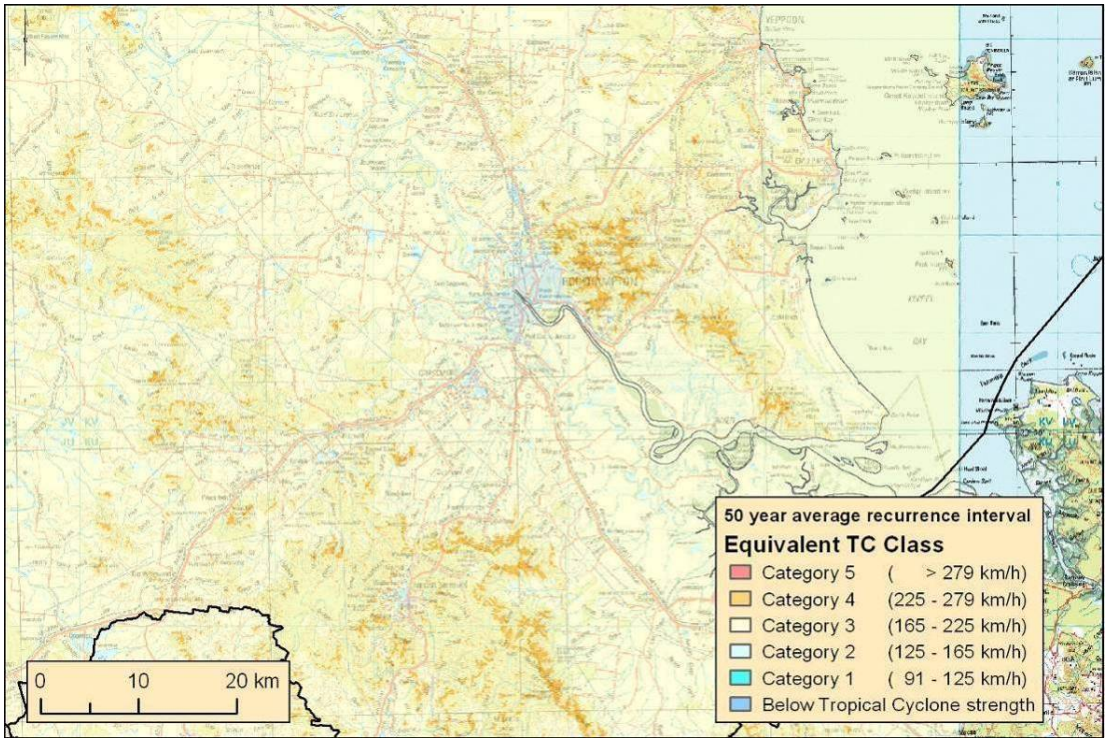

Figure 3.2. 2090 50 year ARI TC wind hazard for the SRES A2 scenario.

[3] The maps show local wind speed hazard in terms of the equivalent TC wind speed categories. The TC categories are only used to facilitate interpretation of the wind speeds; they do not indicate distinct TC events within the study region.

3.3 Discussion

The modelling results agreed with the classification of Rockhampton within Australia's tropical cyclone risk zones as depicted in AS/NZS 1170.2. All hazard estimates were similar to the existing design wind speeds for the region, but were much greater than ARI wind speeds estimated from the observational record at Rockhampton Airport[4].

In the current climate, 50 and 100 year ARI events, the tropical cyclone peak hazard (equivalent to wind speeds from TC Category 4 and 5) is observed in the higher elevations including Mount Archer, Flat Top Range, Mount Morgan and Native Cat Range. The remainder of the study region is mostly exposed to TC Category 3 wind speeds with small areas experiencing lesser wind speeds.

In the future-climate simulation, the TC wind hazard simulations indicated a decline in cyclonic wind hazard. However, it has to be noted that, due to the large inherent variability in modelling methodology, the change in wind hazard modelled for future climate under the SRES A2 emissions scenario was not statistically significantly different.

These results were in line with the current understanding of the shifts in cyclone hazard across Australia. Recent studies indicate that cyclone frequency may decline somewhat overall, but a larger proportion of cyclones will be intense (Category 4 and 5; see for example Abbs, 2012, Zhao and Held, 2012, and Hill and Lackmann, 2011). This shift could produce average hazard levels very similar to those experienced currently. In conjunction, the tracks may tend to occur further southward, especially on the east coast of Australia (Abbs, 2012). While such a shift in tracks suggests some areas in Queensland may experience higher cyclone hazard in the future, this is unlikely to be an issue for Rockhampton as it is already in an active cyclone region.

[4] This illustrates why hazard modelling for extreme events is based on broad, in this case national, 'synthetic' catalogues of potential events, rather than local observations alone.

This page is intentionally blank

4 Bushfire

The dry-tropics of central Queensland result in an annual bushfire threat that generally extends from September to November. Within this study bushfire hazard was defined by the Forest Fire Danger Index.

4.1 Method

In Australia, fire weather hazard is quantified using either the Forest Fire Danger Index (FFDI) or the Grassland Fire Danger Index (GFDI; Luke and McArthur, 1978). Both the FFDI and the GFDI consider weather observations and each index considers a dryness factor: FFDI includes a 'drought factor' and GFDI considers a 'curing factor'. Weather observations (temperature, relative humidity and wind speed) were combined with an estimate of the fuel state to predict likely fire behaviour if an ignition eventuates. The 'drought factor' is used for forests in the combined estimate of fuel state, and is based on daily rainfall and the period of time elapsed since the last rain. For grasslands, the 'curing factor' is used in the combined estimate of fuel state. Curing describes the annual or seasonal cycle of grasses dying and drying out. The curing factor can be measured via destructive sampling, visual observations and remote sensing. For this study only FFDI was calculated and the GFDI was scaled from the historical FFDI/GFDI measurements (for those instances, numbering 22, over nearly 40 years of daily records where FFDI > 50).

A high horizontal spatial resolution (270 m) numerical weather model was utilised to provide spatial texture weather characteristics including temperature, wind speed/direction and relative humidity. This was computed over the Rockhampton region for a range of historical days where bushfire hazard, as measured at the Rockhampton Airport meteorological station, was known to be Severe to Extreme. The weather model simulated the weather conditions across the Rockhampton region from the observations available at the Rockhampton Airport and a range of far-field observations. From the temperature, relative humidity and wind speeds generated by the model, the maximum FFDI for each grid point over each simulated day was calculated, again using a constant drought factor. Each of these FFDI maps was then normalised to the value of the FFDI at the grid point corresponding to Rockhampton Airport. The ARI of FFDI at Rockhampton Airport for the current climate was calculated from observations by fitting Generalised Extreme Value (GEV) distributions.

For current climate, FFDI was obtained utilising the observational record, which spanned four decades at the Rockhampton Airport. High-resolution spatial detail for the FFDI was obtained from the weather model simulations. A number of extreme events (days) that were identified as "typical" of the type of event that would be experienced once in 50 years or once in 100 years (i.e. the synoptic conditions had been determined as being similar to the majority of the extreme fire weather events in the observational record) were downscaled in the simulations. For future climate, this study considered three downscaled GCMs forced by the A2 GHG emission scenario. The ratio of spatial FFDI for the GCMs (involving temperature, relative humidity and wind speed) that was run under both current-climate and future-climate conditions, was then applied to the current-climate bushfire hazard (Rockhampton airport) which resulted in a spatial representation of future-climate bushfire hazard.

4.2 Results/discussion

Figure 4.1 shows the spatial pattern of the current-climate 50 year ARI fire danger rating for the Rockhampton region. Figure 4.2 shows the spatial pattern for the ensemble model average (average of GCMs) for the 2090 climate (A2 emissions scenario). A relatively small increase is observed throughout the Rockhampton region, in both magnitude and extent, through 2050 to 2090. Cluster areas of marginally higher bushfire hazard include:

- south-west of Gracemere
- north of Rockhampton on the eastern side of the Bruce Highway
- south of Rockhampton on the western side of the Bruce Highway.

This relatively small change in FFDI with climate change for this central Queensland coastal community is consistent with other studies that have considered this region (Lucas *et al.*, 2007; Clarke *et al.*, 2011).

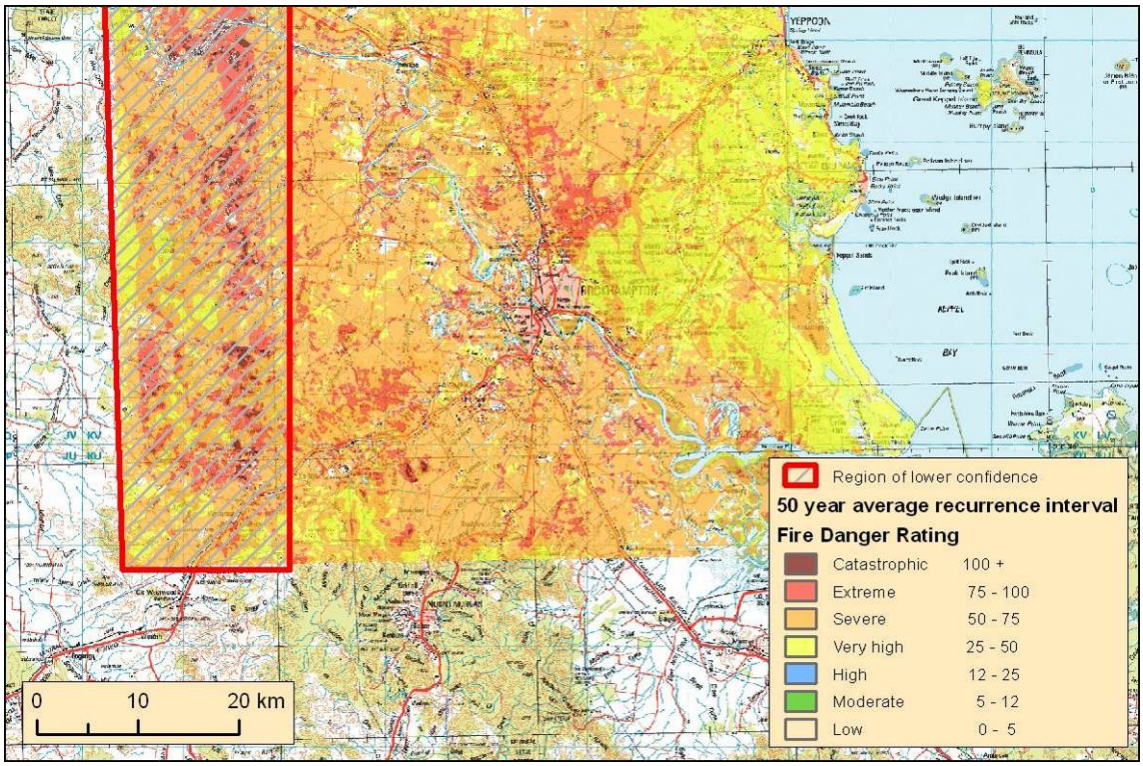

Figure 4.1. Rockhampton region Fire Danger Rating, current-climate – 50 year ARI. See Appendix B for a description/discussion of the region of lower confidence (dashed area).

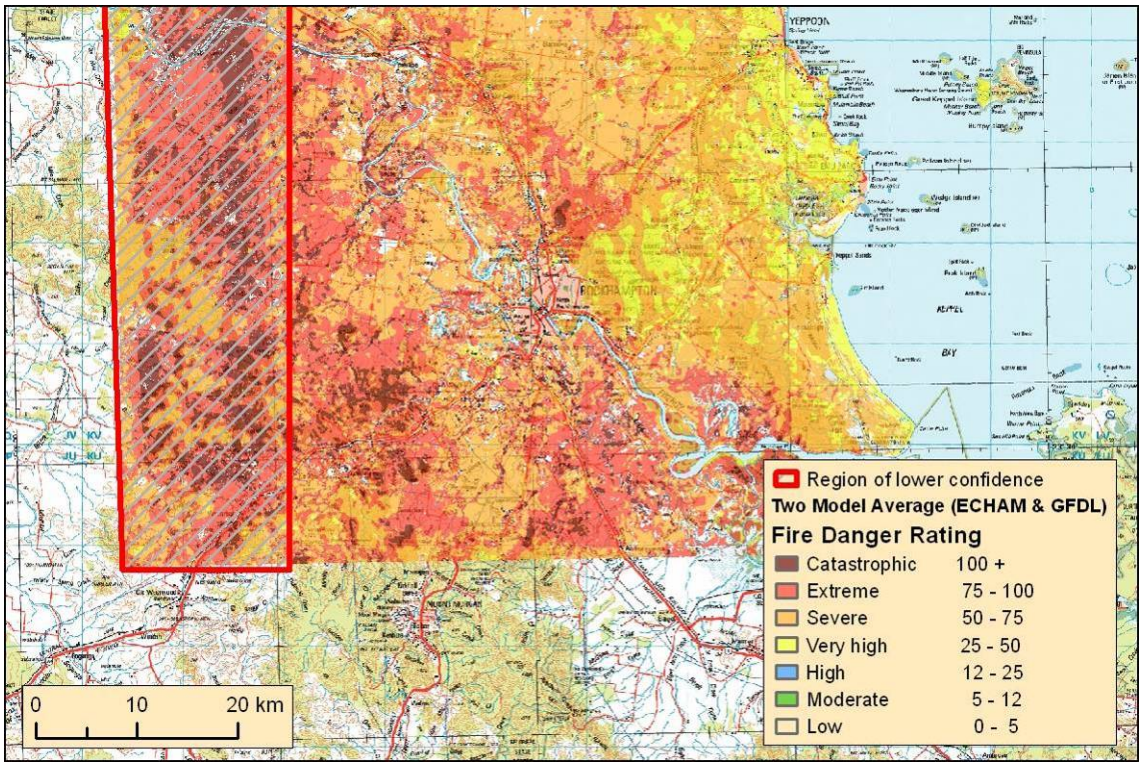

Figure 4.2. Rockhampton region Fire Danger Rating, 2090 – 50 year ARI (A2 scenario). See Appendix B for a description/discussion of the region of lower confidence (dashed area).

This page is intentionally blank

5 Storm tide

The low-lying coastal areas in the Rockhampton region lie within a high-risk cyclone zone, and are susceptible to the impacts of storm tide. For example, the Mackay cyclone of 1918 caused 2.7 m waves in Rockhampton[5]. Storm tide is a combination of storm surge, wave setup and astronomical tide. Storm tides can impact over 100 km of coastline in a single event, causing significant damage to property and endangering lives (CSIRO, 2003). Storm tide event impact depends on the storm's characteristics, its track approaching landfall and the coastal geography including bathymetry and topography.

5.1 Method

The storm tide data used in this study were sourced from a national hydrodynamic modelling study of extreme water levels for current climate (Haigh *et al.,* 2012) undertaken by the University of Western Australia (UWA) for the Antarctic Climate & Ecosystems Cooperative Research Centre (ACE CRC). The outputs of the ACE CRC study consisted of points adjacent to the coastline with defined storm tide water level heights (Mean Sea Level (MSL) + tide + storm surge) for a range of ARIs. The ACE CRC study distinguished between extra-tropical and tropical storm events. However, the ACE CRC study did not model a future-climate storm tide hazard. Therefore, to model the impact of climate change on future storm tide hazard, the following sea-level rise scenarios were added to the ARI probability storm tide inundation heights: + 0.3 m (QLD 2050)[6], + 0.5 m (QLD 2070), + 0.8 m (QLD 2100), + 1.1 m (FED 2100)[7].

A cluster analysis method was then applied to identify spatial patterns and thereby group similar storm tide heights. Two distinct clusters were identified within the study region: Area A and B (Figure 5.1 and Figure 5.2). For each cluster area, the mean water height for each ARI probability event was calculated from the contained storm tide points. The mean water height was then utilised to identify inundation extent. The 'bath-tub' method (Eastman, 1993) was used to determine the inundation extent. This method identifies the areas onshore that are lower than the mean storm tide level. While a bath-tub method is often used as a first-order approximation, it is a rudimentary approach. The bath-tub method does not consider physical barriers that can prevent inundation, such as small hills or sea walls. This can lead to overestimation of the inundation. Alternately, the bath-tub method does not consider the force and momentum of waves, which can result in this method underestimating the inundation extent.

The inundation extent was restricted to within 4 km of the coastline. This limit was applied because the bath-tub method, an approximation of inundation extent, tends to overestimate inundation in large

[5] http://hardenup.org/be-aware/weather-events/events/1910-1919/cyclone-mackay-1918-1918-01-21.aspx

[6] The sources are provided within the Sea-level Rise hazard section on page 31

[7] This methodology and storm tide data also supports the ACE CRC Canute Sea Level Calculator which provides a user interface to identify combined current climate storm tide and sea-level rise around Australia for extra-tropical storms only. http://canute2.sealevelrise.info/slr/Important%20Information

low-lying areas, such as the lower reaches of the Fitzroy River mouth. However, the full extent of the potential inundation, in digital form, has been provided to the Rockhampton Regional Council for consideration.

5.2 Results

To present the range of inundation hazard the lowest (Figure 5.1) and the highest (Figure 5.2) inundation levels are shown. Each figure presents inundation probability from 50 through to 1000 year ARI hazard.

The supplied hazard maps and digital spatial data covering all the results allow more detailed analysis which identifies the following locations are potentially at risk from impact:

- Wetlands, lakes and some buildings were exposed to storm tide inundation in both current-climate and the 2100 future-climate scenario
- Yeppoon-Emu Park Road is exposed to storm tide hazard in the current climate. This can very nearly cut the road to the north of Emu Park. The road is cut by storm tide inundation in the 2100 future-climate scenario
- Keppel Sands Road is exposed to the impacts of storm tide in the 2100 future-climate scenario
- Bajool-Port Alma Road is exposed to storm tide inundation in current climate. It is increasingly exposed in the future climate with the banks of salt evaporators also being over-topped in the 2100 future-climate scenario.

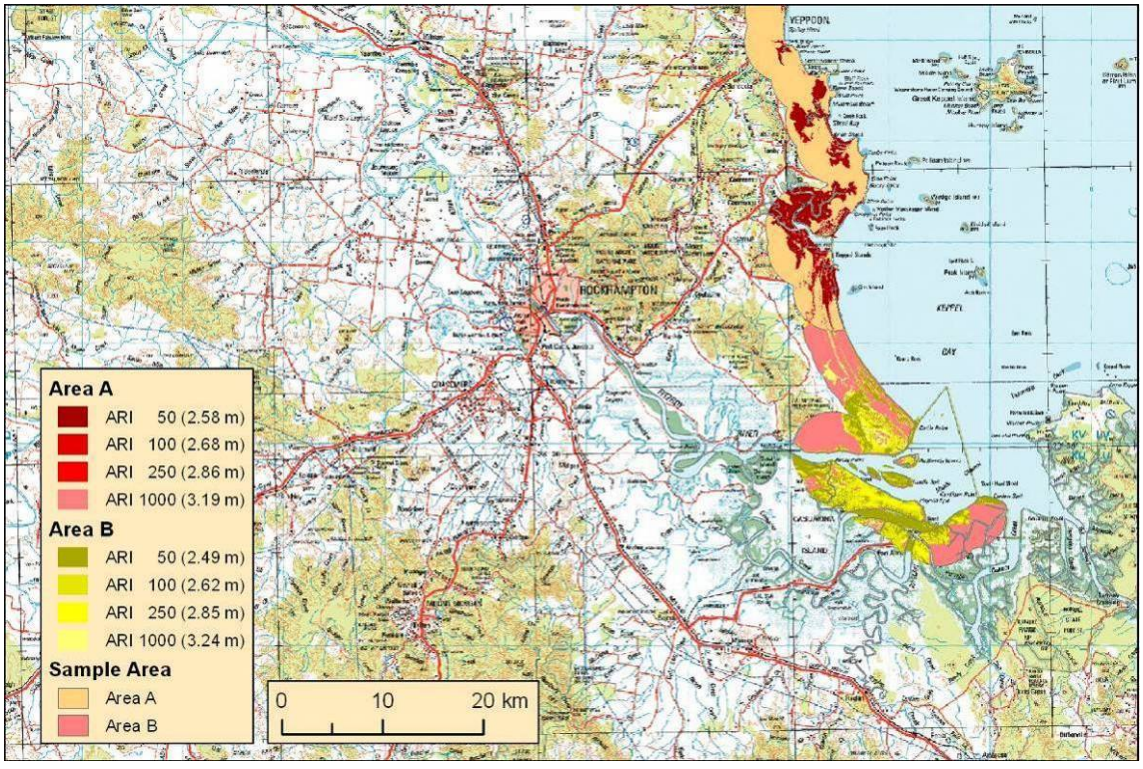

Figure 5.1. Current climate - tropical cyclone storm tide inundation.

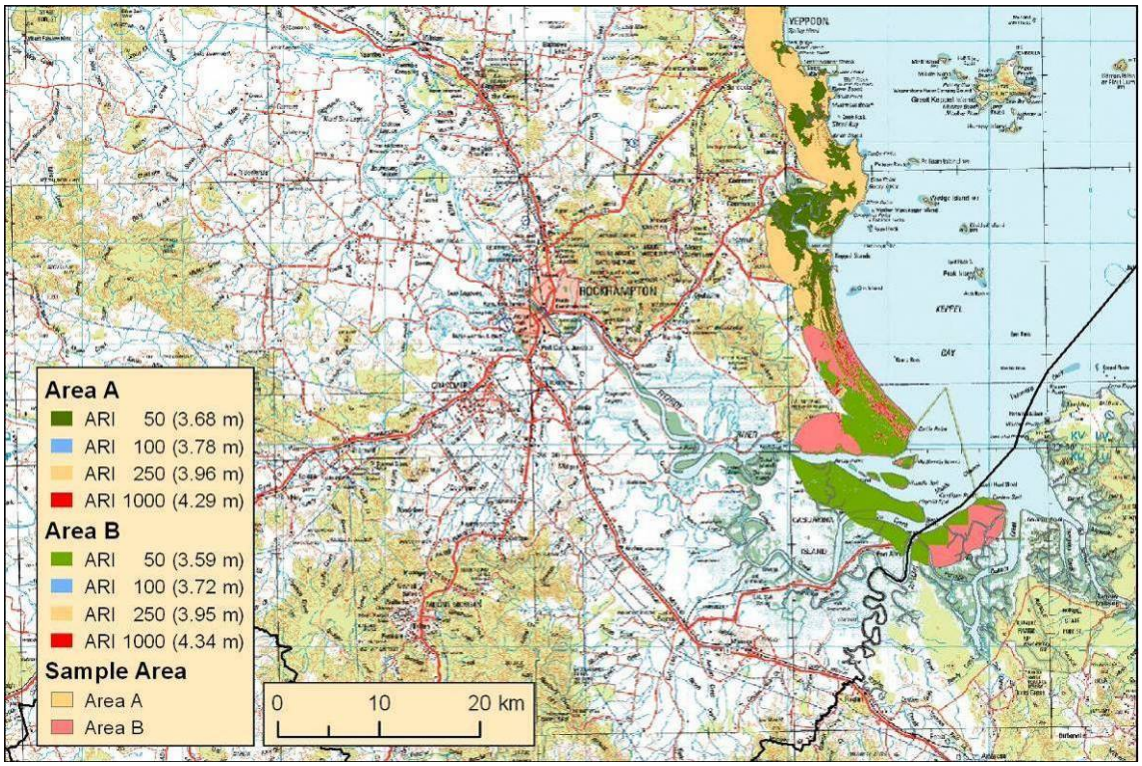

Figure 5.2. Future-climate - 2100 sea-level rise (1.1 m) combined with tropical cyclone storm-tide inundation.

This page is intentionally blank

6 Coastal Erosion

Coastal erosion is a naturally occurring process caused by wave and current processes that continually shape the nature and form of the shoreline. Erosion in the coastal zone is both a short-term problem due to the occurrence of storm events and a long-term problem relating to natural and anthropogenic interruptions to sediment supply. The form and fabric of the geomorphic units in the coastal zone determines the rate and extent of erosion. For example, the unconsolidated sediments within dune and barrier systems are easily eroded over short temporal scales (days to weeks) compared with bedrock cliffs that erode across hundreds of kilometres at geological temporal scales. Coastal erosion results in a reduction of beach width and the creation of dune scraps resulting in the loss of beach amenity as well as damage to property. Coastal erosion due to storms events is often followed by a period of beach recovery. However, over the long-term, with sea-level rise and increased storminess, the loss of land eroded in the coastal zone is likely to be permanent.

For the purpose of this study, coastal erosion was defined as “shoreline recession due to sea erosion causing a permanent loss of land” (DERM, 2012a). This study does not consider the temporary erosion associated with storm events, after which the beach or section of coastline may recover naturally.

6.1 Method

The current and future-climate erosion hazard was determined using the method provided by the Queensland Coastal Hazards Guideline (QCHG, DERM, 2012a). The guideline requires erosion prone area widths to accommodate both short- and long-term erosion for a specific planning period. The current-climate erosion overlays refer to short-term erosion prone areas.

6.1.1 Current Climate

The identification of the current-climate coastal hazard was undertaken by making a visual inspection of the coastline using the high resolution digital aerial photography of the Rockhampton region. The purpose was to identify sections of the coastline that were:

- actively eroding (presence of a dune scrap), or were
- currently protected by a hard engineering structure (e.g. rip-rap wall or sea wall).

In addition, a historical shoreline analysis was undertaken to identify any underlying coastal erosion trends not captured by the first step. The shoreline, defined as the vegetation boundary for ease of identification on the historical black and white photographs was digitised (scale 1:86,000) from two series of historical aerial photographs (captured 05/1961 and 06/1964). The location of the historical shoreline was then compared to the present shoreline from the 2010 image of the Rockhampton

coastline (10 - 50 cm horizontal resolution). This comparison enabled the identification of sections of the coastline that have experienced coastal recession or accretion[8] during this time period.

The current coastline was then digitised from the 2010 aerial photography and buffers applied to eroding sections of coast to represent the areal extent of coastal erosion hazard under current climate as described by the QCHG.

6.1.2 Future Climate

There is considerable debate within the coastal science community about whether or not rising sea levels due to climate change will increase rates of coastal erosion. Sea-level rise does not itself cause coastal erosion as there is too little energy associated with it to mobilise sediment, but rather the higher water level allows wave action to impact higher on the beach resulting in sediment being transported seaward. To date, a simple empirical relationship developed by Per Bruun in the 1950's (Bruun, 1962) has dominated the prediction of the impacts of sea-level rise on sandy beaches. This model estimates the expected coastal erosion, as shoreline retreat, to be approximately 100 times that of the observed rate of sea-level rise. For example, a rise in sea level of 1 m will result in a corresponding erosion of the shoreline by 100 m. Whilst this simple relationship forms the basis of many coastal planning and beach nourishment program, it has never been validated on open coast beach systems or macro-tidal beach systems that exist along the Rockhampton Regional Council coast. This, coupled with the absence of any process studies for these beach types, led to the application of the methodology proposed by the Queensland Department of Environment and Heritage Protection (DERM, 2012a).

Applying the QCHG long-term erosion method, the Queensland Department of Environment and Heritage Protection had identified the exposed coastline and produced a table (Appendix Table D.1) containing the modelled coastal erosion distances for the Rockhampton Regional Council coastline. The coastline segment, identified in each row of the table, was then matched to the coastline spatial data and buffered the coastline with the identified erosion distances.

[8] The process where sediment deposits cause the shoreline to advance seaward.

6.2 Results

Under current climate approximately 0.6 km^2 of shoreline was identified as exposed to the erosion hazard. Under a future climate this estimate increases to 47.3 km^2 of the shoreline being identified as exposed to the coastal erosion hazard.

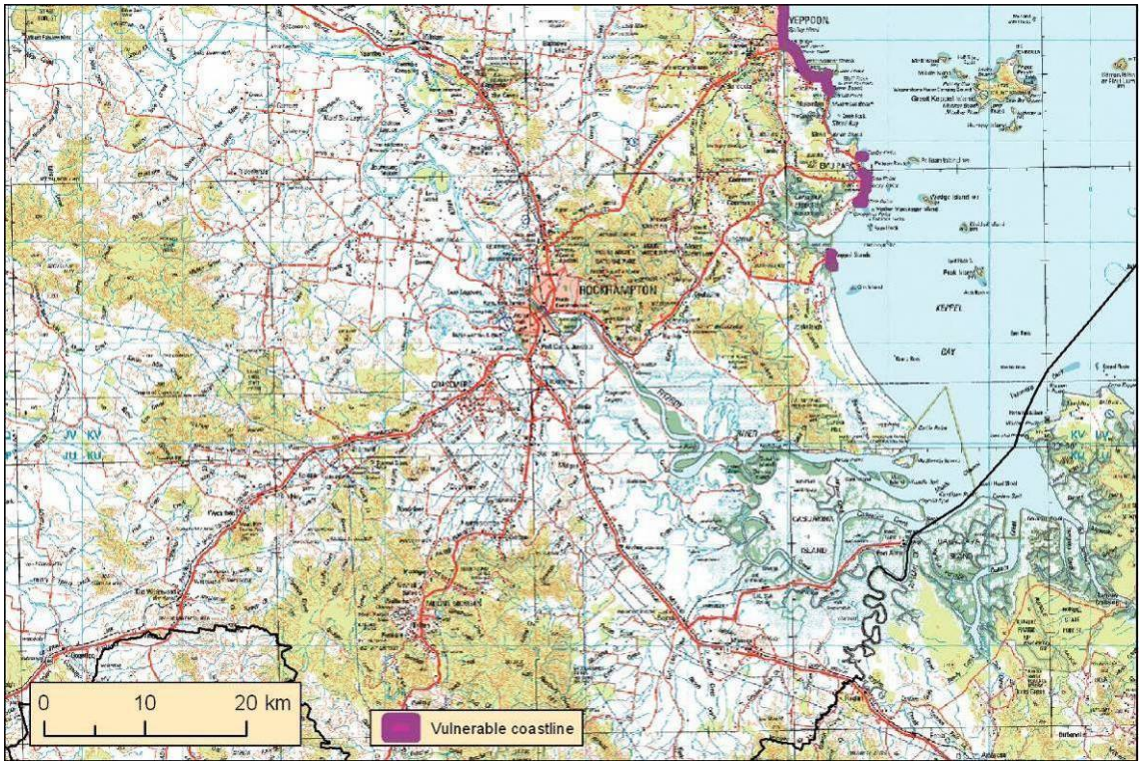

Figure 6.1. Current-climate coastal erosion exposed coastline[9].

6.3 Discussion

The current-climate exposure to coastal erosion is largely confined to the following:

- East facing sections of the coastline directly open to the prevailing wave climate, e.g. Rocky Point Beach and the northern section of Long Beach.
- The southern sections of the predominantly east to east-north-east facing beaches due to wave refraction by the southern headlands concentrating the wave energy, e.g. Tanby Point. This is a natural phenomenon and will continue under current-climate conditions.
- Beaches where there has been significant anthropogenic activity resulting in the loss of sediment from the beach system, and often leading to the construction of hard engineering structures to prevent further losses; e.g. the southern section of Farnborough Beach.

[9] Note: the outline width of the erosion extent has been increased to clearly show the exposed coastline and does not represent the areal extent of the erosion. For the correct erosion extent refer to the provided A3 hazard maps.

Figure 6.2. Future-climate (2100) coastal erosion exposed coastline[10].

The results show that the extent of shoreline exposed to the erosion hazard increases significantly with the future climate. This includes areas with existing development, e.g. Bangalee, Yeppoon (including the Yeppoon-Byfield Road), the Yeppoon-Emu Park Road and Emu Park.

There have been very few studies of the macrotidal beaches in the southern and central part of Queensland (e.g. Brooke *et al,* 2008; Webster and Ford, 2010); of those undertaken even fewer have attempted to model them (Masselink, 1993; Masselink and Short, 1993; Masselink and Hegge, 1995). As a consequence there is considerable uncertainty around how the beaches within the Rockhampton Regional Council LGA will respond to the impacts of climate change. However, in areas of the coastal zone that are already suffering from erosion, it most likely that rising sea levels will exacerbate this erosional trend

The lack of fundamental data, both observational (e.g. near-shore wave climate and storm-tide run-up levels) and instrumental (e.g. bathymetry) for the Rockhampton Regional Council LGA, along with an absence of any suitable morphodynamic models to predict shoreline change on these meso- to macro-tidal beaches (Della Pozza, pers comm.), was a significant limitation to this study. In addition, there was no suitable data from which to gain an understanding of the current beach behaviour, in order to predict or forecast beach behaviour under future climate.

In recognition of these data and modelling gaps, the Queensland Government's erosion prone area width estimates used in this study to generate future-climate coastal erosion overlays were the best available, but are to be considered as indicative only.

[10] As for the footnote relating to Figure 6.1.

7 Sea-level Rise

Long-term sea-level rise is caused by global warming which results in the thermal expansion of the oceans and the melting of water, such as ice sheets and glaciers, into the oceans (CSIRO, 2008). Sea levels have been observed to be currently rising globally at a speed of 3.2 mm per year in the last few decades (Church and White, 2011). Sea level does not rise uniformly along the Australian coast. Current science indicates that sea levels will continue to rise over the next decades, even if it were possible to stop global warming (DCC, 2009).

7.1 Method

The SLR hazard analysis considered the potential inundation from an increased still water level from sea-level rise without the impacts of waves and/or surge. This was completed using a bath-tub method[11] through the addition of sea-level rise heights to the Highest Astronomical Tide (HAT). The HAT is defined by the Australian Hydrographic Service as "…the highest level of water which can be predicted to occur under any combination of astronomical conditions" (AHS, 2012). The 2012 value of the HAT is 3.9 m at Rockhampton (MSQ, 2011). The HAT is considerably higher than the Mean High Water Springs (MHWS) in Rockhampton (2.66 m), and as an extreme tide scenario, HAT implies a conservative approach to risk assessment. HAT is also recommended as a reference tide by the QCHG for coastal recession assessment (DERM, 2012a).

The four sea-level rise scenarios considered were:

- HAT + 0.3 m (QLD 2050)
- HAT + 0.5 m (QLD 2070)
- HAT + 0.8 m (QLD 2100)
- HAT + 1.1 m (FED 2100)

The three Queensland scenarios (2050, 2070 and 2100) were identified within the QCHG. The Federal scenario (HAT +1.1 m by 2100) was identified by CSIRO from the IPCC AR4 and subsequent research (OzCoasts, 2012). The 1.1 m sea-level rise scenario considers the "high-end" hazard including the effects of warming trends on ice sheet dynamics (OzCoasts, 2012).

Utilising the high resolution (1 m) Digital Elevation Model (DEM), the bath-tub method (Eastman, 1993) was applied to identify elevation values that were equal to or less than the scenario value. In the example of the QLD 2050 scenario, land was identified where it was equal to or less than an elevation of 4.2 m (3.9 m (HAT) + 0.3 m) above the Australian Height Datum (AHD).

[11] The bath-tub method is described in the Storm Tide hazard summary and within Appendix C.

7.2 Results/Discussion

Owing to the high value of HAT and the low-lying topography of the Fitzroy River mouth, there is significant inundation from a HAT event under current-climate conditions (Figure 7.1). The Yeppoon Road, Bajool-Port Alma Road, Port Alma, the Scenic Highway South of Yeppoon and buildings in the vicinity of Keppel Sands were identified as inundated by a current-climate HAT event.

The sea level incremental rises from HAT to 5 m results in an increase in the inundation extent between a 3.8% and 6.7% compared with the lesser scenario. The greatest increase to the inundation extent from the addition of SLR scenarios was on the floodplain downstream of Rockhampton. As the inundation height increases, the inundation extent in the Fitzroy River region on the south-western area of the floodplain towards the Bruce Highway increases (Figure 7.1). Nearer to the city of Rockhampton, the Bruce Highway was shown as being potentially inundated to the south of the Capricorn Highway intersection. However, this area of inundation is isolated from the main body of water, and could be an artefact of the bath-tub method (Eastman, 1993).

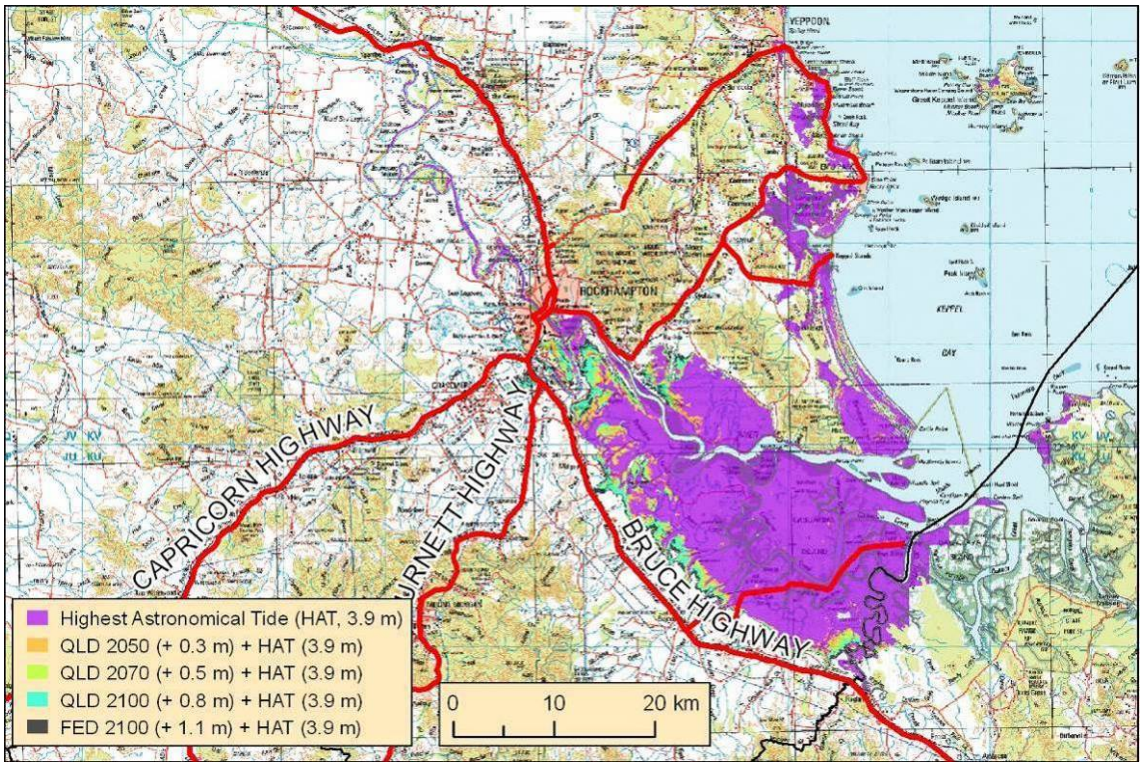

Figure 7.1. Sea-level rise inundation extent.

8 Discussion (all hazards)

This study aimed to identify and quantify the extent of natural hazards in the Rockhampton region under current and future-climate conditions. The study covered many of the most prevalent natural hazards in the region, with the notable exception of flood. This section discusses the results of this study from a 'multi-hazard' perspective.

The hazard modelling in this study identifies hazard at a regional scale, and the outputs are intended for use in regional planning. The results are not suited to fine-scale analysis due to the resolution of various input datasets and/or the models applied. It is important to understand the assumptions used, and the limitations of the methodologies and data to interpret the results of this study correctly. These issues are discussed in detail in the technical appendices for each hazard considered. The outputs from this study are to be incorporated into the Rockhampton Regional Council planning process. Where areas of interest are identified from the outputs of this study, more detailed hazard assessments should be carried out to generate local scale information.

This study did not carry out a formal analysis of the assets at risk from the hazards. Such an analysis could be undertaken using the digital data provided by this study, e.g. by overlaying the hazard layers with council information such as building and infrastructure data. Furthermore, future work could incorporate multiple GHG emissions scenarios, and a wider range of climate models, to produce a range of likely future-climate hazard. This would assist with developing a risk profile for the region and could inform cost/benefit analysis with regards to both building/infrastructure site risk assessments and also climate change adaptation measures.

The tropical cyclone wind hazard was the only hazard not to show a future-climate increase in extent or magnitude. In fact, the results suggest a drop in hazard levels may occur, although the change was not statistically significant.

The sea-level rise analysis predicted greater inundation than the storm tide plus sea-level rise assessment. This was caused by the tidal component applied in the storm tide modelling being sampled from values of the whole tidal cycle. Whereas for sea-level rise hazard, HAT, the theoretical extreme tide scenario, is not based on observation. For Rockhampton HAT is 3.9 m and this is 1.24 m higher than mean of long term observed high waters (MHWS). Within the constraints of this study, there was no opportunity to repeat the storm tide modelling with an explicit tide scenario, such as HAT.

This report is part of a Rockhampton Regional Council project that aims to evaluate the ability of its existing urban planning principles and practices to accommodate climate change and the uncertainty of climate change impacts. The results of the future-climate assessment within this study identify the regional hazard from extreme events for a single GHG emissions scenario. There is still considerable uncertainty around the exact projected emissions, and how the Earth's system will respond to these in terms of atmosphere and ocean, including sea-level rise. The future-climate scenario (A2) used in this study, was considered the most likely scenario, however, this may need to be revised with the release of the next IPCC assessment report (IPCC AR5). Current planning processes, especially for infrastructure with a longer lifetime (>50 years), will need to factor in future hazard levels, and this study provides some indication of how those might differ from the current hazard.

8.1 Study Limitations

The calculation of the future-climate TC wind hazard relied on a single simulation of future-climate TCLV data. As such, these results are sensitive to that single TRCM run and the simulated broader environment. This is due to the small sample size used in training TCRM for future climate as the behaviour of TCLVs is strongly modulated by a range of drivers, including the RCM representation of features such as the El Nino Southern Oscillation (ENSO). This may reduce or enhance the simulated TC activity during the period of sampling (e.g. 2046-2065), or influence the intensity or tracks of TCLVs. In further studies, this could be addressed by running the TCRM multiple times and from each simulation, extracting TCLVs for the periods of interest. However, multiple TCRM simulations downscaled from a single GCM were not available for this project.

Within the bushfire hazard modelling, the vegetation was considered a static layer. The bushfire hazard modelling maintained land cover at the same level (composition and spatial extent) for the whole simulation period (1971-2100) with no seasonal or inter-annual variation, e.g. the response to year-to-year rainfall variability. In addition, significant episodic events such as tropical cyclones and tropical depressions, which are known to cause significant vegetation growth and regeneration in the months following their passage through a region, do not influence either vegetative growth or the drought factor used in the FFDI calculations.

The bath-tub inundation method, used within the sea-level rise and storm-tide hazard modelling, identifies all the elevation heights less than the still-water height of the scenario. This potentially produces an overestimation of inundation in areas where topographic breaks exist, e.g. flood barriers, and the elevation heights are less than the scenario height on the protected side of the break. The bath-tub inundation method also does not consider hydrodynamic processes and interactions such as wave forces, momentum, and the impacts of topography (e.g. headland protection) and bathymetry (e.g. depth of water near-shore and the existence of reefs) resulting in a potential under estimation of inundation.

The methodology used for the coastal erosion assessment was a qualitative approximation that does not account for local processes such as wave climate and availability of sediment. Such an approximation may be less valid for future-climate conditions when there are changes in wave climate, or in the events that can cause erosion, such as storm events. Furthermore, this method was applied to the whole coastline, which is unlikely to uniformly respond to changes under future sea-level rise.

8.2 Treatment of Uncertainty

GCMs are used to predict what will happen to Earth's climate in the future. Groups like the IPCC compare the results from several different climate models as they determine what is most likely to happen on both a global and also regional scale. To evaluate the performance of a climate model, the model is run through a time period for which there are actual measurements of the Earth's climate; e.g. the past 50 - 100 years. The results from the model are compared with the actual measurements of real climate, and if they are similar then the mathematical equations in the model that are used to describe how the Earth functions regarding its climate are considered reasonably accurate. If the model results are very different from the actual measurements, then the model is considered "less useful" with regards to its predictive ability and therefore requires further work. Atmosphere-ocean GCMs represent the pinnacle of complexity in climate models and internalise as many processes as possible. However, they are still under development and uncertainties remain. They may be coupled to models of other processes, such as the carbon cycle, so as to better model feedback effects. Most

recent simulations show "plausible" agreement with the measured temperature anomalies over the past 150 years, when forced by observed changes in greenhouse gases and aerosols, and better agreement is achieved when both natural and man-made forcings are included (IPCC, 2007).

No model perfectly reproduces the system being modelled. However, imperfect models may nevertheless produce useful results. In this context, GCMs are capable of reproducing the general features of the observed global temperature over the past century. Some uncertainty about our future climate remains because there are processes and feedbacks between different parts of the Earth that are not fully understood and therefore not included in models At the present time, scientists are conducting research to learn more about how some of the less well-known processes and feedbacks function.

Confidence in GCM model estimates is higher for some climate variables (for example, temperature) than for others (for example, precipitation). Confidence in the reliability of these models for climate projections has also improved (Alexander and Arblaster, 2009), based on tests of their ability to simulate:

- the present average climate and year to year variability
- observed climate trends in the recent past
- extreme events, such as storms and heatwaves
- climates from thousands of years ago.

Climate models provide credible quantitative estimates of future climate change, particularly at continental scales and above. It is difficult to quantify the uncertainty of future-climate modelling and the compounded uncertainty when considering hazard modelling, which has its own uncertainty, within future-climate simulations. However, this does not necessarily detract from value of applying the methods used in this study as this is the current state of the science. Further information relating to climate modelling reliability is presented by the CSIRO[12]

Existing models show significant and increasing skill in representing many important mean climate features, such as the large-scale distributions of atmospheric temperature, precipitation, radiation and wind, and of oceanic temperatures, currents and sea ice cover. Patterns of climate variability that are well simulated include the advance and retreat of the major monsoon systems, the seasonal shifts of temperatures, storm tracks and rain belts. Simulations that include estimates of natural and human influences can reproduce the observed large-scale changes in surface temperature over the 20th century, including the global warming that has occurred during the past 50 years (DCCEE, 2012).

However, in the Australian region, there are deficiencies in the simulation of tropical rainfall and some important climate processes such as the El Niño-Southern Oscillation and the Madden-Julian Oscillation (DCCEE, 2012). Climate features with smaller space and time scales are also simulated with lower skill, for example, tropical cyclones and thunderstorms. With increasing computer power and better understanding of climate processes, future models will include finer resolution and more processes, which is expected to reduce some of these uncertainties. Even so, there will always be a range of uncertainty in climate projections.

A more complete discussion of climate models is provided in both the IPCC's Third and Fourth Assessment Reports.

[12] http://www.csiro.au/Outcomes/Climate/Reliability-Climate-Models.aspx

This study has been completed using currently available world best-practice methods and only used models which have been verified as producing acceptable results for the current climate of the Australian region. Climate science is a developing field and as such the results of this study need to be compared to future climate research to consider the ongoing validity of the results. Largely, the future-climate simulation in this study has been based on global, and subsequently regional, climate simulations that have, in turn, been based on the IPCC AR4 results. The IPCC Fifth Assessment Report (AR5) is due for release in September 2013. The research world, including such organisations as the CSIRO, is a constantly evolving source of information relating to hazards and future-climate effects.

8.3 Future Work

The future work described below, if undertaken, would allow a more in-depth understanding of the current hazard and reduce the uncertainty in the future-climate hazard predictions. In addition, these efforts would further translate the understanding of hazard into the determination of the risk to local population and council asset that climate change impact poses. Future work includes, but is not limited to extending the hazards considered, extending the future-climate emissions scenarios considered, updating the hazard modelling and completing an exposure or risk assessment.

Flood modelling was not within the scope of this study. Flood modelling should be included within an "all-hazards" approach; specifically as Rockhampton is prone to flood. This work should be undertaken with some urgency, and the spatial analysis of the flood regions included in the hazard GIS information available to the Rockhampton Regional Council. Currently proposed future residential subdivisions as well as infrastructure projects should be re-examined against this new flood hazard information.

The development of climate science is greatly assisted by the IPCC assessment reports; the IPCC Fifth Assessment Report (AR5) is due for release in September 2013. This new climate science information, which for AR5 focuses on improved regional understanding of climate change, should be utilised in future studies to update the current understanding of climate-related hazard within the Rockhampton region. Specifically, the range of resulting future-climate hazard under representative concentration pathways should be determined. To date, the IPCC has published a range of GHG emissions scenarios which are used to drive, or 'force', GCMs used for this and many other studies. These emissions scenarios are shown in Figure 2.2 (p14) and the six GHG emissions scenario groups range from a low emissions scenario, B1, resulting in best estimate of 1.8 ºC increase through to the high scenario, A1FI, resulting in a best estimate of 4.0 ºC increase both by 2090-2099 relative to 1980-1999 global average surface temperatures. Completing hazard modelling for a range of GHG emissions scenarios provides a range of future hazard levels for consideration. The new greenhouse gas concentration trajectories will allow researchers to examine the range of climate model variability based around the premise of a stabilised green house gas concentration.

Revised hazard levels based on IPCC AR5 data should be compared to outputs provided within this report so as to consider the ongoing veracity of the results.

Via this study hazard layers have been produced and provided in map and digital form (for current and future-climate hazards). This hazard data can be combined with other data such as the location of infrastructure (roads, rail, bridges, houses etc) or people to identify the exposure (e.g. Hazelwood and Moore, 2012; Thomas and Burbidge, 2008) of this infrastructure to the hazard. Furthermore, with an understanding of the vulnerability of the infrastructure, or population, to the hazard the risk to the assets, and therefore the impact, can be calculated. Geoscience Australia has broad experience in

completing risk assessments both within Australia (e.g. Cechet *et al.,* 2011, Middelmann-Fernandes, 2010, Jones *et al.,* 2005) and more broadly in the Asia-Pacific region (e.g. Simpson *et al.,* 2008).

This page is intentionally blank

9 Conclusion

This study aimed to identify the natural hazards in the Rockhampton region under current and future-climate conditions. The study covered many of the most prevalent natural hazards in the region, with the notable exception of flood. Hazards considered were tropical cyclone, bushfire, sea-level rise, storm tide and coastal erosion.

This study draws on available scientific work undertaken by other agencies studying current and future climate, including a national storm tide study, and GCM simulations for mid-century (2050) and end of century (2100). This study builds on those outputs by applying hazard modelling techniques to develop an overview of multiple climate hazards in the Rockhampton region under current and future climate. The future-climate scenario considered here was the IPCC AR4 A2 GHG emissions scenario, a mid- to high-level emissions scenario (IPCC, 2007). The sea-level rise scenarios ranged between 0.3 m (for 2050) and 1.1 m (for 2100).

The hazard modelling in this study identifies hazard at a regional scale, and the outputs were aimed at regional planning purposes. The results are not suited to fine-scale (high resolution) analysis due to the resolution of various input datasets and/or the models applied. The outputs from this study could be used to assess areas for potential land development. Where areas of interest are identified from the outputs of this study, more detailed hazard assessments should be carried out to generate local scale information. This study did not carry out a formal analysis of the assets at risk from the hazards. However, such an analysis could be undertaken using the digital data resulting from this study.

The Rockhampton region is already characterised by high hazard levels for all hazards considered in this study. Moreover, almost all hazards showed an increase in hazard level, although this increase was not uniform across the region, and the magnitude of increase varied between the hazards. Notably, the tropical cyclone wind hazard was the only hazard not to show a future-climate increase in hazard extent or magnitude. In fact, the results suggest a drop in hazard levels may be possible, although the change was not statistically significant.

This report is part of a Rockhampton Regional Council project that aims to evaluate the ability of its existing urban planning principles and practices to accommodate climate change and the uncertainty of climate change impacts. The results of this study provide an assessment of regional hazard from extreme events for a particular emissions scenario. Land use planning should consider how the projected future hazard level would impact on proposed development. For some hazards, effective local planning could help neutralise the risk to some extent, such as storm surge or bushfire. Hazard levels across the wider region may need to be considered when it concerns planning of access roads or power lines. The present study did not include flooding, or consider the correlation between hazards such as cyclone and storm surge or flooding, both of which are important components of a full understanding of current and future hazard.

This page is intentionally blank

10 References

Abbs, D., Aryal, S., Campbell, E., McGregor, J., Nguyen, K., Palmer, M., Rafter, A., Watterson, I. and Bates, B., 2006. Projections of Extreme Rainfall and Cyclones: Final Report to the Australian Greenhouse Office, *CSIRO Marine and Atmospheric Research*, Canberra.

Abbs, D., 2012. The impact of climate change on the climatology of tropical cyclones in the Australian region. CSIRO Climate Adaptation Flagship Working paper No. 11. Available online: http://www.csiro.au/en/Organisation-Structure/Flagships/Climate-Adaptation-Flagship/CAF-working-papers.aspx

ACE CRC (2010). Climate Futures for Tasmania climate modelling: the summary, *Antarctic Climate and Ecosystems Cooperative Research Centre*, Hobart, Tasmania. Project reports and summaries are available online: www.climatechange.tas.gov.au

Alexander, L. V., and Arblaster, J. M., 2009. Assessing trends in observed and modelled climate extremes over Australia in relation to future projections. *International Journal of Climatology*. **29**, 417–435

Amiro, B. D., 2001. Paired-tower measurements of carbon and energy fluxes following disturbance in the boreal forest. *Global Change Biology*. **7**, 253–268.

Arthur, W. C., (In prep). A statistical-parametric model of tropical cyclones for hazard assessment. *Geoscience Australia*.

Arthur, W. C., Cechet, R. P., Divi, C. B., Dunford, M., Sanabria, L.A., Thomas, C.M., Wehner, M. and Yang, T., (In prep). National Wind Risk Assessment (NWRA): a preliminary national assessment of wind risk to Australian communities under current and future climates; assessing adaptation options. *Geoscience Australia Professional Opinion,* **2011/12**.

Australian Hydrographic Service (AHS). 2012.http://www.hydro.gov.au/aboutus/glossary.htm

Beach Protection Authority 1979. Report on the Capricorn Coast. Beach Protection Authority, Brisbane.

Betts, R. A., 2006. Forcings and feedbacks by land ecosystem changes on climate change. *Journal of Physics*., **139**, 119–142.

Bonfils, C., and D. Lobell., 2007. Empirical evidence for a recent slowdown in irrigation-induced cooling. *Proceeds of the National Academy of Science*. USA, **104**, 13 582–13 587.

Bowman, D. M. J. S., and Coauthors, 2009. Fire in the Earth system. *Science*, **324**, 481–484.

Brooke, B., Ryan, D., Pietsch, T., Olley, J., Douglas, G., Packett, R., Radke, L. and Flood, P., 2008. Influence of climate fluctuations and changes in land use on Late Holocene and modern beach-ridge sedimentation on a tropical macrotidal coast: Keppel Bay, Queensland. Australia. . *Marine Geology*, **251**, 195-208.

Cai, M., and Kalnay, E., 2004. Response to the comments by Vose et al., and Trenberth. Impact of land-use change on climate. *Nature*, **427**, 214.

Carleton, A. M., Arnold, D. L., Travis, D. J, Curran, S. and Adegoke, J. O., 2008a. Synoptic circulation and land surface influences on convection in the Midwest U.S. “Corn Belt” during the summers of 1999 and 2000. Part I: Composite synoptic environments. *Journal of Climate*, **21**, 3389–3414.

Carleton, A.M., Travis, D. J., Adegoke, J. O., Arnold, D. L., and Curran, S., 2008b. Synoptic circulation and land surface influences on convection in the Midwest U.S. “Corn Belt” during the summers of 1999 and 2000. Part II: Role of vegetation boundaries. *Journal of Climate*, **21**, 3617–3641

Cechet, R., Sanabria, A., Yang, T., Arthur, W. C., Wang, C. H., and Wang, X., 2011. An Assessment of severe wind hazard and risk for Queensland’s Sunshine Coast Region. *19th International Congress on Modelling and Simulation*, Perth, Australia, 12-16 December 2011. Available online: http://www.mssanz.org.au/modsim2011/F7/cechet.pdf

Cechet, R., Hazelwood, M., Skene, D., Griffin, C., Dunford, M., Power, L., Canterford, S., Nadimpalli, K., Taylor, P., Woolf, M. and Anderson, H. 2012. Impacts of climate change on human settlements and other nationally significant infrastructure in the coastal zone. *Geoscience Australia Record,* **2012/65**.

Chambers, S. D., and Chapin, F. S. III, 2003. Fire effects on surface-atmosphere energy exchange in Alaskan black spruce ecosystems: Implications for feedbacks to regional climate. *Journal of Geophysical Research: Atmospheres*, **107**, 8145, doi:10.1029/2001JD000530.

Chambers, S. D., Beringer, J., Randerson, J. T., and Chapin, F. S. III, 2005. Fire effects on net radian and energy partitioning: Contrasting responses of tundra and boreal forest ecosystems. *Journal of Geophysical Research: Atmospheres*. **110**, D09106, doi:10.1029/2004JD005299.

Chase, T. N., Pielke, R. A., Kittel, T. G. F., Nemani, R. R., and Running, S. W., 2000. Simulated impacts of historical land cover changes on global climate in northern winter. *Climate Dynamics*., **16**, 93–105.

Christy, J. R., Norris, W. B., Redmond, K., and Gallo, K. P., 2006. Methodology and results of calculating central California surface temperature trends: Evidence of human-induced climate change? *Journal of Climate*, **19**, 548–563.

Church, J. A., and White, N. J., 2011. Sea-level rise from the late 19th to the early 21st Century. *Surveys in Geophysics*, **32**, 585-602, DOI:10.1007/s10712-011-9119-1.

Clarke H. G., Smith P. L. and Pitman A. J., 2011. Regional signatures of future fire weather over eastern Australia from global climate models, *International Journal of Wildland Fire*, **20**, 550-562

Commonwealth Scientific and Industrial Research Organisation, 2003. http://reg.bom.gov.au/info/cyclone/stormsurge.pdf

Commonwealth Scientific and Industrial Research Organisation. 2008. http://www.cmar.csiro.au/sealevel/sl_drives_longer.html

Commonwealth Scientific and Industrial Research Organisation and the Bureau of Meterology. 2012. State of the Climate 2012. Published by CSIRO and the Australian Bureau of Meteorology. Available online: http://www.csiro.au/Outcomes/Climate/Understanding/State-of-the-Climate-2012.aspx

Corney, S. P., Katzfey, J. J., McGregor, J. L., Grose, M. R., Bennett, J. C., White, C. J., Holz, G. K., Gaynor, S. M., and Bindoff, N. L., 2010. Climate Futures for Tasmania: climate modelling technical report. *Antarctic Climate and Ecosystems Cooperative Research Centre*, Hobart, Tasmania.

Cotton, W. R., and Pielke, R. A. Sr., 2007. Human Impacts on Weather and Climate. 2nd ed. Cambridge University Press, 308 pp.

CSIRO 2012. South East Queensland Climate Adaptation Research Initiative (SEQCARI): Climate Change Projections. Information available online: http://www.csiro.au/en/Organisation-Structure/Flagships/Climate-Adaptation-Flagship/seqcari/Multi-sector-study.aspx

Davey, C. A., and Pielke, R. A. Sr., 2005. Microclimate exposures of surface-based weather stations—Implications for the assessment of long-term temperature trends. *Bulletin of the American Meteorology Society*, **86**, 497–504.

DCCEE 2012. Climate Change in Australia: Australia's future climate. Available online: http://www.climatechangeinaustralia.gov.au/futureclimate.php

Della Pozza, R., 2012. Queensland Department of Environment and Heritage Protection. Personal Communication.

Department of Climate Change. 2009. Climate Change Risks to Australia's Coast. Available online: http://www.climatechange.gov.au/publications/coastline/climate-change-risks-to-australias-coasts.aspx

Department of Environment and Heritage Protection. 2012a. Erosion prone area mapping. State of Queensland report. 16pp. Available online: http://www.ehp.qld.gov.au/coastal/development/assessment/erosion_prone_areas.html

Department of Environment and Heritage Protection. Climate change in the Central Queensland Region: Queensland Government. Available online: http://www.ehp.qld.gov.au/climatechange/pdf/regionsummary-cq.pdf

Department of Environment and Resource Management 2009. ClimateQ: towards a greener Queensland, Department of Environment and Resource Management, Queensland Government. Available online: http://rti.cabinet.qld.gov.au/documents/2009/May/ClimateQ%20toward%20a%20greener%20Qld/Attachments/ClimateQ_Report_web_FINAL_20090715.pdf

Department of Environment and Resource Management. 2012a. Queensland Coastal Hazard Guideline. State of Queensland report. pp21. Available online: http://www.ehp.qld.gov.au/coastalplan/pdf/hazards-guideline.pdf

Devlin, M., Waterhouse, J., Taylor, J., and Brodie, J., 2001. Flood plumes in the Great Barrier Reef: spatial and temporal patterns in composition and distribution. *Great Barrier Reef Marine Park Authority*, Research Publication No. **68**, 113 pp.

Douglas, G., Ford, P., Palmer, M. J., and Noble, R., 2005. Identification of sediment sources in the Fitzroy River Basin and Estuary, Queensland, Australia. *CRC for Coastal Zone, Estuary and Waterway Management*, Technical Report, No. **13**.

Eastman, J. R., Kyem, P. A. K., Toledano, J., and Jin, W., 1993. GIS and decision making. Explorations in Geographic Information Systems Technology, Vol. 4. Geneva: United Nations Institute for Training and Research (UNITAR).

Ezber, Y., Sen, O. L., Kindap, T., and Karaca, M., 2007. Climatic effects of urbanization in Istanbul: A statistical and modeling analysis. *International Journal of Climatology,* **27**, 667–679.

Feddema, J. J., Oleson, K. W., Bonan, G. B., Mearns, L. O., Buja, L. E., Meehl, G. A., and Washington, W. M., 2005. The importance of land-cover change in simulating future climates. *Science*, **310**, 1674–1678.

Flood, P. G., and Walbran, P. D. 1986. A siliciclastic coastal sabkha, Capricorn Coast, Queensland, Australia. *Sedimentary Geology*, **48**, 169-181.

Foley, J. A., Costa, M. H., Delire, C., Ramankutty, N., and Snyder, P., 2003: Green surprise? How terrestrial ecosystems could affect Earth's climate. *Frontiers in Ecology and the Environment*, **1**, 38–44.

Ge, J., 2011: Satellite-Observed Surface Temperature Changes after the 2004 Taylor Complex Fire in Alaska. *Earth Interactions*., **15**, 1–14. doi: http://dx.doi.org/10.1175/2010EI361.1

Ge, J., Qi, J., Lofgren, B. M., Moore, N., Torbick, N., and Olson, J. M., 2007: Impact of land use/cover classification accuracy on regional climate simulations. *Journal of Geophysical . Research*, **112**, D05107, doi:10.1029/2006JD007404

Haigh, I. D., Wijeratne, E. M. S, MacPherson, L. R., Mason, M. S., Pattiaratchi, C. B., Crompton, R. P. & George, S., 2012, Estimating Present Day Extreme Total Water Level Exceedance Probabilities Around the Coastline of Australia, *Antarctic Climate & Ecosystems Cooperative Research Centre,* Hobart, Tasmania. Available online: http://www.acecrc.org.au/access/repository/resource/e8af5cd2-3bb8-1030-998b-40404adc5e91.

Hall, T. M., and Jewson, S., 2007: Statistical modelling of North Atlantic tropical cyclone tracks. *Tellus A*, **59**, 486-498.

Harper, B. A., Kepert, J. D., and Ginger, J. D., 2010: Guidelines for converting between various wind averaging periods in tropical cyclone conditions. *World Meteorological Organization*.WMO/TD-No.1555, Available online: http://www.wmo.int/pages/prog/www/tcp/documents/WMO_TD_1555_en.pdf

Hazelwood, M., and Moore, D., 2012. Regional climate change impact modelling for Mandurah, Western Australia. *Geoscience Australia Record*. **2012/62**. Geoscience Australia: Canberra.

Hekel, H., 1980. Quaternary and marine geology of the Capricorn Coast. *In* Hofmann, G. W. (Ed) Mount Morgan Rundle Range Yeppoon Area, 1980 Field Conference. *Geological Society of Australia,* Inc., Queensland Division. pp. 66-71.

Hennessy, K., Fitzharris, B., Bates, B. C., Harvey, N., Howden, S. M., Hughes, L., Salinger, J. & Warrick, R., 2007. Australia and New Zealand. *Climate Change 2007: Impacts, Adaptation and Vulnerability. Contribution of Working Group II to the Fourth Assessment Report of the Intergovernmental Panel on Climate Change* (eds Parry, M. L., Canziani, O. F., Palutikof, J. P., van der Linden, P. J. and Hanson, C. E.) pp. 507-40. Cambridge University Press, Cambridge.

Hill, K. A. and Lackmann, G. M., 2011. The Impact of Future Climate Change on TC Intensity and Structure: A Downscaling Approach. *Journal of Climate*, **24**, 4644 – 4661.

Holland, G. J., 1980. An Analytic Model of the Wind and Pressure Profiles in Hurricanes. *Monthly Weather Review*, **108**, 1212-1218.

Hosking, J. R. M., 1990. L-moments: Analysis and Estimation of Distributions using Linear Combinations of Order Statistics. *Journal of the Royal Statistical Society*, **52**, 105-124.

IPCC 2001: Climate Change 2001: The Scientific Basis. *Contribution of Working Group I to the Third Assessment Report of the Intergovernmental Panel on Climate Change* [Houghton, J.T., Ding, Y., Griggs, D.J., Noguer, M., van der Linden, P.J., Dai, X., Maskell, K. and C.A. Johnson (eds.)]. Cambridge University Press, Cambridge, United Kingdom and New York, NY, USA. 881 pp.

IPCC, 2007 Summary for Policymakers. Climate Change 2007: The Physical Science Basis. Contribution of Working Group I to the Fourth Assessment Report of the Intergovernmental Panel on Climate Change [Solomon, S., Qin, D., Manning, M., Chen, Z., Marquis, M., Averyt, K. B., Tignor, M., and Miller, H .L. (eds.)]. Cambridge University Press, Cambridge, United Kingdom and New York, NY, USA. p14. Available online: http://www.ipcc.ch/pdf/assessment-report/ar4/wg1/ar4-wg1-spm.pdf

IPCC, 2007a. Contributions of Working Group 1 to the IPCC Fourth Assessment Report; Chapter 10, Global emissions scenarios. *Intergovernmental Panel on Climate Change.* Available online: http://www.ipcc.ch/pdf/assessment-report/ar4/wg1/ar4-wg1-chapter10.pdf

Jones, T., Middelmann, M., and Corby, N., 2005. Natural Hazard Risk in Perth, Western Australia. *Geoscience Australia*: Canberra.

Kalnay, E., and Cai, M., 2003. Impact of urbanization and land use on climate change. *Nature*, **423**, 528–531.

Katzfey, J. J., McGregor, J. L., Nguyen, K. C. and Thatcher, M., 2009. Dynamical downscaling techniques: Impacts on regional climate change signals, *World IMACS/MODSIM Congress*, Cairns

Kelly, J.N. and Wong, W. T., 1996. Sediment transport in the Fitzroy River during flood events. In: I. Rutherford and M. Walker, (Eds) *Proceedings of the 1st National Conference of Stream Management in Australia* (pp. 19-21). Merrijig: IEA.

Kepert, J. D., 2001: The Dynamics of Boundary Layer Jets within the Tropical Cyclone Core. Part I: Linear Theory. *Journal of Atmospheric Sciences*, **58**, 2469-2484.

Kleypas, J. A. and Burrage, D. M., 1994. Satellite observations of circulation in the southern Great Barrier Reef, Australia. *International Journal of Remote Sensing*, **15**, 2051-2063.

Kuleshov, Y., Qi, L., Fawcett, R., and Jones, D., 2008. On tropical cyclone activity in the Southern Hemisphere: Trends and the ENSO connection. *Geophysical Research Letters*, **35**, 5.

Lavender, S., Walsh, K., Abbs, D., Thatcher, M., Arthur, C., and Cechet, B., 2011. Regional Tropical Cyclone Hazard for Infrastructure Adaptation to Climate Change. National Research Flagships, *CSIRO*.

Laycock, J. W. 1980. The brine-field at Port Alma. *In* Hofmann, G. W. (Ed) Mount Morgan Rundle Range Yeppoon Area, 1980 Field Conference. *Geological Society of Australia*, Inc., Queensland Division. pp. 79-84.

Lawrence, P. J., and Chase, T. N., 2007. Representing new MODIS consistent land surface in the Community Land Model (CLM 3.0). *Journal of Geophysical Research*., **112**, G01023, doi 10.1029/2006JG000168.

Leslie, L. M., Karoly, D. J., Leplastrier, M. and Buckley, B. W. 2007. Variability of Tropical Cyclones over the Southwest Pacific Ocean using High Resolution Climate Model, *Meteorology and Atmospheric Physics*. **97** (Special Issue on Tropical Cyclones), Available online: ftp://ftp.gfdl.noaa.gov/pub/rt/Leslieetal97.pdf

Lucas, C., Hennessy, K., Mills, G. and Bathols, J., 2007. Bushfire weather in southeast Australia: recent trends and projected climate change impacts. *Bushfire Cooperative Research Centre and CSIRO Marine and Atmospheric Research*. Consultancy Report prepared for The Climate Institute of Australia

Lucas, C., 2010. A historical fire weather dataset for Australia. *Australian Meteorological and Oceanographic Journal* **60**, 1–14.

Luke, R. H. and McArthur, A. G., 1978. Bushfires in Australia. A*ustralian Government Publishing Service,* Canberra. 359pp

McGregor, J., and Dix, M. R., 2008. An Updated Description of the Conformal-Cubic Atmospheric Model. *High Resolution Numerical Modelling of the Atmosphere and Ocean* K. Hamilton, and W. Ohfuchi, Eds., Springer 51-75.

McGregor, J.L., 2005. CCAM: geometric aspects and dynamical formulation, CSIRO Marine and Atmospheric Research report, Melbourne, Victoria

McNider, R. T., A. J. Song, D. Casey, P. J. Wetzel, W. Crosson, and R. M. Rabin, 1995. Toward a dynamic– thermodynamic assimilation of satellite surface temperature in numerical atmospheric models. *Monthly Weather. Review*, **122**, 2784–2803.

Mahmood, R., Foster, S. A., and Logan, D., 2006a. The GeoProfile metadata, exposure of instruments, and measurement bias in climatic record revisited. *International Journal of Climatology,* **26**, 1091–1124.

Mahmood, R., Foster, A., Keeling, T., Hubbard, K.G., Carlson, C., and Leeper, R., 2006b. Impacts of irrigation on 20th century temperatures in the Northern Great Plains. *Global Planetary. Change*, **54**, 1–18.

Mahmood, R., and Co-authors, 2010. Impacts of land use/land cover change on climate and future research priorities. *Bulletin of the American Meteorological Society*, **91**, 37–46, doi: http://dx.doi.org/10.1175/2009BAMS2769.1

Maritime Safety Queensland (MSQ). 2011. http://www.msq.qld.gov.au/~/media/msqinternet/msqfiles/home/tides/tidal%20planes/semidiurnal_planes_2012.pdf

Marshall, J. F., 1977. Marine geology of the Capricorn Channel area. Bureau of Mineral Resources, *Geology and Geophysics Bulletin*, **163**, 81 pp.

Marshall, J.F. and Davies, P.J. 1975. High-magnesium calcite ooids from the Great Barrier Reef. *Journal of Sedimentary Petrology*, **45**, 285-291.

Masselink, G., 1993. Simulating the effects of tides on beach morphodynamics. *Journal of Coastal Research,* **8**, 180-197.

Masselink, G., Short, A.D., 1993. The effect of tide range on beach morphodynamics and morphology: a conceptual beach model. *Journal of Coastal Research,* **9**, 785-800.

Masselink, G., Hegge, B., 1995. Morphodynamics of meso and macrotidal beaches: examples from central Queensland, Australia. *Marine Geology*, **129**, 1-23.

Middelmann-Fernandes, M. H., 2010. Flood damage estimation beyond stage–damage functions: an Australian example. *Journal of Flood Risk Management*, **3**: 88–96. doi: 10.1111/j.1753-318X.2009.01058.x. Available online: http://onlinelibrary.wiley.com/doi/10.1111/j.1753-318X.2009.01058.x/full

Murray, C.G., 1980. General geology of the Rockhampton area. *In* Hofmann, G. W. (Ed) Mount Morgan Rundle Range Yeppoon Area, 1980 Field Conference. *Geological Society of Australia*, Inc., Queensland Division. pp. 4-24.

Nakicenovic, N. and Swart, R., Eds. 2000. Special Report on Emissions Scenarios. *IPCC Special Reports*. Cambridge, England, Cambridge University Press, 608pp.

National Research Council, 2005. Radiative Forcing of Climate Change: Expanding the Concept and Addressing Uncertainties. *National Research Council*, 208 pp.

Nuñez, M. N., Ciapessoni, H. H., Rolla, A., Kalnay, E., and Cai, M., 2008. Impact of land use and precipitation changes on surface temperature trends in Argentina. *Journal of Geophysical Research*, **113**, D06111, doi:10.1029/2007JD008638.

Office of Economic and Statistical Research, Qld Department of Treasury and Trade. 2012. Population and Dwelling Profile Rockhampton Regional Council. Available Online: http://www.oesr.qld.gov.au/products/profiles/pop-housing-profiles-lga/pop-housing-profile-rockhampton.pdf

OzCoasts. 2012.http://www.ozcoasts.gov.au/climate/sd_visual.jsp

Peters, G. P., Andrew, R. M., et al., 2012. The challenge to keep global warming below 2 [deg]C. *Nature Climate Change* (advance online publication). Available Online: http://www.nature.com/nclimate/journal/v3/n1/full/nclimate1783.html.

Pielke, R. A., Sr., Adegoke, J., Beltra´n-Przekurat, A., Hiemstra, C. A., Lin, J., Nair, U. S., Niyogi, D. and Nobis, T. E., 2007. An overview of regional land-use and land-cover impacts on rainfall. *Tellus*, **59B**, 587–601.

Pielke, R. A., Sr., Davey, C. and Coauthors, 2007a. Unresolved issues with the assessment of multi-decadal global land surface temperature trends. *Journal of Geophysical. Research*., **112**, D24S08, doi:10.1029/2006JD008229.

Pielke, R. A., and Coauthors, 2007b: Documentation of uncertainties and biases associated with surface temperature measurement sites for climate change assessment. *Bulletin of the American Meteorological Society*, **88**, 913–928.

Pitman, A. J., Narisma, G. T., Pielke, R. and Holbrook, N. J., 2004. The impact of land cover change on the climate of southwest Western Australia. *Journal of Geophysical. Research*, **109**, D18109, doi:10.1029/2003JD004347.

Radke, L.C., Ford, P.W., Webster, I.T., Douglas, G., Oubelkheir, K., Atkinson, I., Robson, B., Verway, P., MacKensie, K., and Clemonson, L., 2005. Results of two dry-season surveys of Keppel Bay and Casuarina Creek: biogeochemical properties of the water column and underlying sediments. *Geoscience Australia Record.* **2005/18**, 121 pp.

Ramanathan, V., Crutzen, P. J., Kiehl, J. T. and Rosenfeld, D., 2001. Aerosols, climate, and the hydrological cycle. *Science*, **294**, 2119–2124.

Running, S. W., 2008. Ecosystem disturbance, carbon, and climate. *Science,* **321**, 652–653.

Ryan, D. A., Bostock, H. C., Brooke, B. P., Skene, D., 2009. Sedimentology and acoustic stratigraphy of Keppel Bay, south-east Queensland, Australia. *Geoscience Australia, Record*, **2009/14**, 107 pp.

Rümpf, J., Weindl, H., Höppe, P., Rauch, E. and Schmidt, V., 2009. Tropical cyclone hazard assessment using model-based track simulation. *Natural Hazards*, **48**, 383-398.

Searle, D. E., 1978. Continuous seismic profiling survey in Keppel Bay. Department of Mines, *Geological Survey of Queensland Record* **1978/20**, 21 pp.

Silverman, B. W., 1986. Density Estimation for Statistics and Data Analysis. Monographs on Statistics and Applied Probability, Chapman and Hall, 175.

Simpson, A., Cummins, P., Dhu, T., Griffin, G. and Schneider, J., 2008. Assessing natural disaster risk in the Asia-Pacific region. *AusGeo News*: **Issue No.90**. Available online: http://www.ga.gov.au/ausgeonews/ausgeonews200806/disaster.jsp

Smith, I. and Chandler, E., 2009. Refining rainfall projections for the Murray Darling Basin of south-east Australia - the effect of sampling model results based on performance. *Climatic Change*, DOI 10.1007/s10584-009-9757-1

Solomon, S., Qin, D., Manning, M., Marquis, M., Averyt, K., Tignor, M. M. B., Miller, H. L. Jr., and Chen, Z., Eds., 2007. Climate Change 2007: The Physical Science Basis. *Cambridge University Press*, 996 pp.

Steyaert, L. T., and Knox, R. G., 2008. Reconstructed historical land cover and biophysical parameters for studies of land–atmosphere interactions within the eastern United States. *Journal of Geophysical Research*, **113**, D02101,doi:10.1029/2006JD008277.

Strack, J. E., Pielke, R. A. Sr., Steyaert, L. T., and Knox, R. G., 2008. Sensitivity of summer near-surface temperatures and precipitation in the eastern United States to historical land cover changes since European settlement. *Water Resources Research*. **44**, W11401, doi:10.1029/2007WR00654.

Thomas, C. and Burbidge, D., 2008. A Probabilistic Tsunami Hazard Assessment of the Southwest Pacific Nations. *Geoscience Australia Record*. **2009/002**.

Trenberth, K. E., 2004. Rural land-use change and climate. *Nature,* **427**, 213.

Trenberth, K. E., Jones, P. D., Ambenje, P., Bojariu, R., Easterling, D., Klein Tank, A., Parker, D., Rahimzadeh, R., Renwick, J. A., Rusticucci, M., Soden, B. & Zhai, P., 2007. Observations: Surface

and Atmospheric Climate Change. In: Climate Change 2007: The Physical Science Basis. Contribution of Working Group I to the Fourth Assessment Report of the Intergovernmental Panel on Climate Change (eds. Solomon, S., D. Qin, M. Manning, Z. Chen, M. Marquis, K.B. Averyt, M. Tignor and H.L. Miller). *Cambridge University Press*, Cambridge.

Vickery, P. J., 2005. Simple Empirical Models for Estimating the Increase in the Central Pressure of Tropical Cyclones after Landfall along the Coastline of the United States. *Journal of Applied Meteorology*, **44**, 1807-1826.

Vose, R. S., Karl, T. R., Easterling, D. R., Williams, C. N., and Menne, M. J., 2004. Impact of land-use change on climate. *Nature*, **427**, 213–214.

Walsh, K. J. E., Nguyen, K. C. and McGregor, J. L., 2004. Finer resolution regional climate change on tropical cyclones near Australia. *Climate Dynamics*, **22:1**, Available online: http://www.springerlink.com/content/brmpmturdqvxh3vv

Webster, I.T, and Ford, P.W. 2010. Delivery, deposition and redistribution of fine sediments within macrotidal Fitzroy Estuary/Keppel Bay: Southern Great Barrier Reef, Australia. *Continental Shelf Research*, **30**, 793-805.

Welp, L. R., Randerson, J. T., and Liu, H. P., 2007. The sensitivity of carbon fluxes to spring warming and summer drought depends on plant functional type in boreal forest ecosystems. *Agricultural and Forest Meteorology*, **147**, 172–185.

Whetton, P.W., 2011. Future Australian climate scenarios. Chapter 3, Climate Change: Science and Solutions for Australia, *CSIRO Publishing*, 168pp, Available at http://www.publish.csiro.au/pid/6558.htm

Willmott, W. F., O'Flynn, M. L., and Trezise, D. L., 1984. Australia 1:100,000 Geological Special Rockhampton Region, Queensland. Geological Map, *Department of Mines*, Brisbane.

Woodhead, P. M. J., 1970. Sea surface circulation in the southern region of the Great Barrier Reef, spring 1966. *Australian Journal of Marine and Freshwater Research,* **21**, 89-102.

World Bank 2012. "Turn down the heat: Why a 4^{O}C warmer world must be avoided", A report for the World Bank by the Potsdam Institute for Climate Impacts Research and Climate Analytics. *International Bank for Reconstruction and Development / The World Bank.* 106pp Available online: http://climatechange.worldbank.org/sites/default/files/Turn_Down_the_heat_Why_a_4_degree_centrigrade_warmer_world_must_be_avoided.pdf

Yokoyama, Y., Purcell, A., Marshall, J. F. and Lambeck, K., 2006. Sea level during the early deglaciation period in the Great Barrier Reef, Australia. *Global Planetary Change,* **53**, 147-153.

Zhao, M. and Held, I. 2012. TC-Permitting GCM Simulations of Hurricane Frequency Response to Sea Surface Temperature Anomalies Projected for the Late-Twenty-First Century. *Journal of Climate*, **25**, 2995-3009.

This page is intentionally blank

Appendix A Tropical Cyclone Wind

Contents

Figures

Tables

A.1 Method

A.1.1 Current Climate

A.1.1.1 The Tropical Cyclone Risk Model

The hazard assessment uses Geoscience Australia's statistical-parametric TCRM[13] (Arthur *et al*., 2011; Arthur, in prep.). The TCRM generates a synthetic catalogue of 5000 years of events that are statistically similar to the input dataset, e.g. a set of observed historical storms. TCRM then calculates a parametric wind field around each track to determine the swath of winds from each event in the synthetic catalogue. The resulting wind fields were ranked and an extreme value distribution fitting procedure applied to determine ARI wind speeds.

A.1.1.2 Data

The Australian Bureau of Meteorology's best-track dataset, for seasons 1981–2005 (Kuleshov *et al.,* 2008) was used as the input dataset. This is a quality controlled, homogenised catalogue of Tropical Cyclone (TC) observations of date, time, position and intensity (measured as estimated central pressure). This dataset does impart a slight bias, due to the high proportion of El Niño events over the 25-year period. Tropical cyclone activity in the eastern Australian region is generally decreased under El Niño conditions, and this may result in a slight underestimation of wind hazard (this period was relatively quiescent compared to the entire 20th Century). However the actual value should be within the upper and lower 90% confidence estimates indicated in Appendix Figure A.1 and Appendix Figure A.2.

A.1.1.3 Track model

The track model is composed of four components: TC genesis, track behaviour, landfall decay and TC lysis (termination).

The genesis of TCs is modelled as a Poisson process based on the historical frequency and spatial Probability Density Function (PDF) derived from historical genesis points. The PDF is generated using kernel density estimation (Silverman, 1986), utilising a 2-dimensional Gaussian kernel with automatically selected bandwidth.

TC tracks display significant autocorrelation for speed, bearing and the rate of intensity change. Using the approach of Hall and Jewson (2007) and Rümpf *et al.* (2009), TCRM uses an autoregressive method to model the future behaviour of each synthetic TC. Initial statistics of tropical cyclone parameters (speed of forward motion, bearing, rate of intensity change) were determined from the historical record, and the lag-1 autocorrelation for each parameter calculated on a spatial grid. The behaviour of a TC at a given time step is a combination of the value at the preceding time step plus a random innovation. The magnitude of this random variation is related to the strength of the autocorrelation for that parameter.

The filling rate of TCs after making landfall is modelled in the same manner as Vickery (2005), where the central pressure increases as a function of time over land (t) and the pressure deficit at the time of first landfall. The landfall decay component of the model has not been calibrated for eastern Australian

[13] The TCRM code is available online at http://code.google.com/p/tcrm

conditions and so the estimated wind speeds well inland (more than 100 km inland) may be inaccurate.

Lysis of a synthetic tropical cyclone occurs when the central pressure deficit falls below an arbitrary threshold, either due to the decline in intensity following landfall, or through the autoregressive process described above. Tropical cyclones were also terminated on exiting the predefined area of interest.

A.1.1.4 Wind field model

To estimate the swath of destructive winds around each of the synthetic cyclones, the TCRM applies a parametric wind field comprised of a radial wind profile and a simplified boundary layer model to incorporate the effects of surface friction and forward motion of the TC. The wind field around each tropical cyclone is calculated at high spatial resolution (0.02°) to ensure the peak wind speeds near the TC eye are accurately captured. TCRM first uses a radial profile to estimate the gradient level wind associated with the circulation. For this study, the Holland (1980) radial profile was applied, with a fixed peakedness (β) parameter.

To relate the wind speed at the gradient level to the near-surface wind speed, the TCRM applies the linear boundary layer model of Kepert (2001), which utilises a bulk formulation for the boundary layer with the drag coefficient set to a constant value of 0.002 and the turbulent diffusivity for momentum set to 50 $m^2\ s^{-1}$. A gust factor of 1.38 is applied to estimate the likely peak wind gust, corresponding to the recommended values for off-water, over-land conditions from Harper *et al.* (2010). The resulting wind fields represent a 10 m above-ground, 3-second gust wind speed[14] over open, flat terrain, and this is carried across the entire model domain, including over-water areas.

The boundary layer model assumes uniform land surface, but these effects were incorporated through site-exposure multipliers that are evaluated separately. The site-exposure multipliers combine effects of topography, land cover (e.g. forests, croplands, urban areas and water bodies) and the shielding effects provided by closely-spaced buildings.

A.1.1.5 Extreme value distribution

Once wind swaths for a simulated storm season have been generated, the annual maximum wind speeds for each grid point is stored. TCRM uses the method of L-moments (Hosking, 1990) to fit parameters to the Generalized Extreme Value (GEV) distribution of extreme wind speeds. ARI wind speeds were in turn estimated from the GEV parameters using Equation 1:

$$w(t;\mu,\sigma,\xi) = \mu - \frac{\sigma}{\xi}\left[1 - \left(-\ln\left(1-\frac{n}{t}\right)\right)^{-\xi}\right] \quad \text{Equation 1}$$

where w is the wind speed with an ARI of t years. μ, σ and ξ are the location, scale and shape parameters of the fitted GEV distribution respectively, and n is the length of record in years over which the maximum values are taken. This parameter fitting is performed at each point across the region of interest, leading to a spatial representation of ARI wind speeds.

[14] This corresponds to the average wind speed recorded over a 3-second period.

Confidence intervals of the estimated ARI wind speeds were calculated using a sub-sampling process for each point over the domain. A randomly sub-sampled set of the simulated wind speed values at each grid point were passed to the GEV fitting routine, and the resulting ARI wind speed estimates were ranked and percentile values returned (for example the 5th and 95th percentile ARI wind speed values) for each ARI.

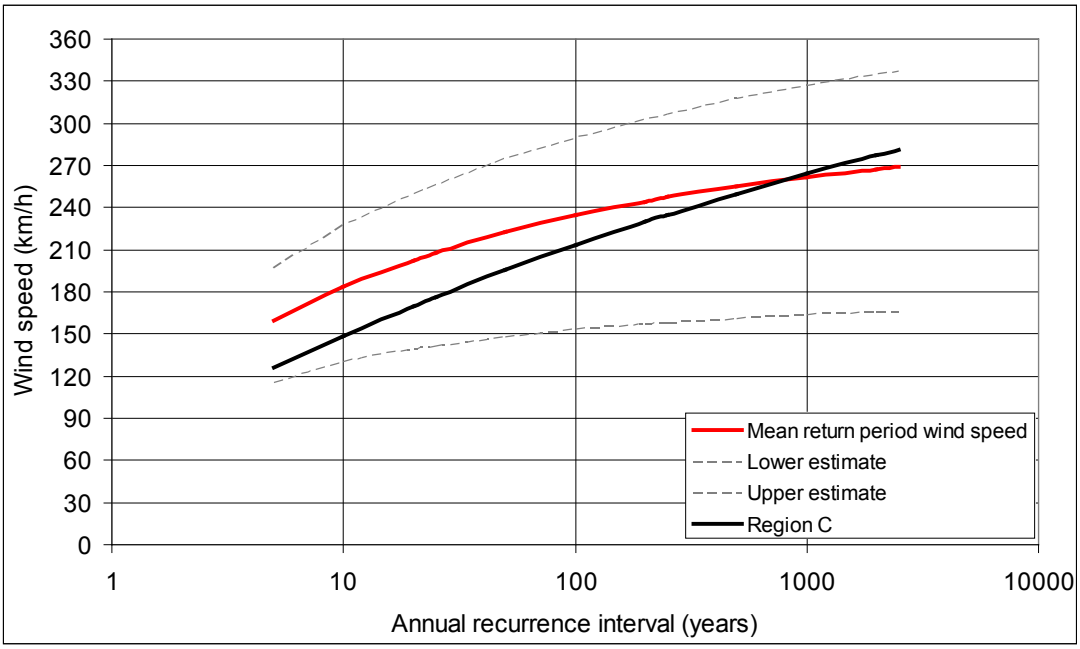

Appendix Figure A.1. ARI regional 3-second gust wind speeds for Rockhampton Airport (23.375°S, 150.47°E). The corresponding ARI wind speeds from wind standard AS/NZS 1170.2 (2011) are shown for reference ('Region C').

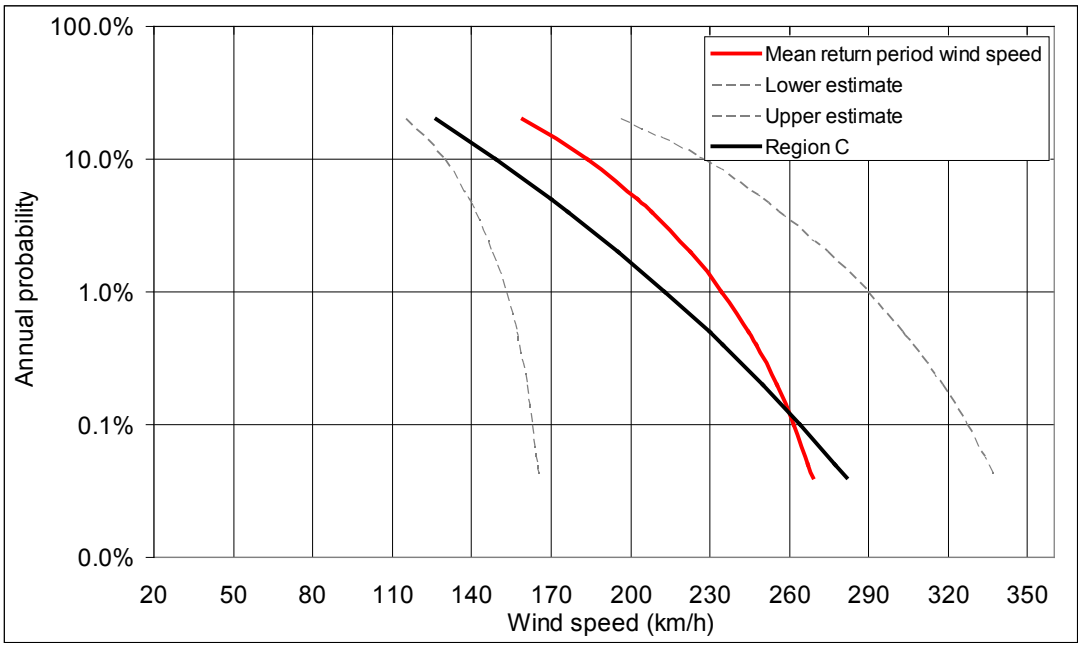

Appendix Figure A.2. Annual exceedance probability 3-second gust wind speeds for Rockhampton Airport (23.375°S,150.47°E). As for Appendix Figure A.1, the corresponding exceedance probabilities for Region C in wind standard AS/NZS 1170.2 (2011) are shown.

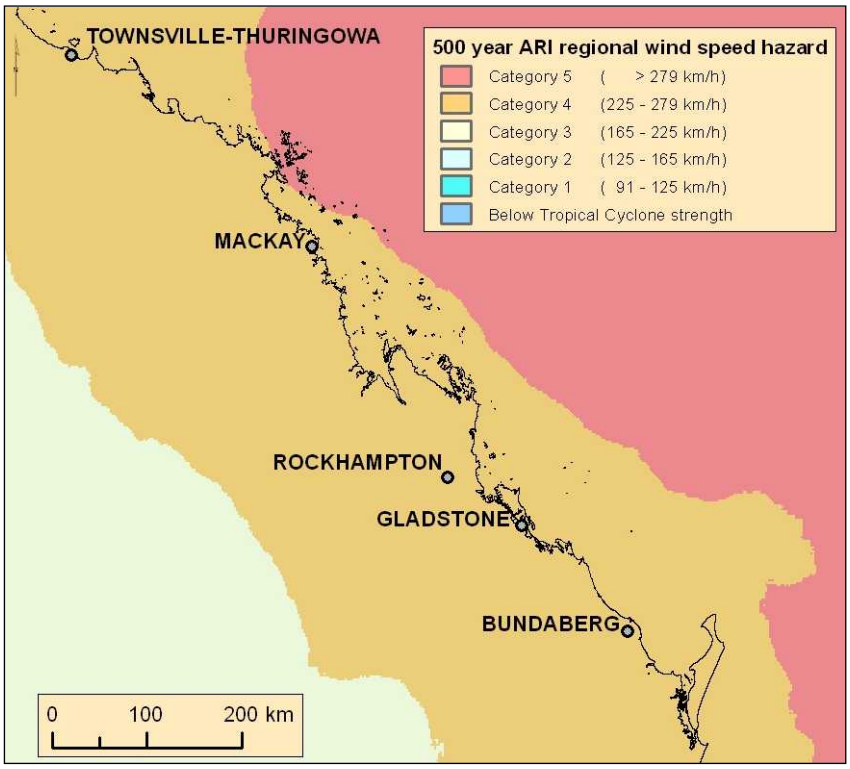

Appendix Figure A.3. 500-year ARI (0.2% annual exceedance probability) regional 3-second gust wind speed(symbolised in TC wind speed categories) map for the central Queensland region. Local effects (e.g. topography, land cover) have not yet been incorporated.

A.1.1.6 Wind multipliers

The model incorporates the effects of the land surface on the wind through so-called site-exposure multipliers. The site-exposure multipliers combine effects of topography, land cover (e.g. forests, croplands, urban areas and water bodies) and the shielding effects provided by closely-spaced buildings. The wind multipliers are location specific values that convert the regional return wind speed[15] (Appendix Figure A.3) into local wind speed estimates at building height. The combined wind multiplier raster is developed from the combination of four multiplier rasters:

- the wind direction multiplier (cyclonic winds all directions = 0.95)
- the terrain/height multiplier (effect of surface roughness on wind speed)
- the shielding multiplier (upwind shielding from buildings)
- the topographic multiplier (hill slope).

When the combined site-exposure multiplier raster is applied to the regional (ARI) wind speed raster, nine rasters were produced: eight cardinal directions with the ninth a maximum wind speed based on the other eight. The maximum wind speed raster for each ARI considered has been provided in the results and the wind hazard map sheets.

[15] Three second gust estimated at 10 m above ground level.

A.1.2 Future Climate

There were four steps in modelling future-climate TC hazard:

- Extract TC-Like Vortices (TCLVs[16]) from high-resolution regional climate simulations for 1981-2000, 2046-2065 and 2081-2100
- Use each TCLV dataset as input to the TCRM to evaluate TC wind hazard for that time period
- Compare resulting TC wind hazard estimates, identifying areas where the change is significant[17]
- Apply relative change in hazard from TCLVs to the observed current-climate (historical) hazard.

Five thousand years of TC activity were simulated based on the input TCLV dataset for each twenty year time period (1981-2000, 2046-2065 and 2081-2100), and then the associated ARI wind fields calculated for each of those simulated years. For each time period, the TC severe wind hazard (quantified in ARI wind speeds) and the 90th percentile range of the hazard was evaluated.

The 90th percentile range was calculated by fitting an extreme value distribution to a subset of the simulated wind fields many times and calculating the 95th and 5th percentiles of the resulting wind speed values at each ARI. This gives an indication of the possible range of hazard levels arising from a short input dataset. For example, between any two 20-year periods there will be differences in the frequency of TC events. The resulting hazard levels from the two 20-year periods will be different. This process to calculate the 90th percentile range aims to capture the potential variability.

A.1.2.1 Data sources

Historical TC tracks were from the Bureau of Meteorology's southern hemisphere best track dataset for the southern hemisphere, from 1981 to 2010[18]. This represents a quality controlled, homogenised set of TC observations, independently constructed from all available TC warning centres across the world.

Future-climate TCLV data was obtained as part of the Regional Tropical Cyclone Hazard for Infrastructure Adaptation to Climate Change CSIRO Climate Adaptation Flagship (Lavender *et al.*, 2011). These data represent TCLVs extracted from a 15 km horizontal resolution regional climate model (CCAM – McGregor and Dix, 2008) for a number of time periods, where the GCM used for external forcing is the CSIRO Mark 3.5 model forced with the SRES A2 GHG emission scenario (Nakicenovic and Swart, 2000).

[16] Tropical Cyclone-Like Vortex – a feature in either General Circulation Models (GCMs) or Regional Climate Models (RCMs) that has characteristics similar to observed tropical cyclones (e.g. a persistent closed circulation, forming in tropical areas). These can be identified in model output using objective detection and tracking algorithms.

[17] Change is considered statistically significant when the mean future climate TC wind hazard estimate lies outside the 90th percentile range of the current climate estimate.

[18] available online at: http://www.bom.gov.au/cyclone/history/tracks/index.shtml

A.2 Results

A.2.1 Current Climate

The local wind speed results have been provided for the 50, 100, 250 and 1000 year ARI wind hazard. The 50 and 100 year ARI wind hazard is shown, Appendix Figure A.4 and Appendix Figure A.5 respectively, with the 250 and 1000 year ARI wind hazard provided in the hazard maps.

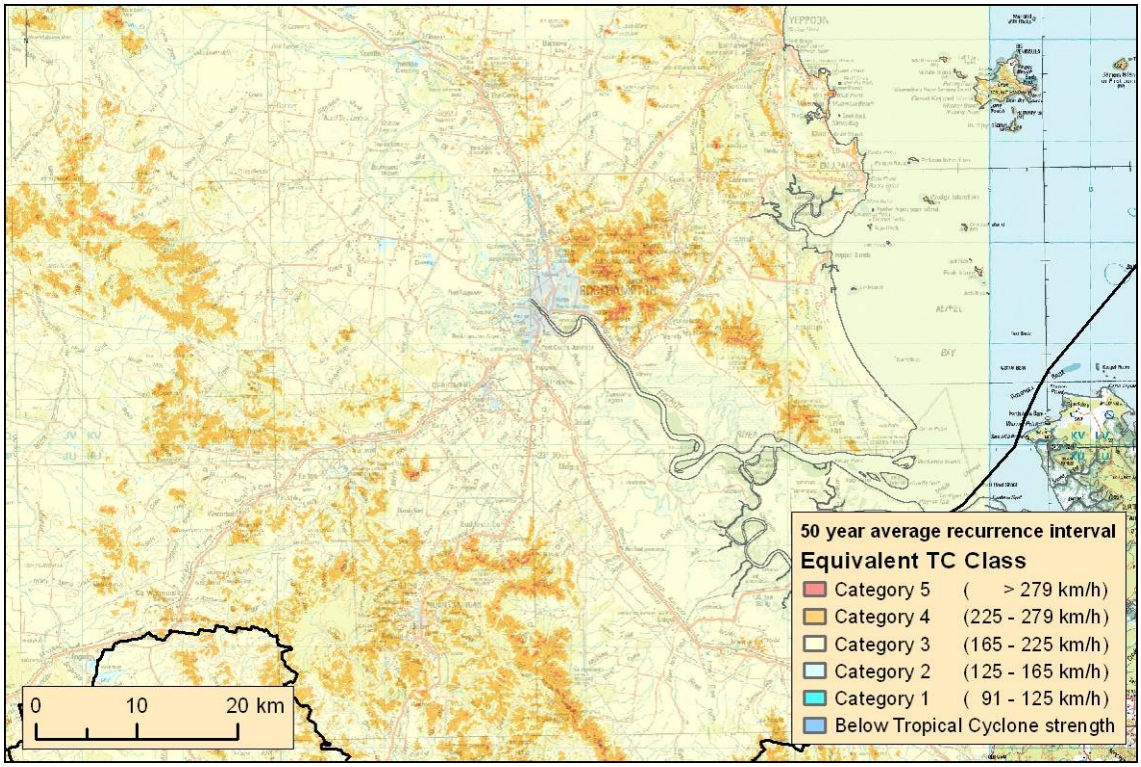

Appendix Figure A.4. 50 year ARI TC wind hazard.

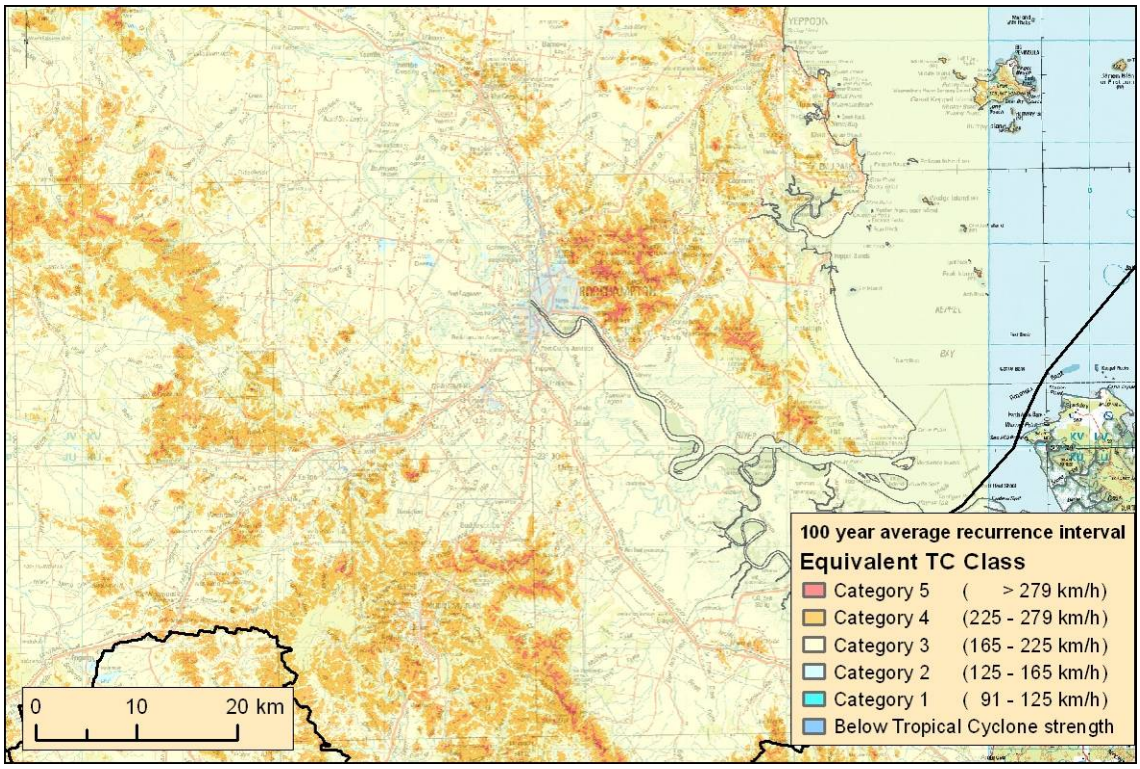

Appendix Figure A.5. 100 year ARI TC wind hazard.

A.2.2 Future Climate

A.2.2.1 Regional wind speed

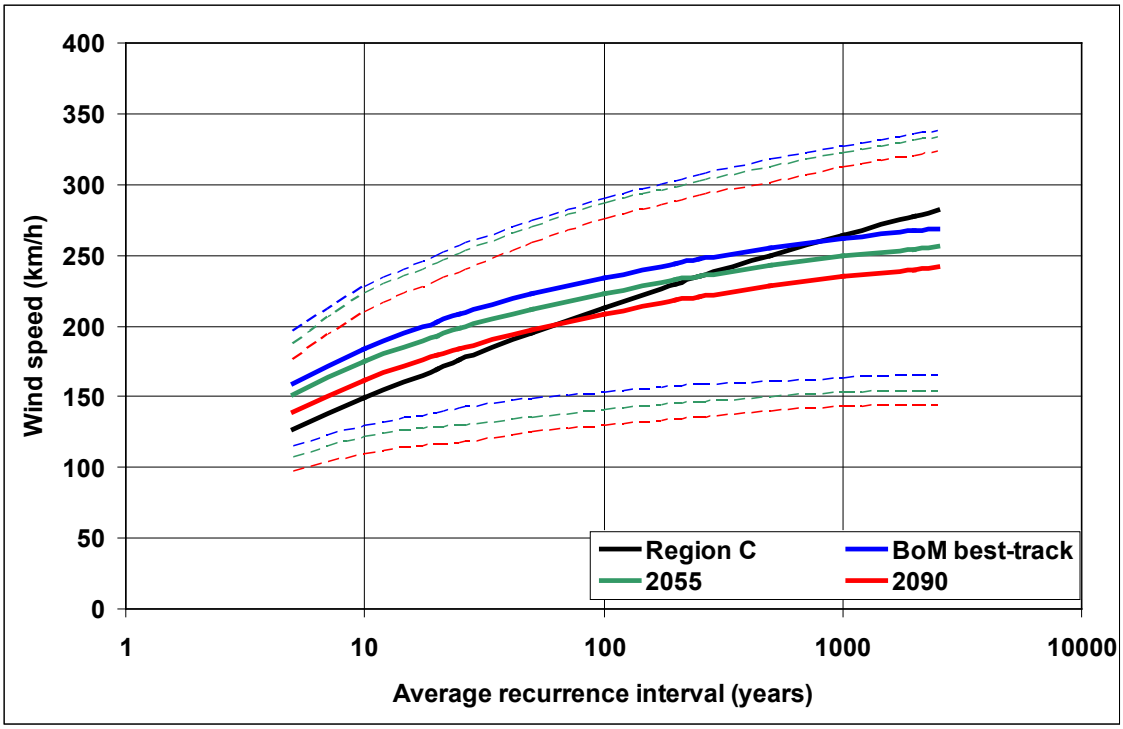

Appendix Figure A.6. ARI wind speeds for Rockhampton. "BoM best-track" refers to wind speeds estimated from TCRM simulation using BoM best-track data as input. "Region C" refers to AS/NSZ 1170.2:2011 Wind Loading Region design wind speeds. Thin dashed lines indicate the 90th percentile range for each period.

The simulations indicate a decline in TC wind hazard into the future, though none of the changes were considered statistically significant[19]. All estimates are similar to the existing design wind speeds for the region, but are much greater than ARI wind speeds estimated from the observational record at Rockhampton Airport (not shown). By 2090, there is approximately a 10-12% reduction in the ARI wind speeds for all recurrence intervals. Critically though, this does *not* imply the region will not experience intense TCs (Category 4 and 5) under future-climate conditions.

A.2.2.2 Local wind speed

As per the current-climate wind hazard results the 50 and 100 year ARI wind hazard is provided for 2055 and 2090 with all ARI wind hazard being provided in the hazard maps.

[19] Change is considered statistically significant when the mean future climate TC wind hazard estimate lies outside the 90th percentile range of the current climate estimate.

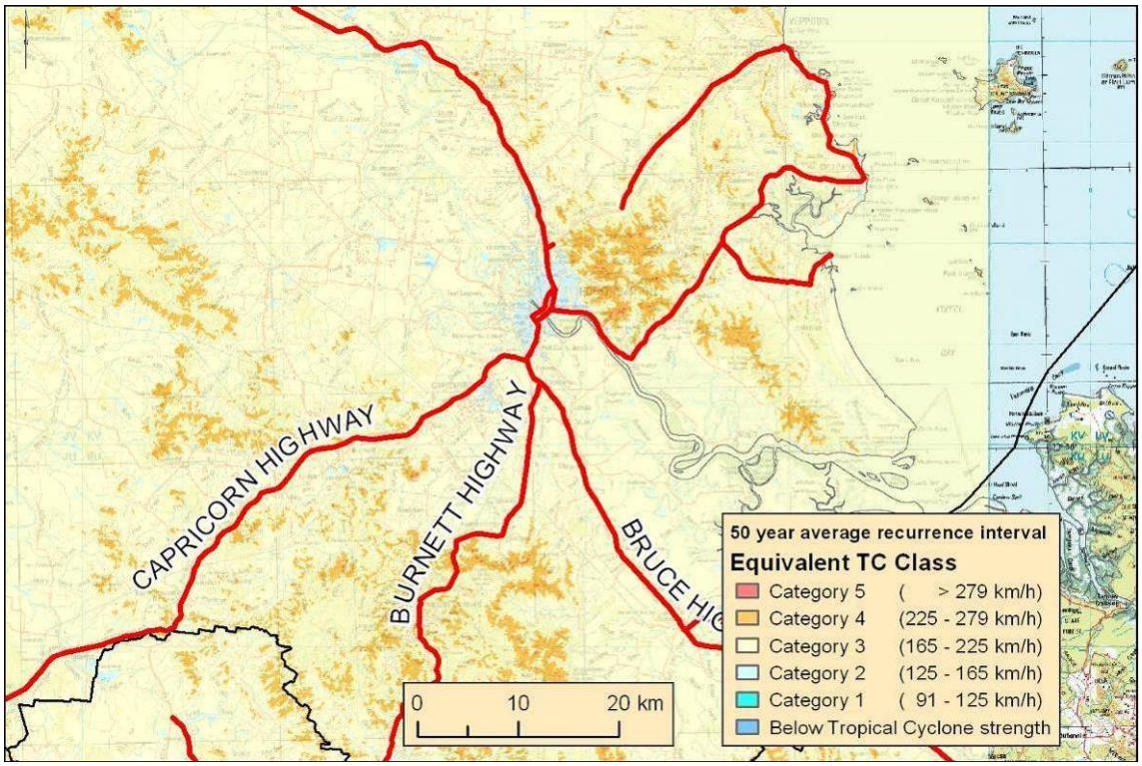

Appendix Figure A.7. 2055, 50 year ARI TC wind hazard.

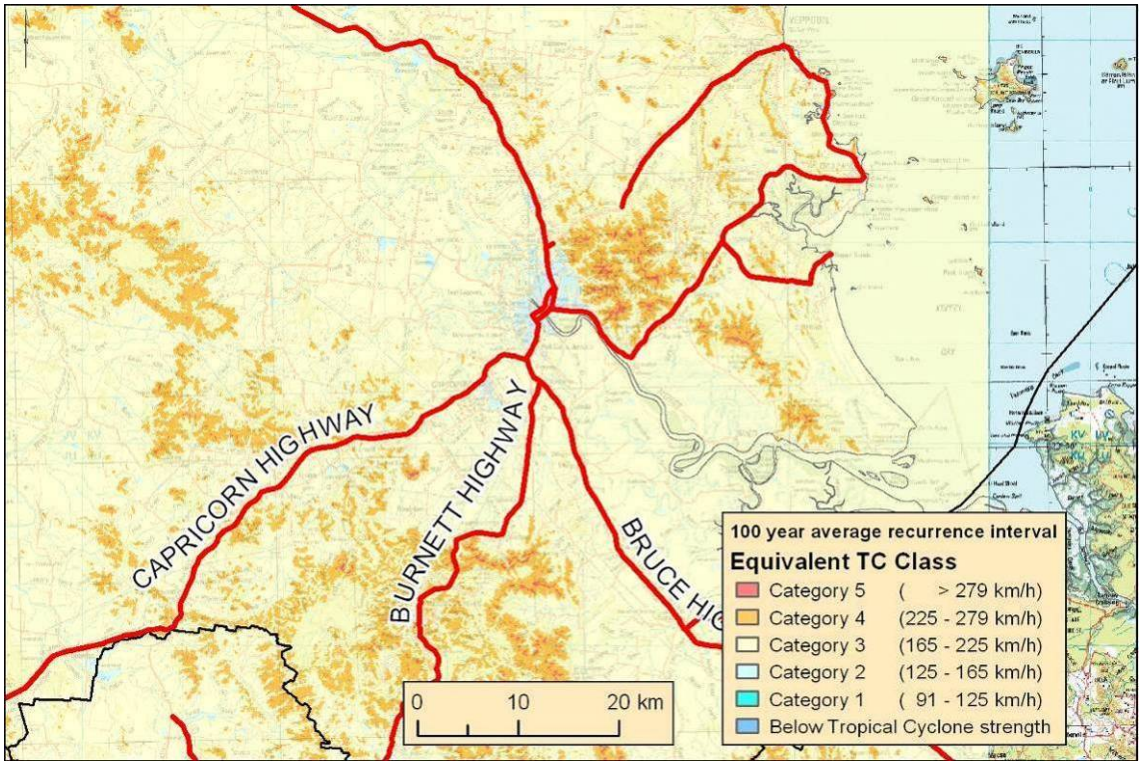

Appendix Figure A.8. 2055, 100 year ARI TC wind hazard.

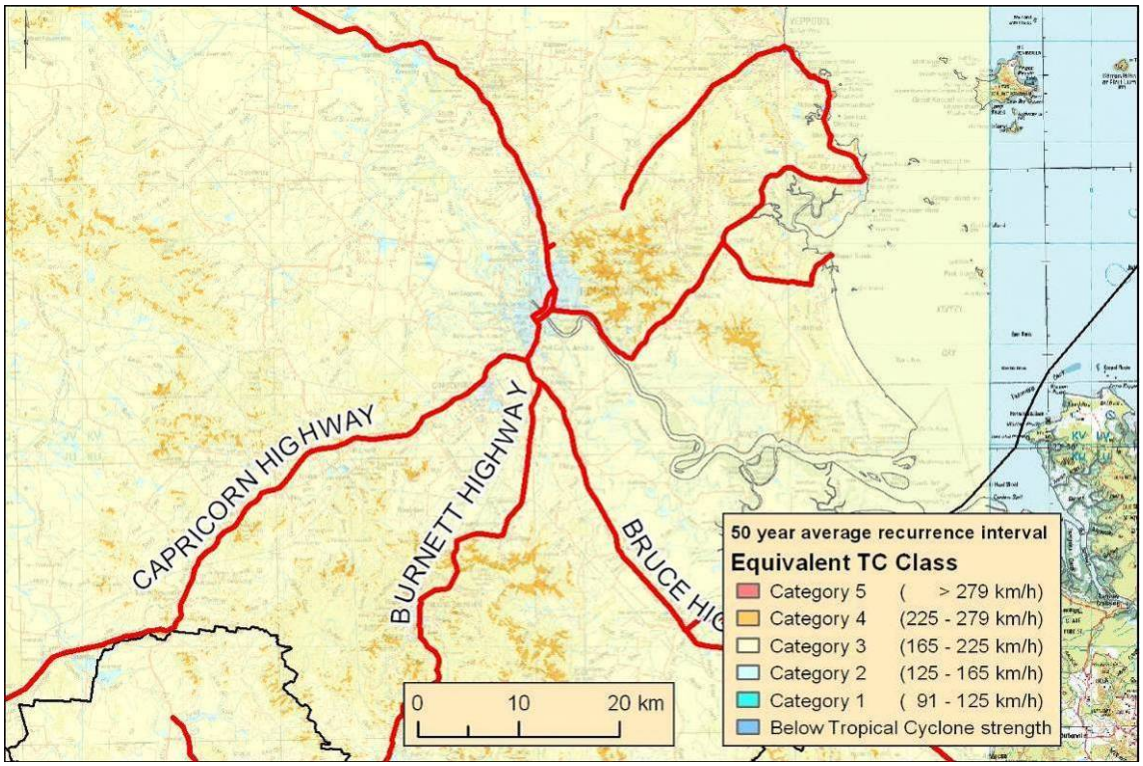

Appendix Figure A.9. 2090 50 year ARI TC wind hazard.

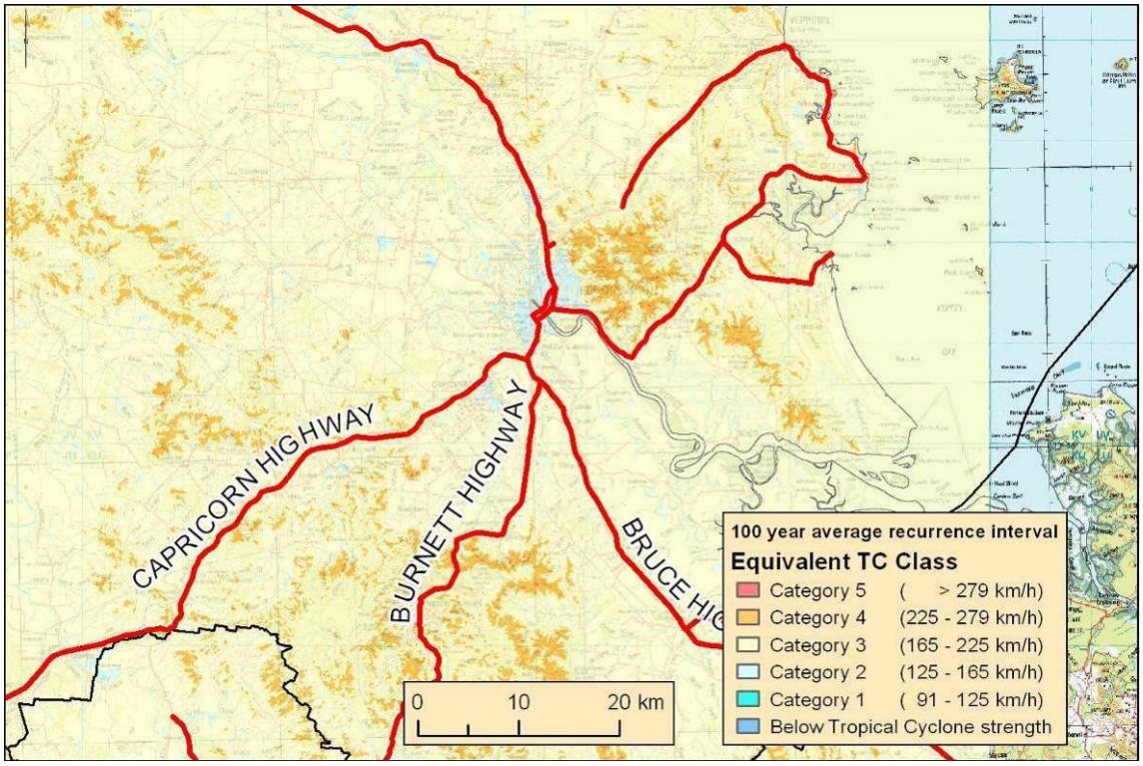

Appendix Figure A.10. 2090, 100 year ARI TC wind hazard.

A.3 Discussion

A.3.1 Current Climate

As an example, the current-climate 500 year ARI wind hazard demonstrates wind speeds of TC category 3 and above within the study area (Appendix Figure A.11). The TC category 3, 4 and 5 wind speeds are the threshold at which the Bureau of Meteorology (BoM) indicates significant structural damage occurs (Appendix Table A.1).

Appendix Table A.1. Bureau of Meteorology TC category and damage description.

Category	Description
Category 3	*"Some roof and structural damage. Some caravans destroyed. Power failures likely."*
Category 4	*"Significant roofing loss and structural damage. Many caravans destroyed and blown away. Dangerous airborne debris. Widespread power failures."*
Category 5	"*Extremely dangerous with widespread destruction."*

Appendix Figure A.11 shows areas of wind hazard by TC category and the higher hazard values occurring in the higher elevations and/or higher gradients within the study region and conversely the lower wind hazard occurring on the lower elevations and/or flatter terrain.

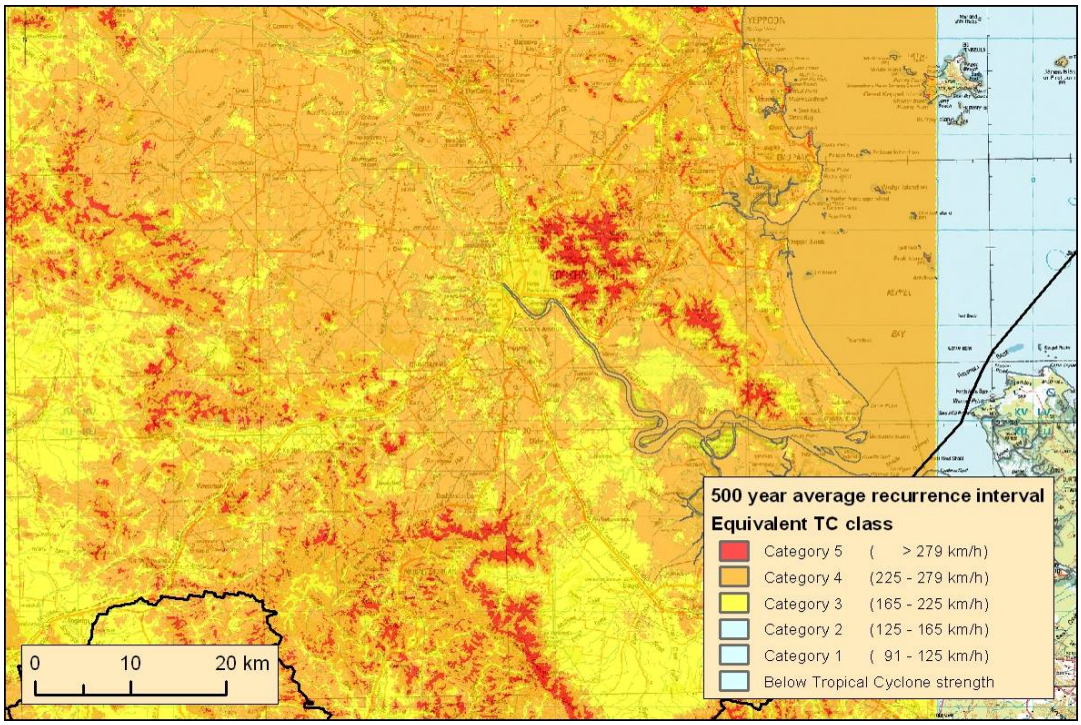

Appendix Figure A.11. 500 year ARI wind hazard combining TC category 4 (split) and 5 wind hazard and combining the remaining wind hazard categories.

The larger homogenous, less exposed areas (TC category 3 wind speeds) in proximity to Rockhampton include:

- an arc east to north-west of Rockhampton
- south of Rockhampton between the Bruce and Burnett highways
- eastern side of the Capricorn Highway (Gracemere to Bouldercombe)
- south of Bajool and Marmor.

Notable areas of peak hazard include:

- Flat Top Range
- Mount Morgan
- Mount Archer National Park.

These peak areas show higher TC wind hazard in the 50 year ARI hazard which increases throughout the range through to the 1000 year ARI hazard. For the area of interest generally, as expected, the wind speeds increases as the events become rarer although the rate of increase varies across the landscape. The comparison between current climate local ARI wind hazard is shown in Appendix Figure A.12, Appendix Figure A.13 and Appendix Figure A.14.

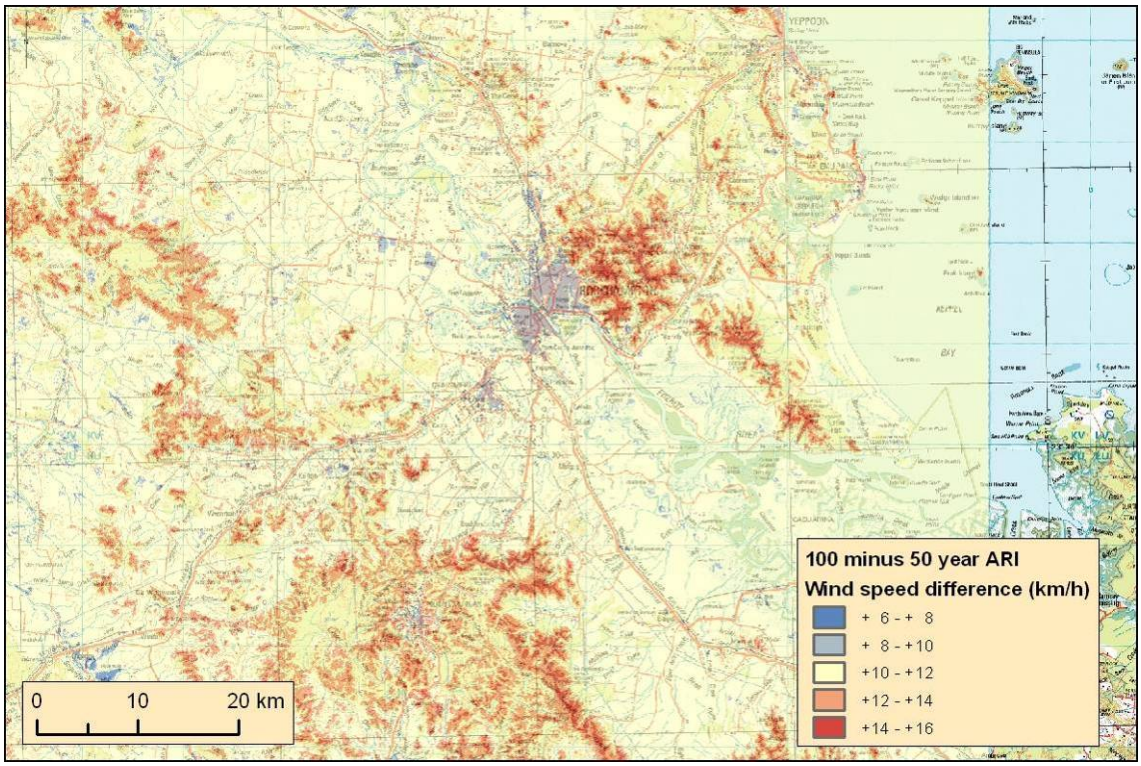

Appendix Figure A.12. Difference between 100 year ARI wind speed and 50 year ARI wind speed.

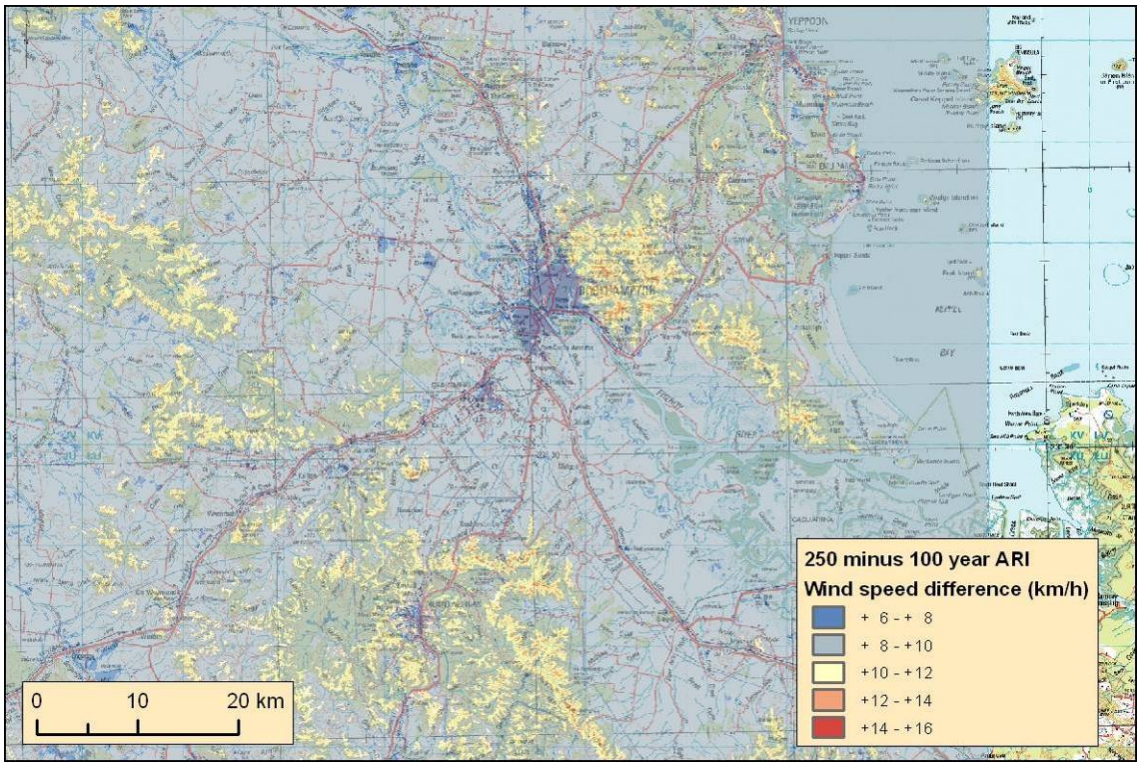

Appendix Figure A.13. Difference between 250 year ARI wind and 100 year ARI wind speed.

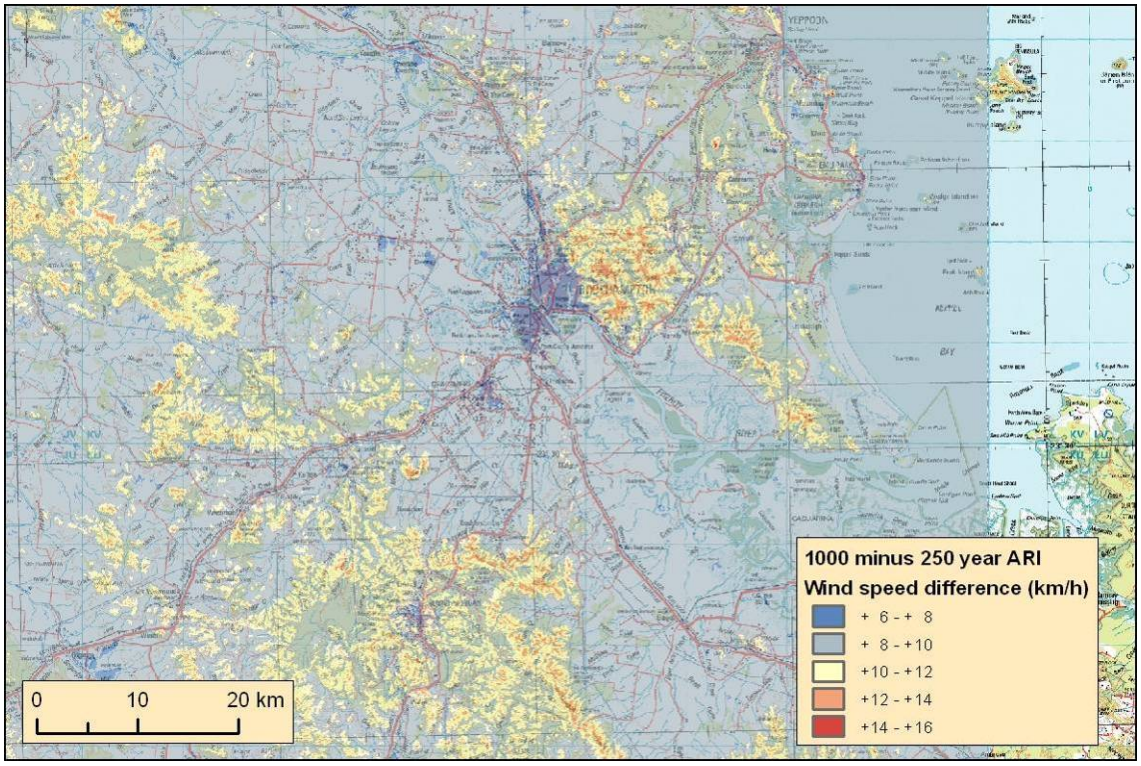

Appendix Figure A.14. Difference between 1000 year ARI wind and 250 year ARI wind speed.

A.3.2 Future Climate

The results in this study are in line with current understanding of the projected changes in cyclone hazard across Australia associated with climate change. Recent studies indicate that in the future cyclone frequency may decline overall, but a larger proportion of those cyclones will be intense (Category 4 and 5). This shift could result in average hazard levels very similar to those experienced currently. Cyclone tracks may also occur further southward, especially on the east coast of Australia (Abbs, 2012). While such a shift in tracks might mean an increase in cyclone risk for some areas of Queensland, this may not be an issue for Rockhampton, which is already in an active cyclone region.

Predicted ARI wind hazard for 2050 can be compared to the current-climate ARI hazard. Although the regional ARI wind hazard has declined (Appendix Figure A.6), spatially there is variation in the local wind hazard. A comparison was completed between current climate and 2050 wind hazard (Appendix Figure A.15 to Appendix Figure A.18) and subsequently for the 2050 and 2090 wind hazard (Appendix Figure A.19 to Appendix Figure A.22). The predicted change in local wind speeds is caused by the topography and shielding. Throughout the comparisons there is a consistent pattern of the greatest reduction in wind hazard occurring at the higher elevations.

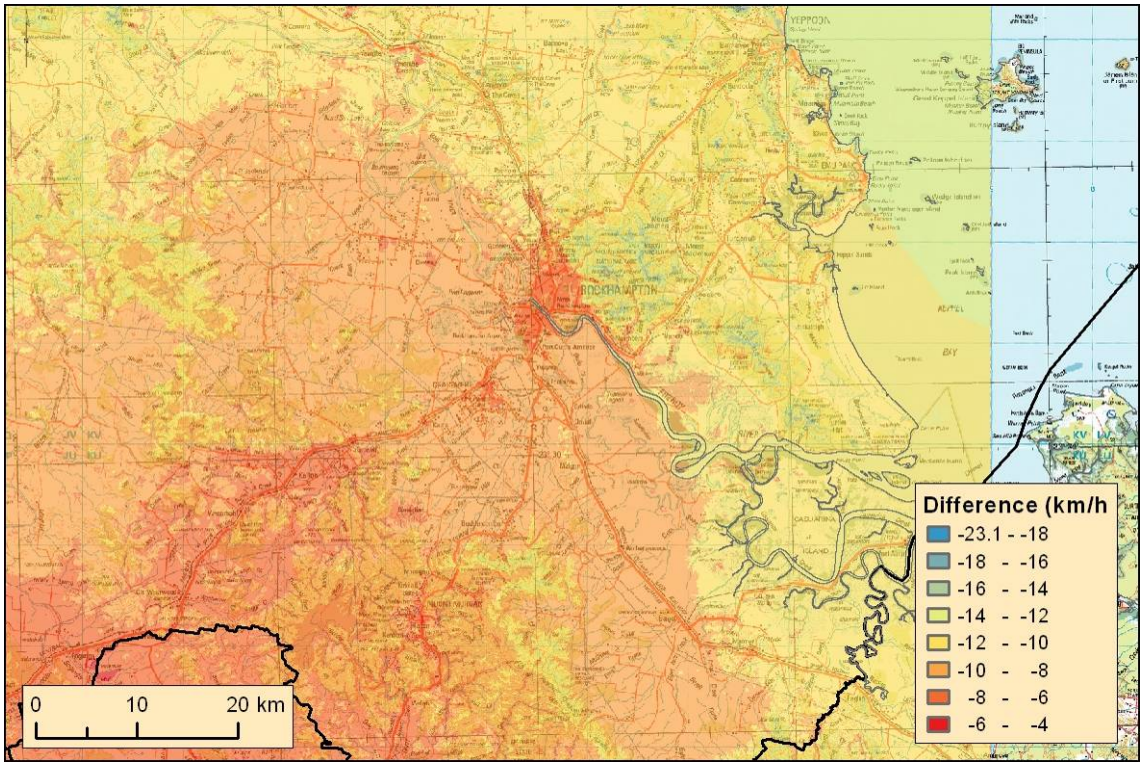

Appendix Figure A.15. 2050 – 50 year ARI minus current-climate 50 year ARI.

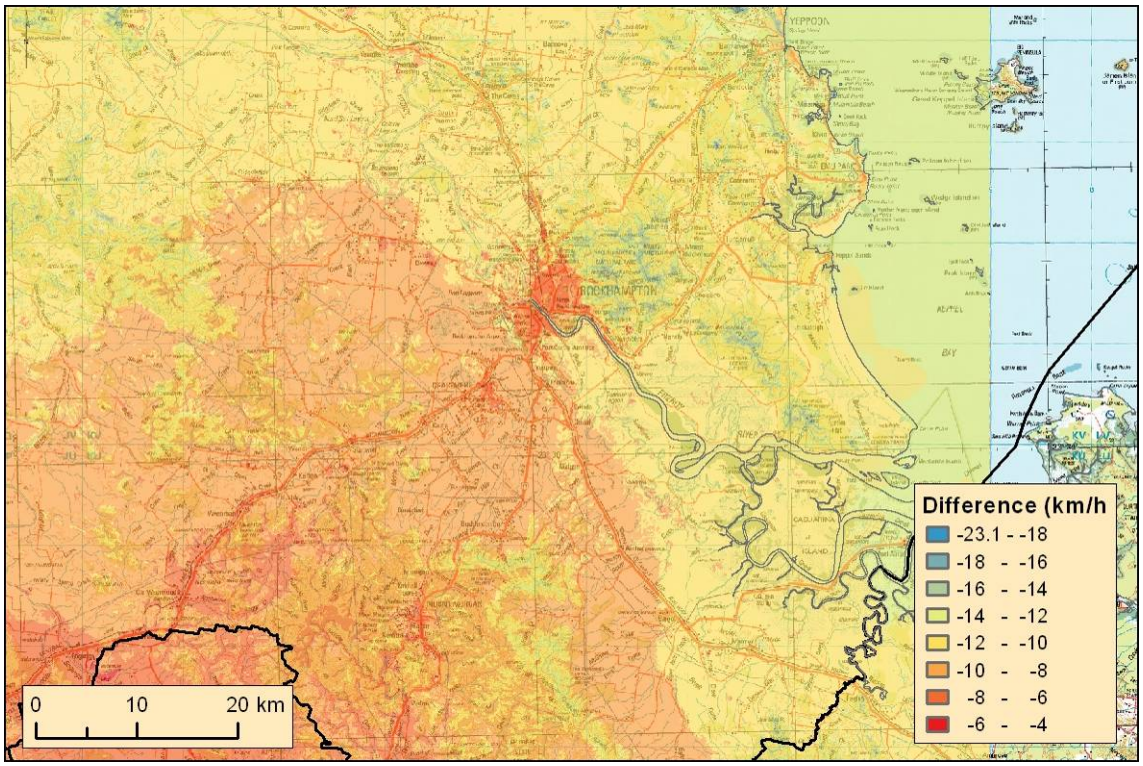

Appendix Figure A.16. 2050 – 100 year ARI minus current-climate 100 year ARI.

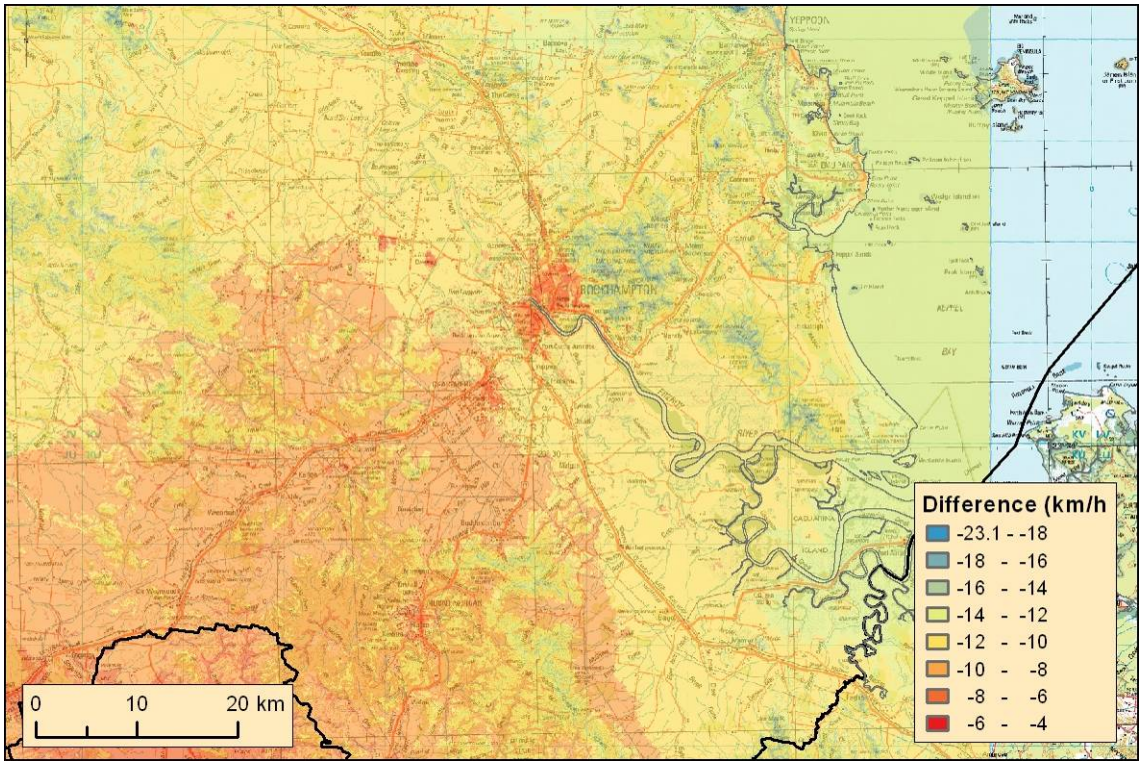

Appendix Figure A.17. 2050 – 250 year ARI minus current-climate 250 year ARI.

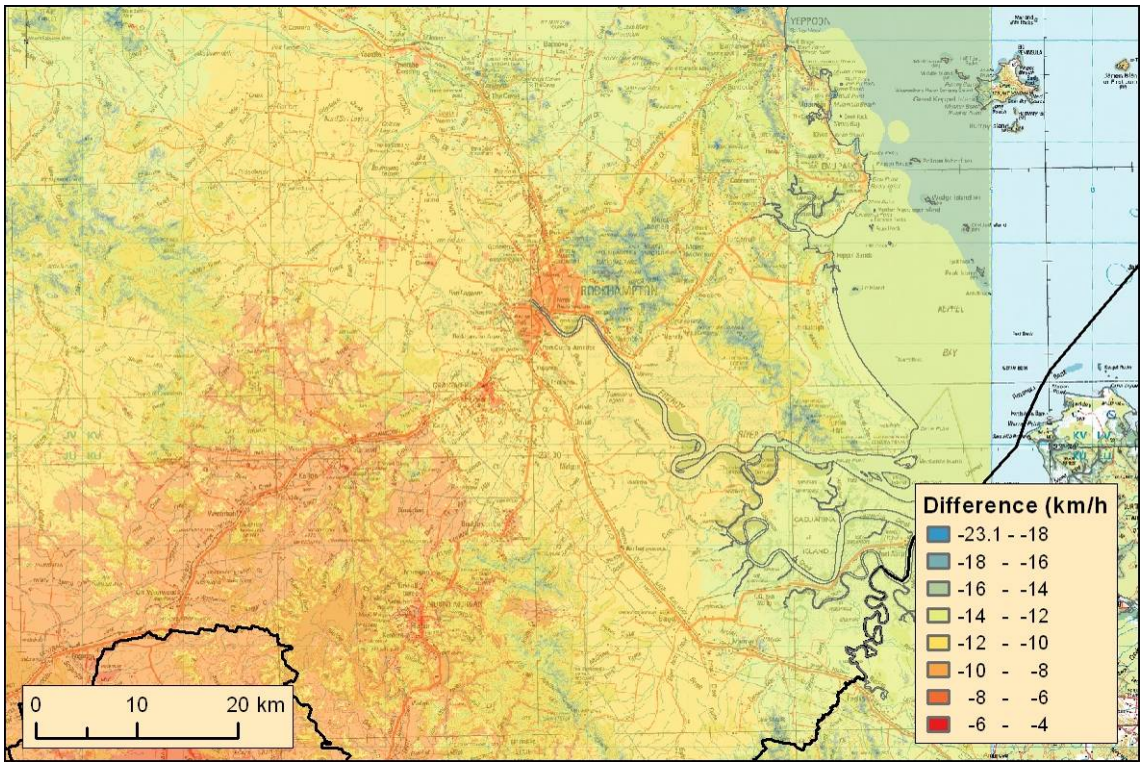

Appendix Figure A.18. 2050 – 1000 year ARI minus current-climate 1000 year ARI.

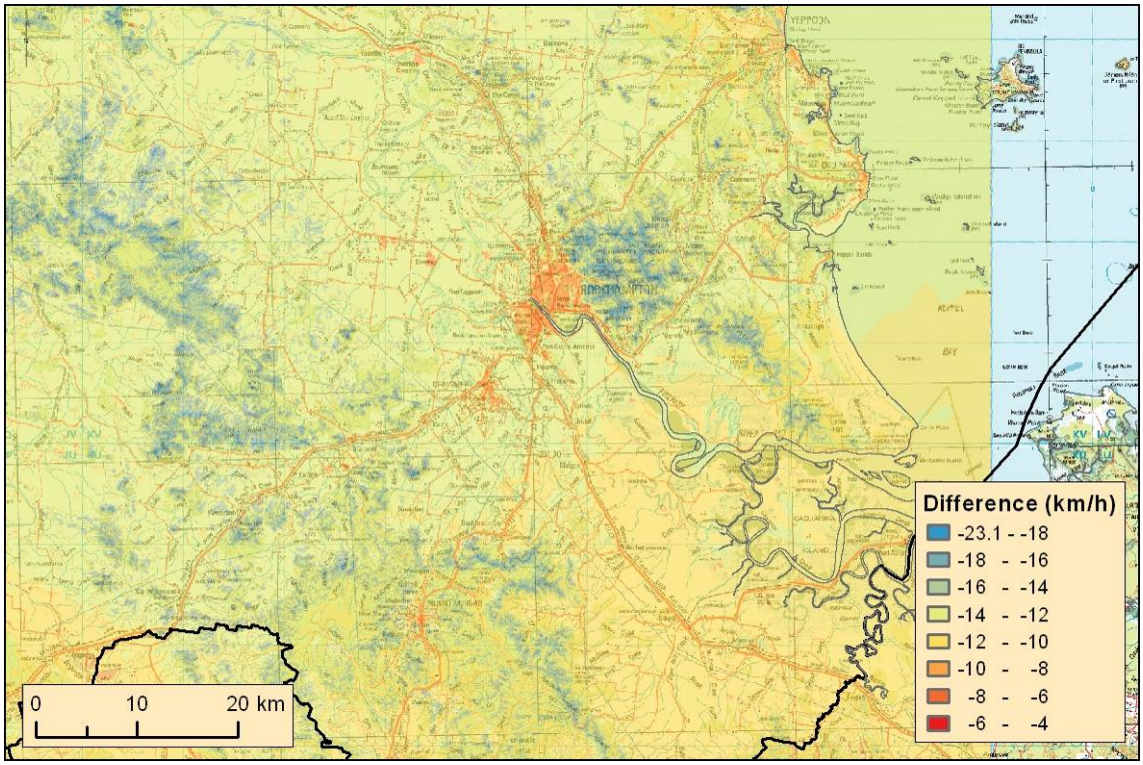

Appendix Figure A.19. 2090 – 50 year ARI minus 2050 - 50 year ARI.

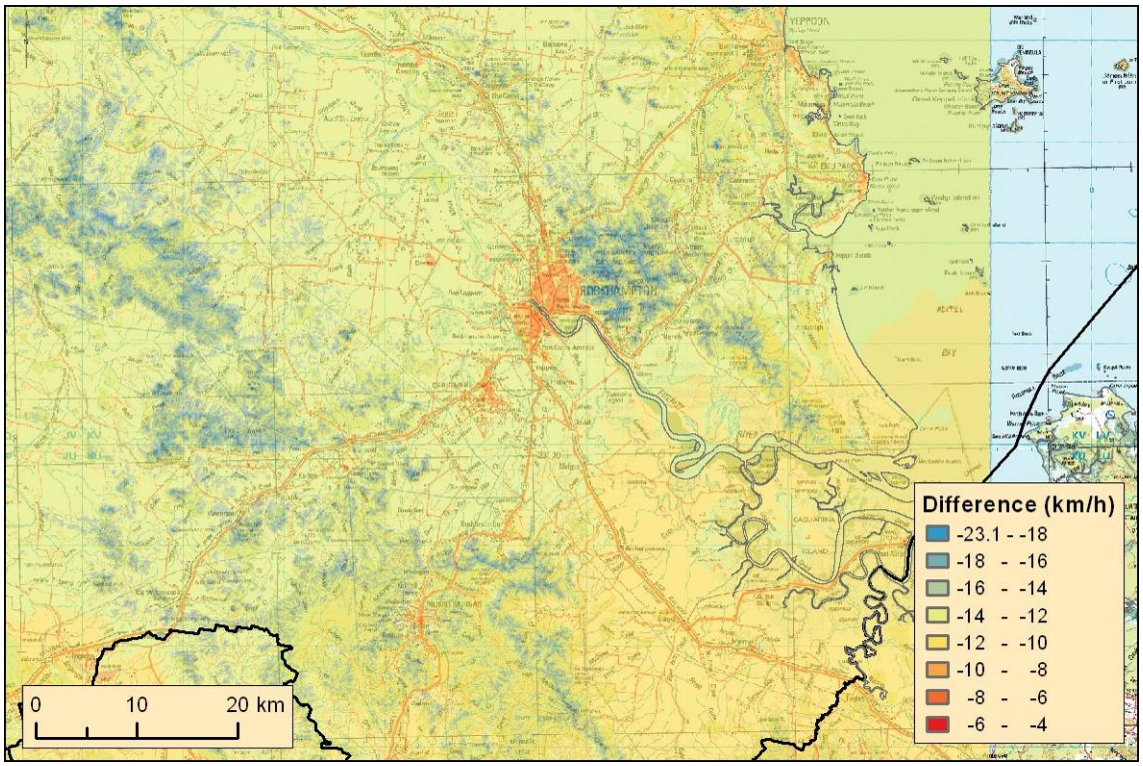

Appendix Figure A.20. 2090 – 100 year ARI minus 2050 – 100 year ARI.

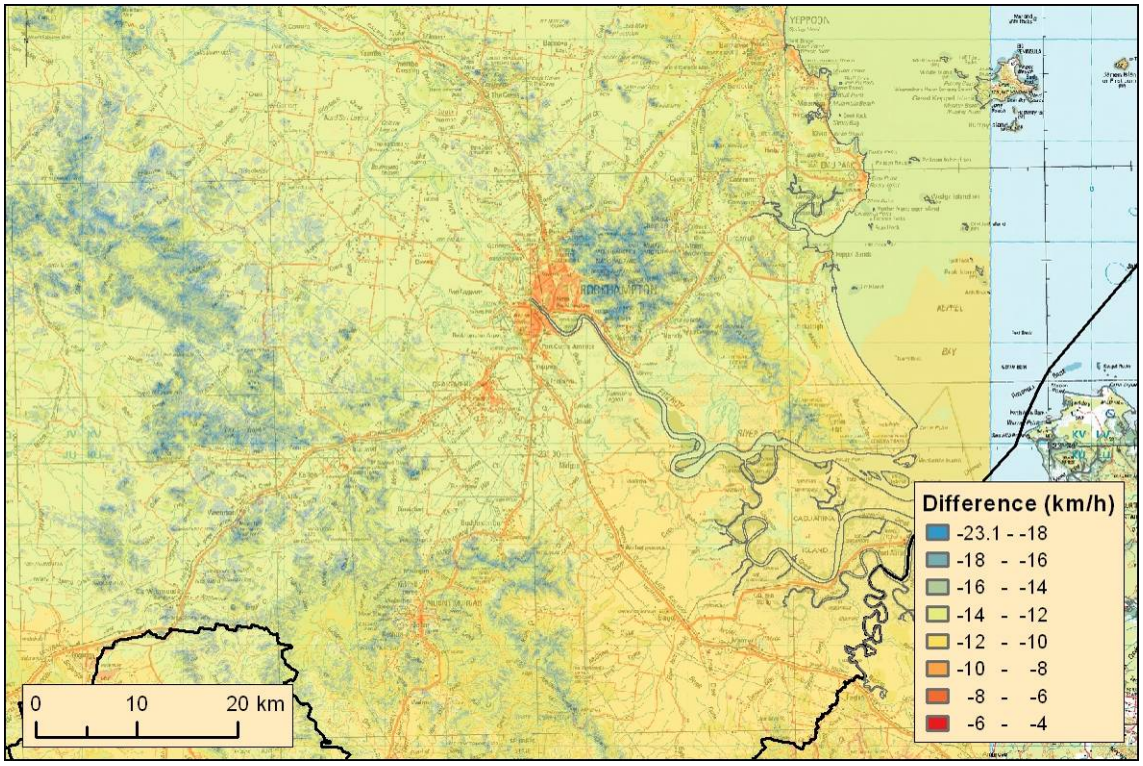

Appendix Figure A.21. 2090 – 250 year ARI minus 2050 – 250 year ARI.

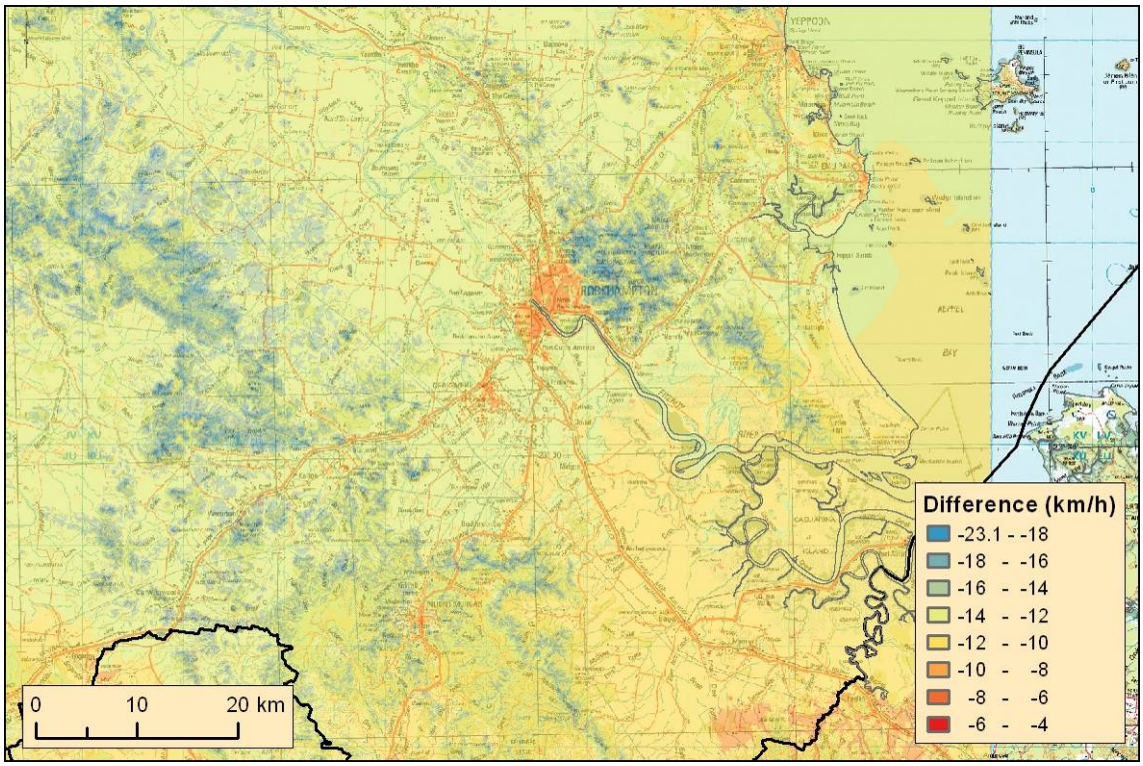

Appendix Figure A.22. 2090 – 1000 year ARI minus 2050 1000 year ARI.

A.3.3 Limitations

There were two significant limitations in the process used for this analysis:

- Sensitivity to downscaling technique
- Use of a single simulation of future-climate TCLV data.

The first limitation was identified through comparing the distribution of minimum central pressures from historical TC events used in the analysis and the same data from the TCLV dataset representing current-climate conditions (1981-2000). Due to the relatively coarse nature of the Regional Climate Model (RCM[20]) data (in this case 15 km horizontal resolution), the fine scale processes that control TC intensity cannot be properly resolved, so the TCLVs will in general display a lower mean intensity when compared to the historical record. To address this issue, the relative change in TC wind hazard between the 2055 and current-climate simulations was calculated and combined with the historical record to result in the 2055 TC wind hazard (and similarly for the 2090 simulation). This results in a baseline estimate and a change relative to that baseline for the two future time periods.

The second limitation was the small sample size used in training TCRM for future climate. The behaviour of TCLVs is strongly modulated by a range of drivers, including the RCMs representation of features such as the El Niño–Southern Oscillation (ENSO). This may reduce or enhance the simulated TC activity during the period of sampling (e.g. 2046-2065), or influence the intensity or tracks of TCLVs. As such, the results were sensitive to that single RCM run and the simulated broader

[20] Regional Climate Model – a higher-resolution atmospheric model, which is run over a reduced domain. The model is forced at its external boundaries with data extracted from a GCM.

environment. This could be addressed by running the RCM multiple times and from each simulation, extracting TCLVs for the periods of interest. Multiple RCM simulations downscaled from one GCM were not available for this project.

This page is intentionally blank

Appendix B Bushfire

Contents

Figures

Tables

B.1 Introduction

The dry-tropics of central Queensland result in an annual significant bushfire threat period that generally extends from September to November.

Bushfire hazard is correlated with temperature and precipitation patterns, as well as with fuel state and availability. According to IPCC AR4, Australia has experienced increases in average maximum and minimum temperatures of 0.6 °C and 1.2 °C respectively over the last century (Hennessy *et al.,* 2007). Furthermore, the rate of warming appears to be increasing globally (Trenberth *et al.,* 2007). Bushfires are exacerbated by the occurrence of heatwaves and droughts. Australian climate change projections based on the IPCC information (Whetton, 2011) indicate a significant increase in the number of days with maximum temperatures in excess of 35 °C for a range of capital cities and major regional centres. Projections also indicate longer periods of extreme heat and more severe droughts interspersed with wetter phases leading to flooding (CSIRO and BoM, 2012). Concurrent changes in precipitation and other environmental factors such as fire regimes are likely to have a significant effect on the diversity and distribution of species and ecosystems. All of these factors can have a significant impact on future bushfire risk to urban and peri-urban communities.

A recent report "Turn down the heat: Why a 4 °C warmer world must be avoided" commissioned by the World Bank (World Bank, 2012) warns that the world will heat up by 4 °C at the end of the century if the global community fails to act on climate change. In line with the above, investigation into the impact of climate change on bushfire hazard considered the IPCC SRES A2 emissions scenario which projects an average surface air temperature of 3.4 °C and a range of 2.0 – 5.4 °C (global warming) from the results of a number of complex climate models with a range of climate sensitivities (IPCC, 2007a). Three GCMs utilising the A2 emissions scenario were employed to consider the projection for the future climate of the Rockhampton region. The climate change projections utilised indicate that the Rockhampton region is likely to become hotter and possibly slightly drier in the future.

B.2 Method

B.2.1 Current Climate

In Australia, fire weather hazard is quantified using either the Forest Fire Danger Index (FFDI) or the Grassland Fire Danger Index (GFDI) (Luke and McArthur 1978). The FFDI is used in all States and Territories as a standard measure of fire danger. The FFDI is designed for forested vegetation types, therefore an additional weighting, based on the vegetation type, needs to be applied to account for less heavily-loaded areas (e.g. open forests, grasslands or urban areas). Both the FFDI and the GFDI consider weather observations and each index considers a dryness factor: FFDI includes a 'drought factor' and GFDI considers a 'curing factor'. Weather observations (temperature, relative humidity and wind speed) were combined with an estimate of the fuel state to predict likely fire behaviour if an ignition eventuates. The 'drought factor' is used for forests in the combined estimate of fuel state, and is based on daily rainfall and the period of time elapsed since the last rain. For grasslands, the 'curing factor' is used in the combined estimate of fuel state. Curing describes the annual or seasonal cycle of grasses dying and drying out, and is defined as the progressive senescence and drying out of grass (100% is fully cured grass). The curing factor can be measured via destructive sampling, visual observations and remote sensing. For this study only FFDI was calculated and the GFDI was scaled from the historical FFDI/GFDI measurements (for those instances at Rockhampton airport numbering 22 over nearly 40 years of daily records where FFDI > 50).

Previously, studies of bushfire exposure have included analysis of the fuel, e.g. remote sensing and deriving a fuel map from vegetation classifications, or FFDI has been calculated for a single location, e.g. a weather observation station or location for a prescribed burn and been considered representative of the region. The calculation of FFDI for a region based on a weather observation point is limited in application where the area being considered is not well represented by the single point location. In the case of calculating FFDI at the Rockhampton Airport, this location does not represent the Rockhampton region's diversity in fuel (vegetation) and topography including the impact that the proximity of the sea has on local weather conditions, including temperature. To consider the spatial variation in FFDI vegetation data was derived for the region and the varying weather conditions across the region were modelled using fine scale weather modelling techniques. In this way FFDI can be calculated to represent the spatial variation across the region due to varying fuel and weather factors.

To assess the bushfire hazard across the Rockhampton landscape, the observational weather record at Rockhampton Airport was used to determine suitable dates for fine-scale simulation of extreme fire weather conditions using a numerical weather prediction model, the Weather Research & Forecasting Model (WRF[21]). Analysis of the observation record at Rockhampton Airport (1 January 1973 – 30 June 2011) determined the worst 20 weather fire days, based on FFDI calculated from daily observations and assuming a constant drought factor. Bushfires had occurred in the Rockhampton region on some of these days.

From these 20 days, 6 were chosen (05/11/1994, 06/11/1994, 07/11/1994, 14/10/2009, 15/10/2009, and 16/10/2009) for high-resolution simulation using the WRF model at 270 m resolution over the Rockhampton study region. The WRF model simulated the weather conditions across the Rockhampton region from the Rockhampton Airport observations and a range of far-field observations. Boundary conditions for the WRF model were supplied from the US National Center for Environmental Prediction (NCEP) operational analyses available at http://mag.ncep.noaa.gov/NCOMAGWEB/appcontroller .

The numerical weather model was run on a smaller area than the Rockhampton study region to ascertain the appropriateness, accuracy and timeliness of the numerical weather prediction model. Model output at the grid-point corresponding to the location of Rockhampton Airport and Yeppoon were compared to the observations for the corresponding dates, to estimate the magnitude and direction of bias in the simulations. Comparison of quantiles of simulated and observed temperature, relative humidity and 10 m height wind speed revealed a reasonable match between the modelled and observed values of the first two elements, but wind speed was significantly underestimated in the simulations. A simple correction factor was applied to improve the quality of the match between the observed and simulated 10 m height wind speeds.

From the temperature, relative humidity and wind speeds generated by the simulations (and corrected where appropriate), the maximum FFDI for each simulated day was calculated, again using a constant drought factor. Each of these FFDI maps were then normalised to the value of the FFDI at the grid point corresponding to Rockhampton Airport – i.e. each grid point in the map defines the ratio of the FFDI at that point relative to the FFDI at Rockhampton Airport. The final output was an average of the six days of FFDI ratio maps, providing a map of the spatial distribution of FFDI for extreme fire weather days.

[21] http://www.wrf-model.org/index.php

The ARI of FFDI at Rockhampton Airport was calculated from observations (Lucas, 2010). For ARIs greater than the length of the record (39 years) the observations of FFDI were fitted with a Generalised Extreme Value (GEV) distribution (Generalised Pareto Distribution) permitting the calculation of ARI hazard outside the range of the dataset (Appendix Figure B.1).

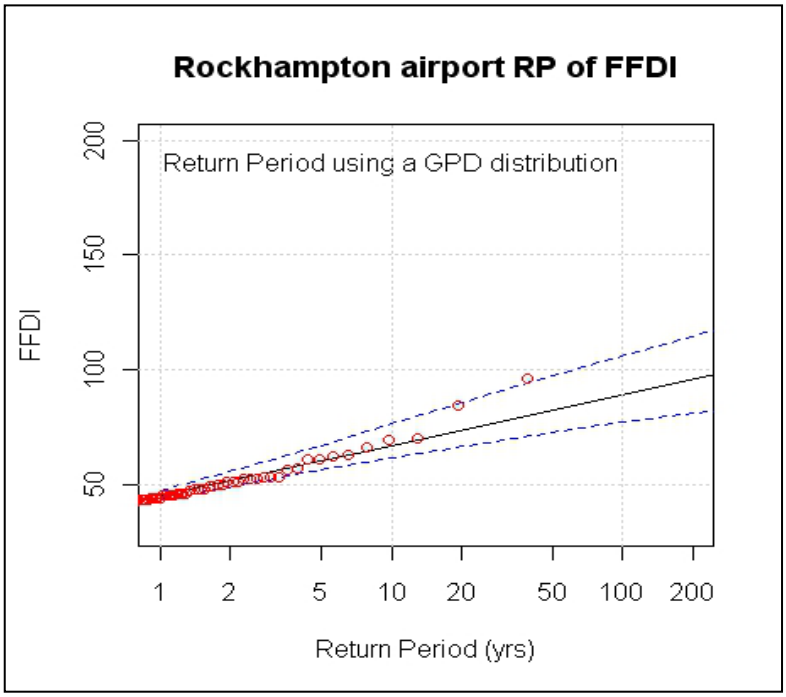

Appendix Figure B.1. Rockhampton airport Return Period[22] of FFDI calculated using observations. The broken lines represent the 95% confidence limits for the predicted FFDI (black solid line).

The GPD was used to obtain the optimum fit for the FFDI dataset. The GPD has been utilised for ARI analysis for a range of environmental parameters (e.g. Sanabria and Cechet, 2007). The broken lines shown in Appendix Figure B.1 depict the 95% confidence limits for the optimal fit of the GPD to the observed values (shown in Appendix Figure B.1 as open circles). It should be noted that the highest observed FFDI value (open circle to the right-most edge of Appendix Figure B.1) is just outside the 95% confidence limit for the extreme value distribution (GPD) fit to the observed data. This indicates that the occurrence of this extreme fire danger day within the 39 years of observed data is indeed very rare.

The observed (Rockhampton Airport) ARI FFDI values (50, 100 years) were then combined with the FFDI ratio maps generated from the weather simulations discussed previously to provide spatial representation of the FFDI ARI hazard across the Rockhampton study region. FFDI alone does not provide the complete picture of fire hazard. FFDI needs to be initially combined with a weighting based on the vegetation type as FFDI is based solely on forested vegetation. The weighting required is calculated based on the vegetation type created by:

- Obtaining the vegetation map for the region (From Landsat 5 TM satellite at 25 m resolution captured during May-August 2011)

[22] Return Period (RP) is equivalent to ARI.

- Classifying and merging the vegetation layers into:
  - Closed Forest (weighting 1.0
  - Open Forest[23] (weighting 0.8)
  - Grassland[24] (weighting 0.7)
  - None[25] (weighting 0.0).

A Bushfire hazard map was produced, with symbology classified into the following ratings (Appendix Table B.1) as developed for the new fire danger rating system for bushfires by the National Bushfire Warnings Taskforce, established following the Victorian bushfires of February 2009 (Table 2).

Appendix Table B.1. Fire danger classification.

Rating	Range
Moderate	(FFDI x weighting > 5 and <=11.9)
High	(FFDI x weighting >=12 and <=24.9)
Very High	(FFDI x weighting >=25 and <=49.9)
Severe	(FFDI x weighting >=50 and <=74.9)
Extreme	(FFDI x weighting >=75 and <=99.9)
Catastrophic	(FFDI x weighting >=100)

This bushfire hazard map does not supply details of where the bushfire hazard can be minimised to allow for future development. To address this, two factors were added, “setback from closed forest” and “slope”, to generate the final bushfire hazard map as follows:

- For setback, the Queensland Rural Fire Service (QRFS) uses the Building Code AS3959 which only addresses radiant heat impact on structures. New South Wales and Victoria allow a setback of 100 m from closed forest which goes some way to addressing both radiant heat and ember attack. For this analysis, the closed forest areas were extended to include a 100 m buffer zone (Appendix Figure B.2).
- For slope, the QRFS uses AS3959 which states that development should not occur on land which has a slope of greater than 20 degrees. Areas where the slope is greater than 20 degrees are shown in red in the Appendix Figure B.3. Note that most of these areas occur in the closed forest and setback areas.

[23] The open forest weighting factor of 0.8 was employed as a fire in this mix of vegetation more closely approximates a grass fire than a forest fire.

[24] For Grasslands the GFDI was not employed to determine the fire weather hazard for the region. Geoscience Australia used the FFDI for the grassland regions and then scaled these values dependent on the observed ratio (average weighting) of the GFDI to FFDI when observed FFDI was greater than or equal to 50 during the period January 1973 to June 2011 (22 occasions in the record). For FFDI >50 (1973-2011): average weighting = 0.7.

[25] “None” consists of regions where the vegetation was classified as urban, unclassified, mudflat or water.

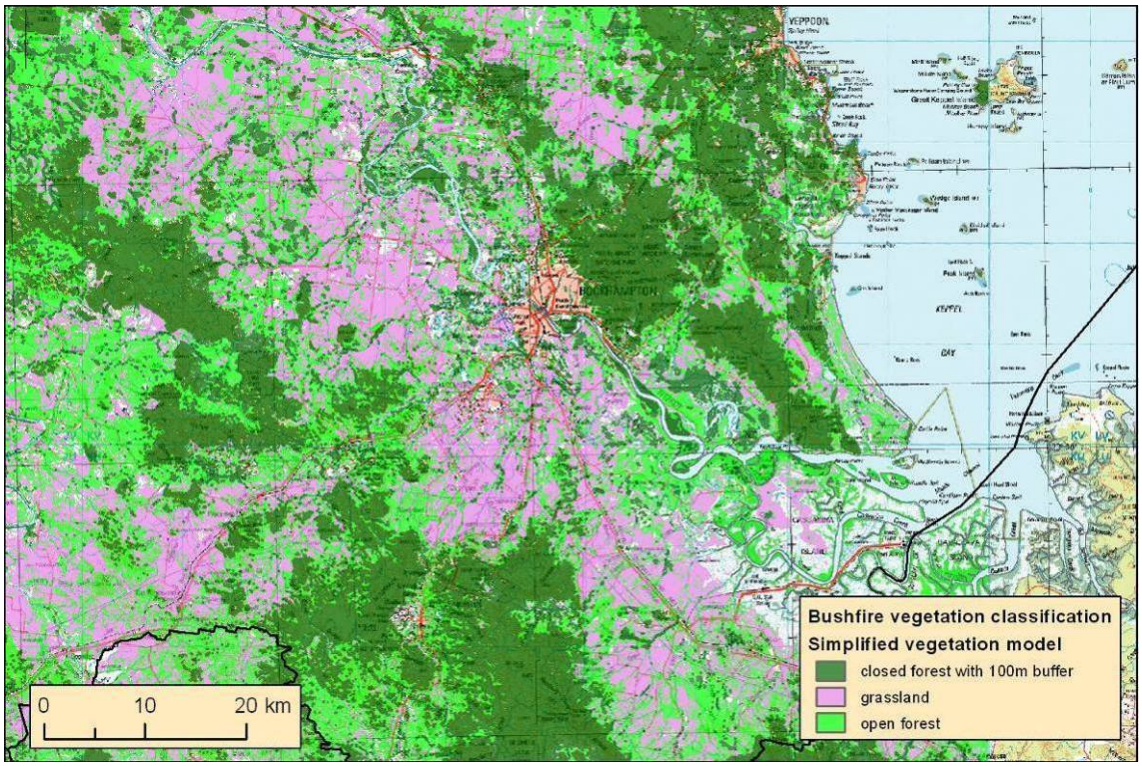

Appendix Figure B.2. Bushfire vegetation classification.

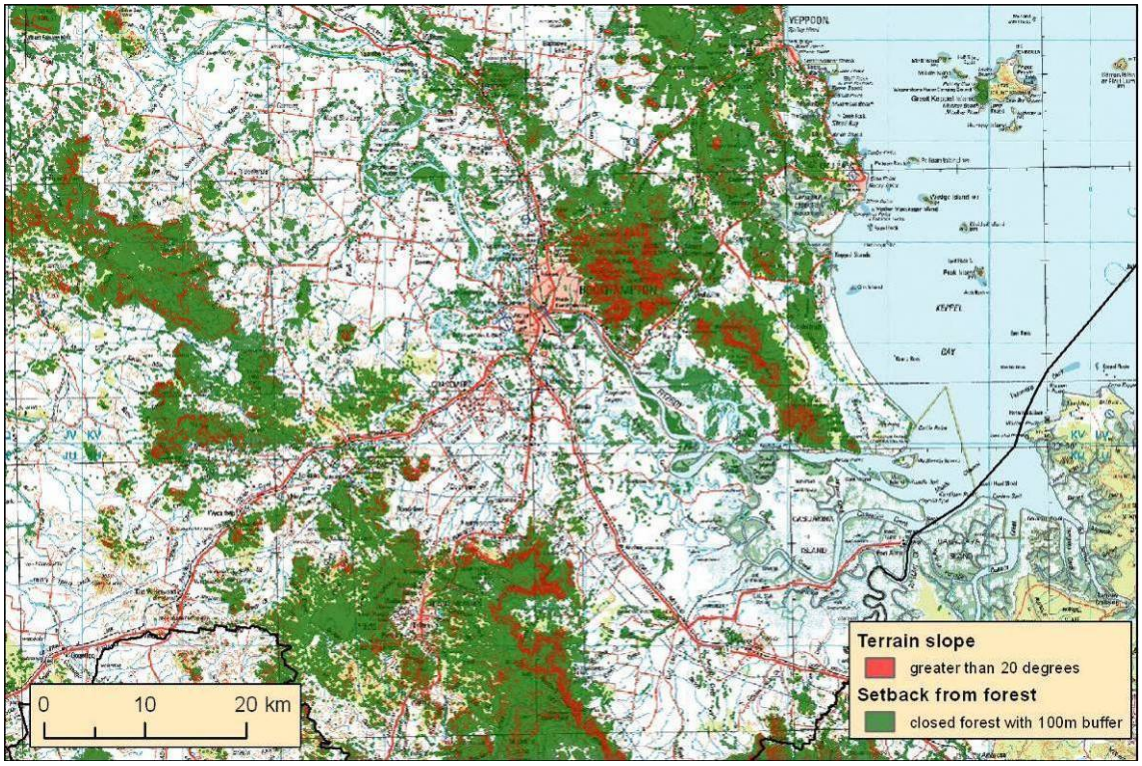

Appendix Figure B.3. AS3959 bushfire constraints.

B.2.2 Future Climate

This study utilised data (climate simulations) from three GCMs all being forced by the A2 SRES GHG emissions scenario.

CSIRO Marine and Atmospheric Research (CMAR) has produced high-resolution climate change projections for the eastern part of the Australian continent as part of the *South East Queensland Climate Adaptation Research Initiative* (SEQCARI) project (CSIRO, 2012). A key component of the project was to establish possible changes to climatic extreme events as a consequence of climate change up to the end of the 21st century. We utilised the new high-resolution projections provided by CSIRO to obtain a 0.15° grid of meteorological parameters (approx. 15 km horizontal resolution) across the eastern part of the continent (Latitude -10°S to -50°S; Longitude 135°E to 155°E) generated by downscaling the global GCMs using the CSIRO Conformal Cubic Atmospheric Model (CCAM).

Three GCMs were dynamically downscaled using the CCAM model (McGregor, 2005; McGregor and Dix, 2008) at the grid resolution of 0.15 degrees for the period 1971-2100. The GCMs selected are detailed in Appendix Table B.2. The model selection was based on an assessment by Smith and Chandler (2009) that examined the ability of selected models to reproduce the present-day climate of the Australian region. A single SRES emission scenario for atmospheric greenhouse gas emissions (A2; see Nakicenovic and Swart, 2000) was used to provide a mid- to high-range response for the likely projected future of the region. The IPCC SRES A2 emissions scenario provides an average global warming of 3.4 °C and a range of 2.0 - 5.4 °C (global warming) when considering a number of complex climate models with a range of climate sensitivities (IPCC, 2007a).

Appendix Table B.2. Parent GCM model (driver) for the CCAM climate simulations (regional downscaling).

CCAM "parent model" (driver)	Institution
ECHAM 5	Max-Planck Institut (Germany)
GFDL_CM 2.1	Princeton Univ./NOAA (USA)
MIROC 3.2 medres	Interdisciplinary Research on Climate (Japan)

A regional downscaling approach utilising the CCAM dynamical downscaling model (Katzfey *et al.,* 2009) was employed to model the spatial variability of the regions climate. It uses a stretched-grid global model with forcing data taken from a host GCM. The result is a fine-scale grid of information over the area of interest (dynamically downscaled region). A two stage downscaling process was required to achieve the final resolution of 0.15°. The first stage (intermediate model) involved downscaling from the host GCM to a grid with the high-resolution face of the cubic conformal grid covering all of Australia at a resolution of approximately 0.5°. The second stage placed the high-resolution face over the eastern part of the continent. Appendix Figure B.4 demonstrates the average annual precipitation totals for Tasmania at the three grid resolutions (a typical GCM and the two stages of downscaled results; demonstrated by GFDL-CM2.1 model). A typical GCM resolution (Appendix Figure B.4a, Typical GCM Projection) only has two or three grid cells covering the state. The 0.5° resolution model (Appendix Figure B.4b, 0.5° intermediate downscaled projection) shows an improved spatial pattern of precipitation, with the predominantly dryer eastern and wetter western regions starting to be defined. The finest 0.15° resolution model (Appendix Figure B.4c, 0.15° downscaled projection) closely resembles the observed spatial pattern of annual precipitation. It was concluded that the high-resolution 0.15° dynamical downscaling process had the ability to model the

local climate of a region such as Central Queensland accurately across the downscaled models, including seasonality, spatial variance and relationships between the different climate variables.

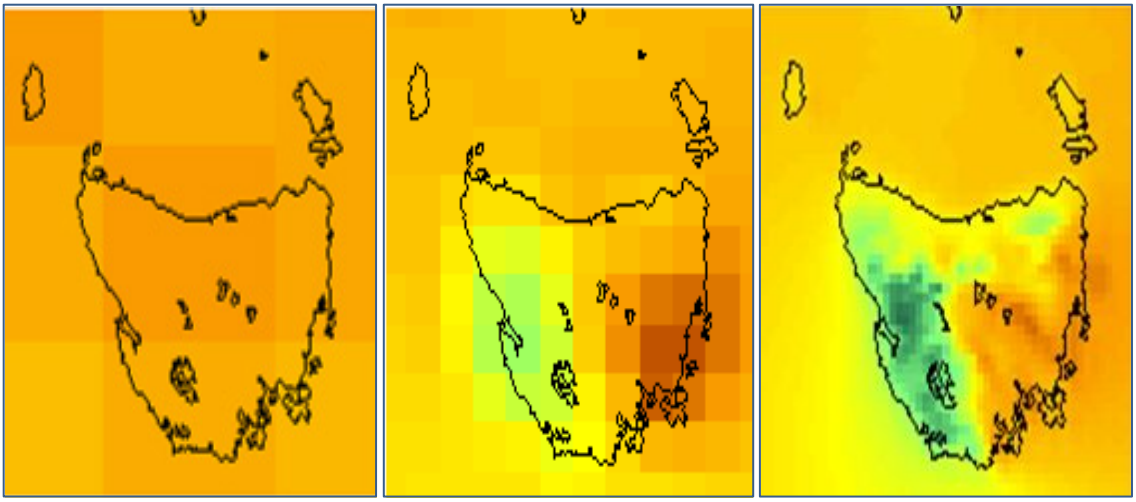

a) b) c)

Appendix Figure B.4. Average annual precipitation totals for Tasmania projected on typical a) GCM, b) 0.5° and c) 0.15° grids (Corney et al., 2010). Precipitation scaled from 0-3000 mm per annum.

B.2.3 Forest Fire Danger Index

For current climate, the FFDI was obtained utilising the observational record, which spanned four decades in the Central Queensland region. High-resolution spatial detail for the FFDI was obtained by using a modelling approach that considered a number of extreme events that were identified as "typical" of the type of event that would be experienced for a 50 year ARI or 100 year ARI event (i.e. the synoptic forcing had been determined as being similar to the majority of the extreme fire weather events in the observational record).

For future climate, three downscaled GCMs forced by the A2 GHG emissions scenario for atmospheric greenhouse gas emissions were considered. The models were initially run in "control" mode where the present-day (1990) atmospheric forcings were kept constant. From 1991 to 2100 the atmospheric forcing followed the A2 scenario (Nakicenovic and Swart, 2000) resulting in a change within each model from the "control" climate. Three periods of the simulation within each of the three models were considered:

- (Dataset 1) 1971 – 1990 (considered as the current-climate [CC] simulation)
- (Dataset 2) 2041 – 2060 (considered as the simulated climate of 2050)
- (Dataset 3) 2081 – 2100 (considered as the simulated climate of 2090)

The maximum FFDI for the Rockhampton region was calculated for each day in these datasets (as with the observed current-climate data) and extreme value statistics were employed to determine the magnitude of the 50 year ARI [50ARI] and 100 year ARI [100ARI] FFDI event. Finally, the FFDI for the observed current-climate data was scaled by the simulated data (Appendix Table B.3) to determine how the FFDI would be modified in a new climate.

Appendix Table B.3 Future climate bushfire hazard calculation.

	Calculation
2050 – 50 year ARI	[50ARI (2041-2060) / 50ARI (1971-1990)] x 50ARI (observed current climate)
2050 – 100 year ARI	[100ARI (2041-2060) / 100ARI (1971-1990)] x 100ARI (observed current climate)
2090 – 50 year ARI	[50ARI (2081-2100) / 50ARI (1971-1990)] x 50ARI (observed current climate)
2090 – 100 year ARI	[100ARI (2081-2100) / 100ARI (1971-1990)] x 100ARI (observed current climate)

NOTE: The ensemble average of the three downscaled GCMs was used to provide estimates for the 50 year ARI and the 100 year ARI FFDI predictors that inform the future climate FFDI. For the 100 year ARI estimate for 2090, the MIROC3.2 model was not used as it gave extremely high FFDI values when compared with the other two models with a highly unlikely spatial distribution. The FFDI is an exponential index, therefore care needs to be taken that any significant model bias has been removed before calculating the FFDI values. It was also decided not to use the MIROC3.2 model for the 2090 climate simulation due to the very high values and the highly unlikely spatial distribution of FFDI where, for 2090, the derived FFDI was a maximum near the coast. The three model constituents that combined to identify extremely high FFDI on the coast were a maximum wind speed near the coast, a lack of temperature gradient (with distance from the coast), and a lack of humidity (driven by an offshore wind direction).

B.3 Results

B.3.1 Current Climate

For the 50 and 100 year ARI scenarios the bushfire danger rating is shown in Appendix Figure B.5 and Appendix Figure B.6 respectively. The bushfire hazard is in part based on the simplified vegetation model (Appendix Figure B.2) and the "Vegetation type (including 100 m setback from closed forest) and slope" (Appendix Figure B.3) which was used to create the bushfire hazard maps. Note that the current vegetation (May-August 2011 Landsat 5 TM image) has been used in calculating the 50 year and 100 year bushfire hazard maps, and that a change in the vegetation caused by land use practices or perhaps wet or dry decades (compared to average rainfall) will alter these results.

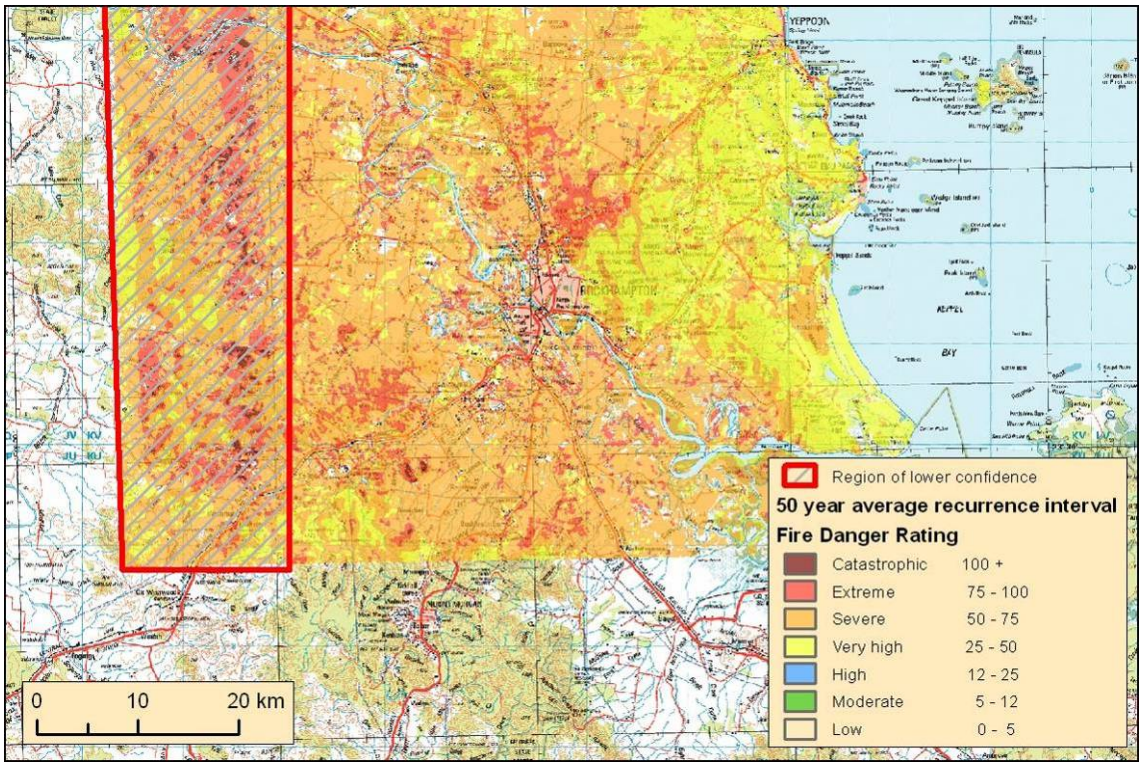

Appendix Figure B.5. Fire danger rating – current-climate 50 year ARI. The dashed area indicates a region of lower confidence; see the Discussion section.

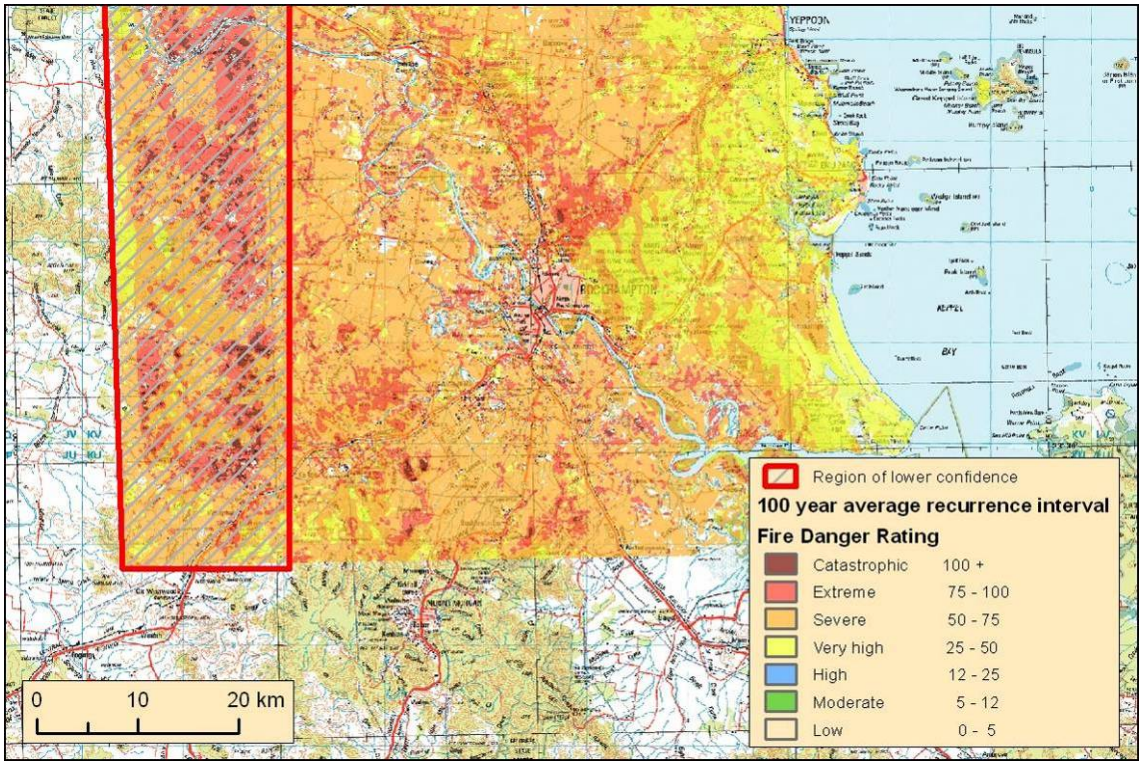

Appendix Figure B.6. Fire danger rating – current-climate 100 year ARI. The dashed area indicates a region of lower confidence; see the Discussion section.

B.3.2 Future Climate

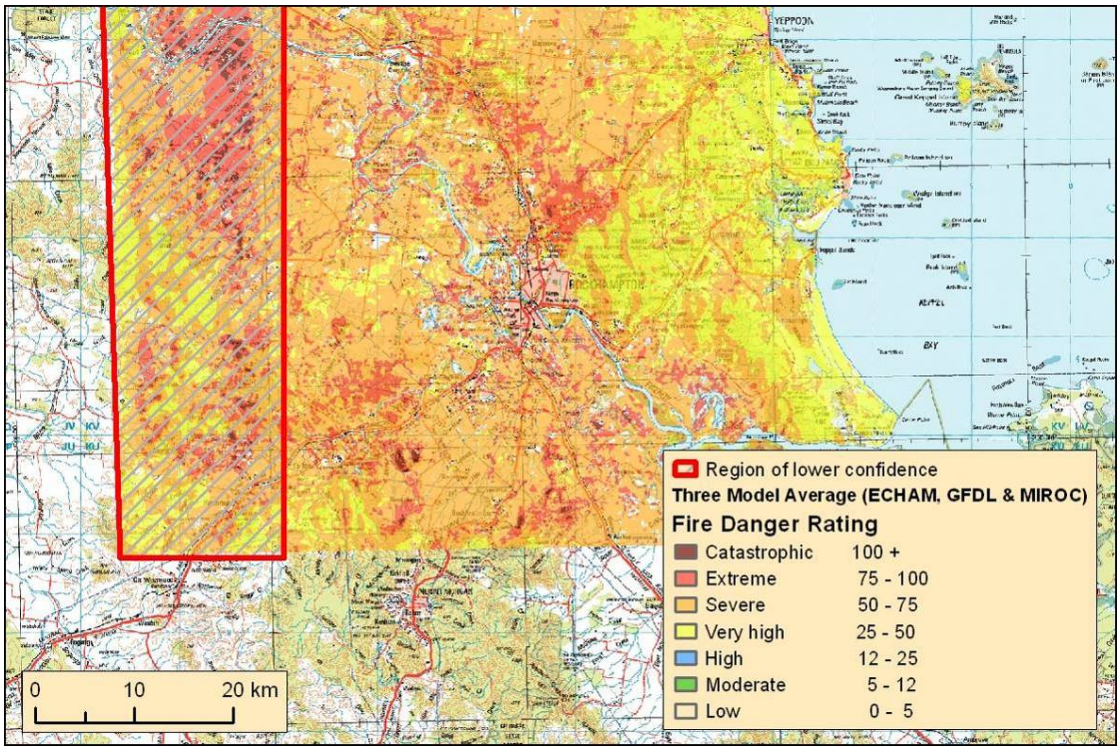

Appendix Figure B.7. Fire Danger Rating, 2050 – 50 year ARI. The dashed area indicates a region of lower confidence; see the Discussion section.

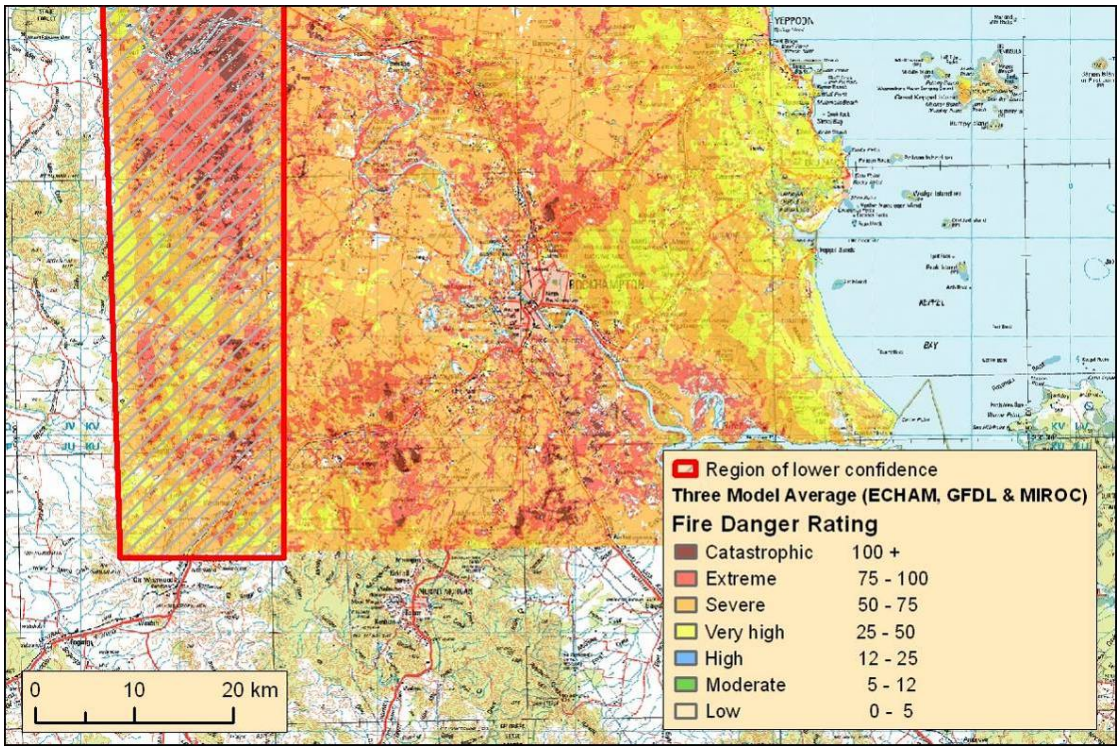

Appendix Figure B.8. Fire Danger Rating, 2050 – 100 year ARI. The dashed area indicates a region of lower confidence; see the Discussion section.

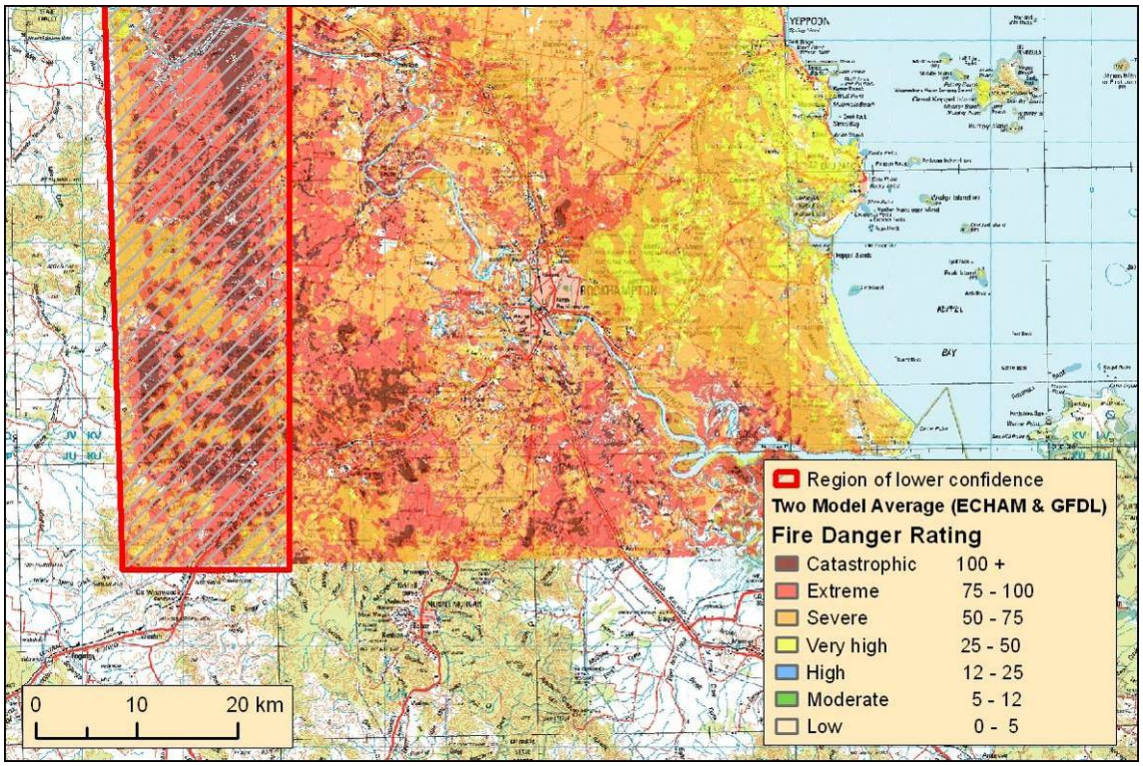

Appendix Figure B.9. Fire Danger Rating, 2090 – 50 year ARI. The dashed area indicates a region of lower confidence; see the Discussion section.

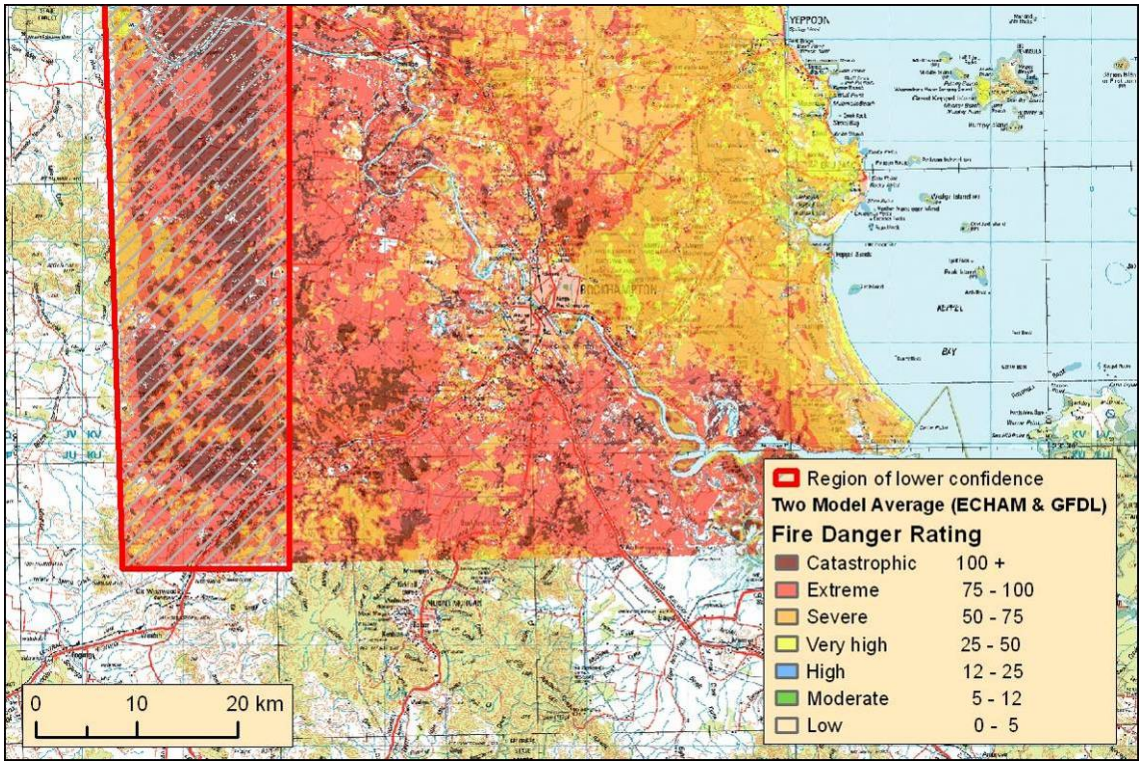

Appendix Figure B.10. Fire Danger Rating, 2090 – 100 year ARI. The dashed area indicates a region of lower confidence; see the Discussion section.

B.4 Discussion - Current Climate

The Bushfire hazard has been reclassified into three classes to more clearly show the lesser and greater hazard in the 50 year and 100 year ARI events, Appendix Figure B.11 and Appendix Figure B.12 respectively. The existing hazard has been reclassified into three classes: Class 1 - Low, Moderate and High; Class 2 - Very High and Class 3 - Severe, Extreme and Catastrophic. A summary of the business and home risk from the Queensland Rural Fire Service[26] is replicated below:

Appendix Table B.4. Fire Danger Rating description – Queensland Rural Fire Service.

Rating	Description
Catastrophic	A fire with a rating of "Catastrophic" may be uncontrollable, unpredictable and fast moving. The flames will be higher than roof tops. Many people will be injured and thousands of homes and businesses will be destroyed. During a "Catastrophic" fire, well prepared, constructed and defended homes may not be safe. Leaving is the safest option for your survival.
Extreme	A fire with an "Extreme" rating may be uncontrollable, unpredictable and fast moving. The flames will be higher than roof tops. During an "extreme" fire, people will be injured and hundreds of homes and businesses will be destroyed. During a fire with an "Extreme" rating, only well prepared, well constructed and actively defended houses are likely to offer any safety during a fire. Leaving is the safest option for your survival.
Severe	A fire with a "Severe" rating may be uncontrollable and move quickly, with flames that may be higher than roof tops. A severe fire may cause injuries and some homes or businesses will be destroyed. During a fire with a "Severe" rating, leaving is the safest option for your survival. Only use your home as a place of safety if it is well prepared and you can actively defend it.
Very High	A fire with a "Very High" danger rating is a fire that can be difficult to control with flames that may burn into the tree tops. During a fire of this type some homes and businesses may be damaged or destroyed. During a fire with a "Very High" danger rating, you should only use your home as a place of safety if it is well prepared and you can actively defend it.
High	A fire with a "High" danger rating is a fire that can be controlled where loss of life is unlikely and damage to property will be limited. During a fire with a "High" danger rating, you should know where to get more information and monitor the situation for any changes.
Low - Moderate	A fire with a "Low to Moderate" rating can be easily controlled and post [*sic*] little or no risk to life or property. During a fire with a "Low to Moderate" rating, you should know where to get more information and monitor the situation for any changes.

The location of greater and lesser hazard is consistent with the TC wind hazard although the area in the larger bushfire clusters is less than the 500 year ARI wind hazard.

[26] http://www.ruralfire.qld.gov.au/national_warning_system.asp

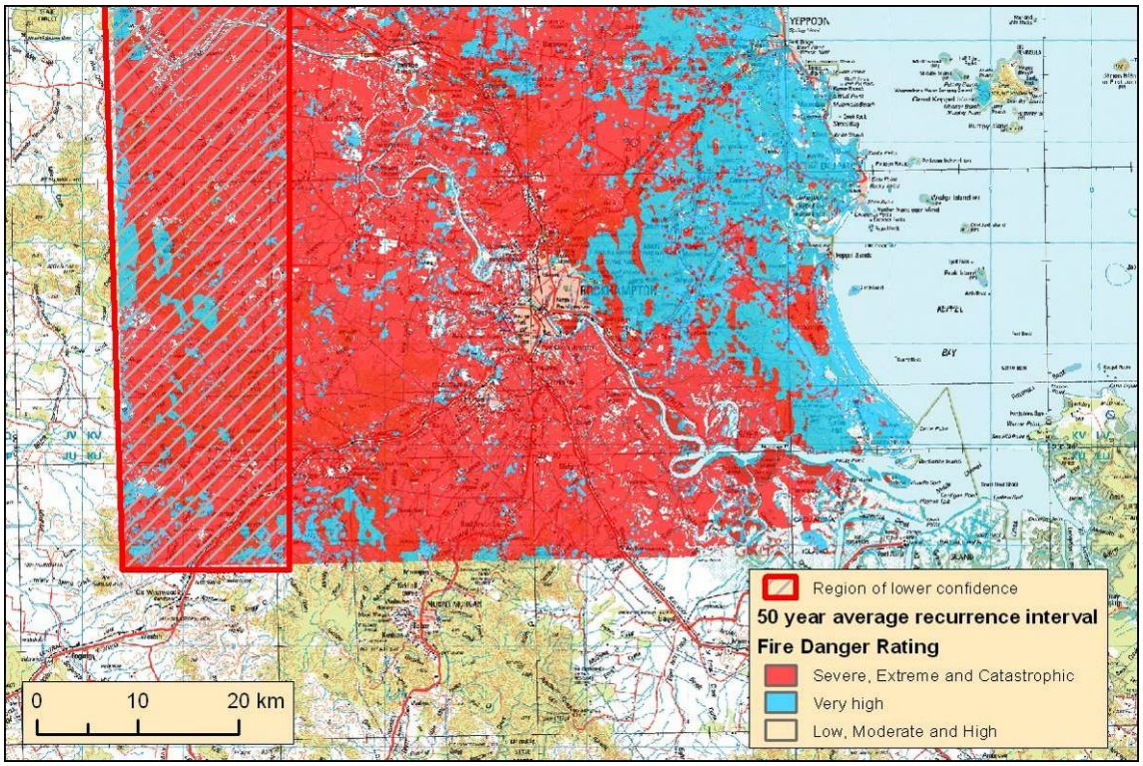

Appendix Figure B.11. Current-climate 50 year ARI bushfire hazard reclassified.

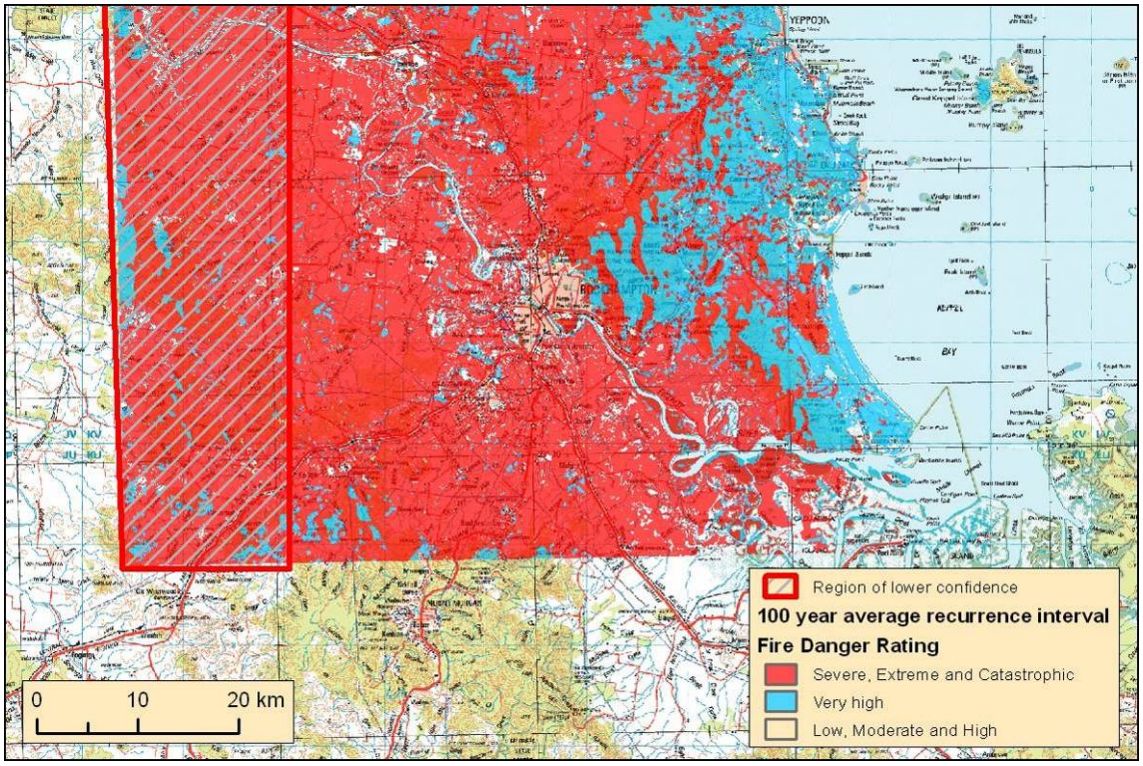

Appendix Figure B.12. Current-climate 100 year ARI bushfire hazard reclassified.

The dashed area in the bushfire hazard depicts a region of lower confidence in the assessment associated with the numerical model and modelling technique utilised. The area of lower confidence

has been affected by gravity waves in the modelled atmosphere caused by westerly flow over the nearby mountain ranges (called mountain waves). The influence on turbulent mixing and on the boundary layer winds is important enough that gravity waves are included in weather and climate models by parameterisation, which is an active area of research. In this study we have averaged the output from four simulations which is considered insufficient to average the gravity influence in the region of lower confidence. As the weather simulations are an input into the future-climate modelling this issue is therefore present in all the future-climate results. It is unclear how inaccurate these results are without further weather simulations being completed (extreme fire weather case studies) to attempt to investigate this anomaly, which was not possible within the project timelines. Otherwise outside the area of lower confidence, the results conform generally with expectations of the spatial distribution of bushfire hazard relating to weather characteristics, such as the proximity of the ocean increasing the relative humidity and reducing fire hazard.

Without considering the red box area, the larger blocks of less exposed land closer to Rockhampton include:

- north-west of Rockhampton
- south of Rockhampton between the Bruce and Capricorn highways.

The hazard modelling extent does not extend far enough south to compare with the lesser wind exposed areas south of Bajool and Marmor.

The Fitzroy floodplain to the east of the Bruce Highway shows mixed areas of high and low hazard whereas the lesser wind hazard was relatively homogenous in comparison.

Notable areas of peak hazard include:

- Flat Top Range and to south to the Fitzroy River
- Mount Archer National Park.

It should be noted that there is only a small difference in FFDI between the 50 year ARI and 100 year ARI. This is also reflected in Appendix Figure B.1 (Rockhampton airport FFDI observations). Appendix Figure B.13 shows a map of the difference between the 50 year ARI and 100 year ARI assessments. Most of the region (about 70%) has a difference below 4 FFDI units, whilst less than 5% of the region has a difference above 6 FFDI units.

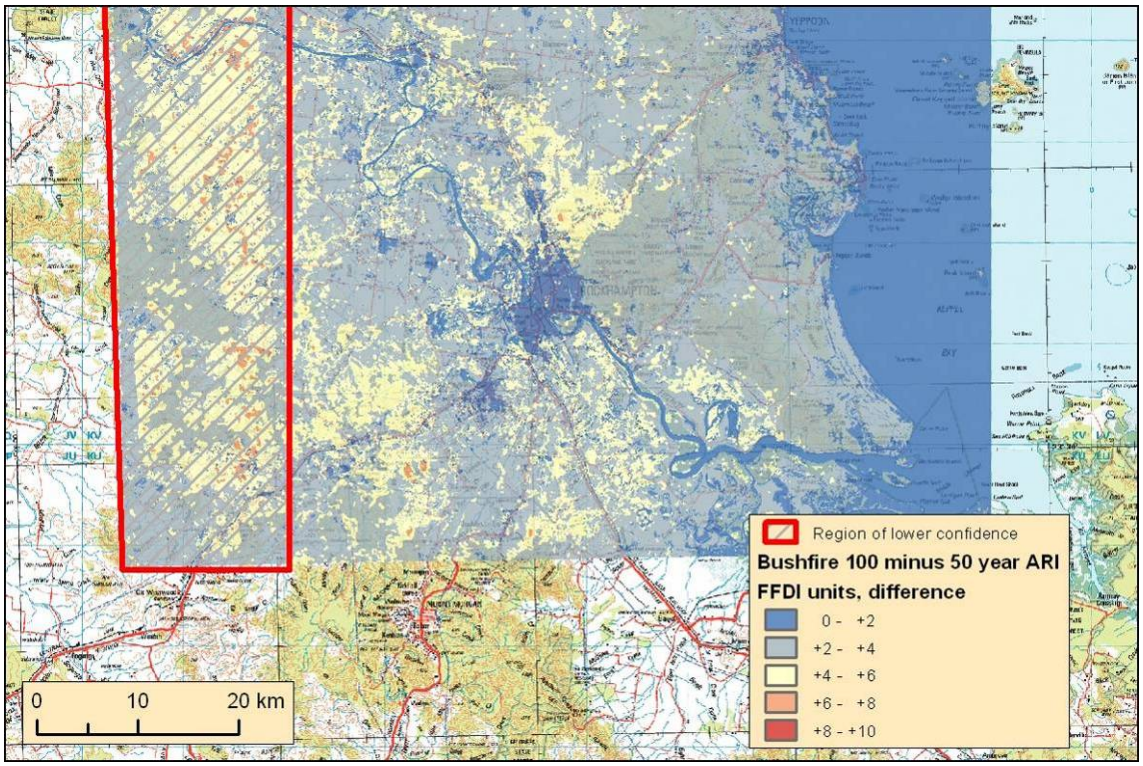

Appendix Figure B.13. Bushfire hazard difference – 100 year ARI minus 50 year ARI.

B.5 Discussion - Future Climate

Larger homogenous areas showing Extreme hazard in the 2050 50 year ARI hazard (Appendix Figure B.7) include:

- south-west of Gracemere
- north of Rockhampton on the eastern side of the Bruce Highway
- south of Rockhampton on the western side of the Bruce Highway.

The common trend between the 2050 50 year ARI hazard (Appendix Figure B.7), 2050 100 year ARI hazard (Appendix Figure B.8), 2090 50 year ARI hazard (Appendix Figure B.9) and the 2090 100 year ARI hazard (Appendix Figure B.10) is the increasing bushfire hazard. This can be seen from the increasing extent of the higher bushfire hazard classes and the decreasing extent of the lower bushfire classes when the previous scenario is compared (e.g. 2050 100 year ARI vs. 2050 50 year ARI).

B.5.1 Bushfire hazard reclassified

As shown in the current-climate discussion of bushfire hazard, the future-climate bushfire hazard has been reclassified to combine hazard categories to focus on risk to buildings and people as described by QRFS in Appendix Table B.4. The 2050 reclassified bushfire hazard is presented in Appendix Figure B.14 and Appendix Figure B.15, for 50 and 100 year ARI, respectively, and the 2090 reclassified bushfire hazard is presented in Appendix Figure B.16 and Appendix Figure B.17, for 50 and 100 year ARI, respectively.

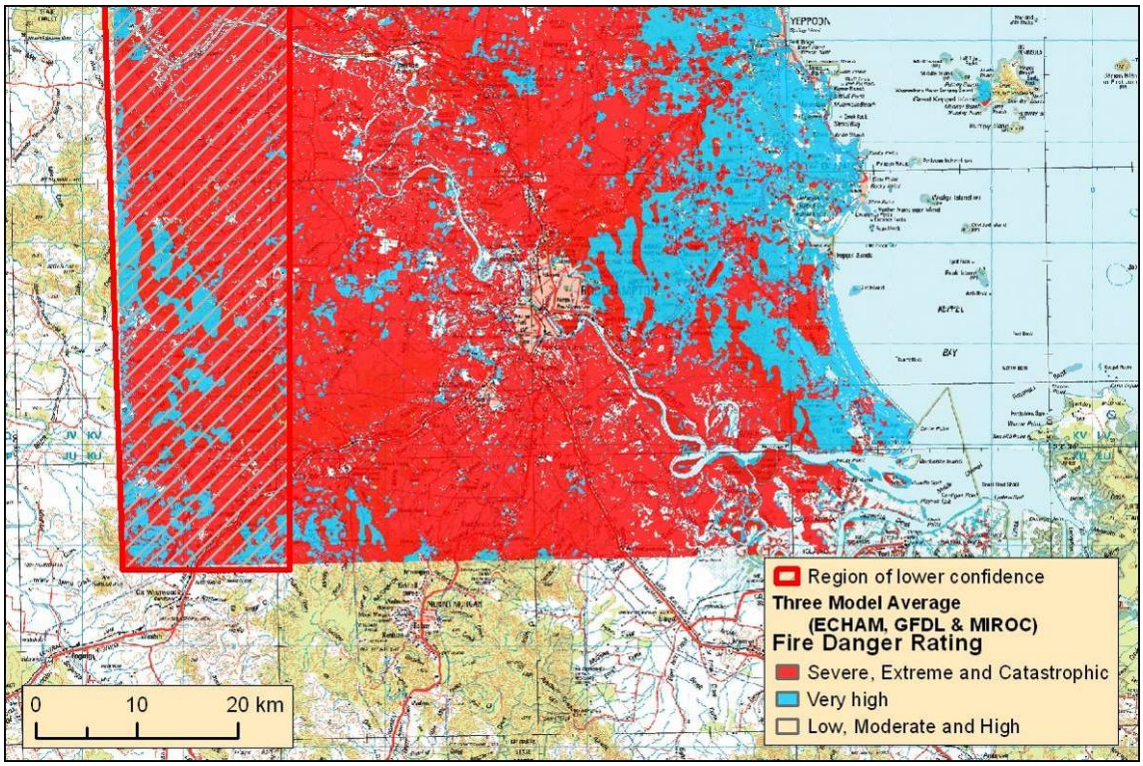

Appendix Figure B.14. 2050 50 year ARI bushfire hazard reclassified.

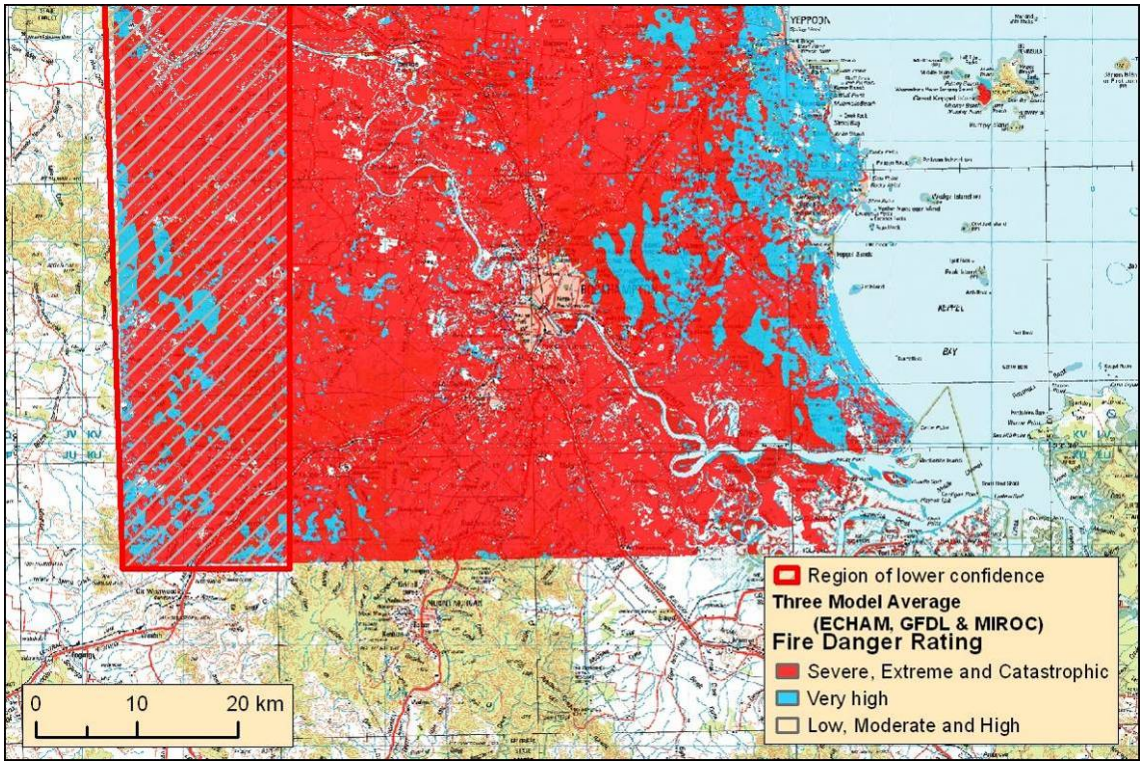

Appendix Figure B.15. 2050 100 year ARI bushfire hazard reclassified.

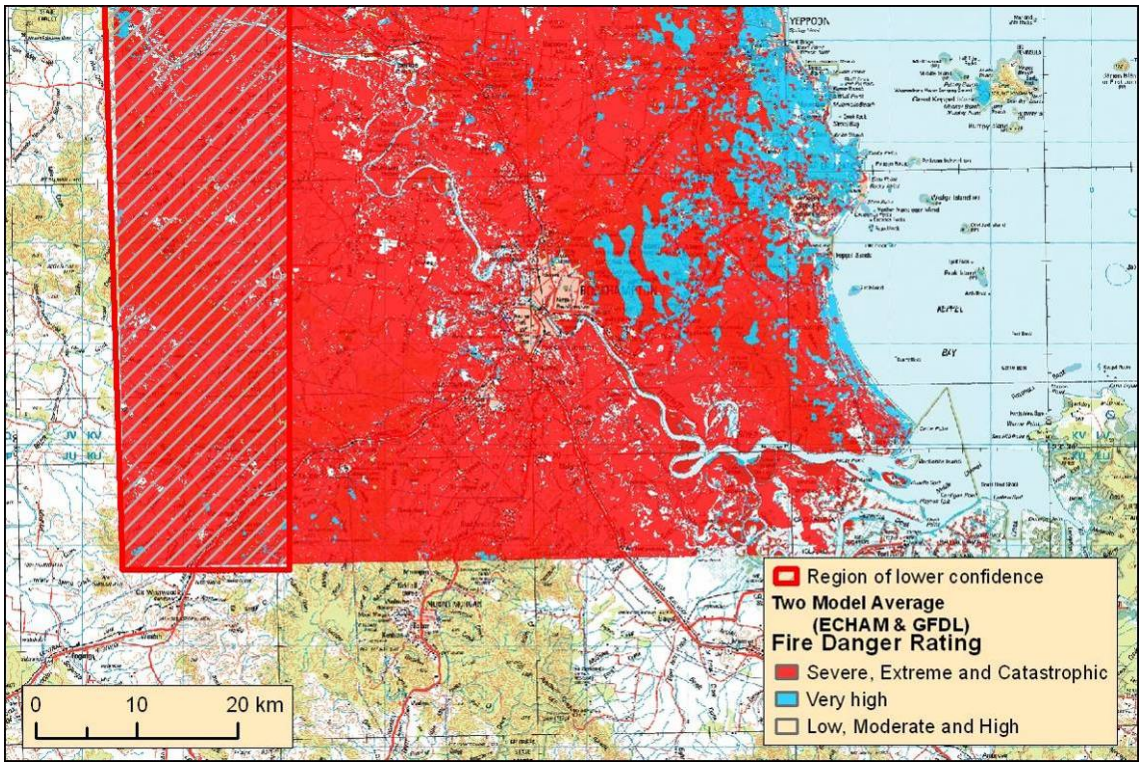

Appendix Figure B.16. 2090 50 year ARI bushfire hazard reclassified.

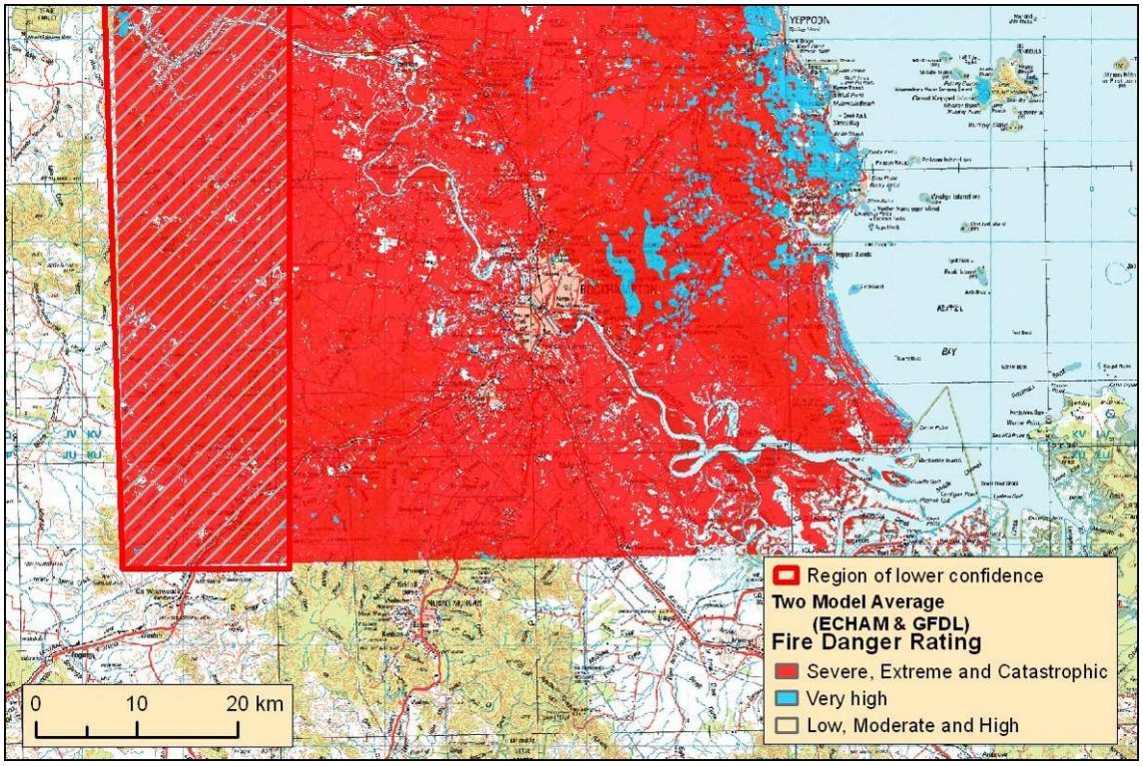

Appendix Figure B.17. 2090 100 year ARI bushfire hazard reclassified.

B.5.2 Future-climate 50 vs. 100 year ARI bushfire hazard

It should be noted that for the future-climate simulations there is, similar to current climate, a small difference in bushfire hazard between the 50 year ARI and 100 year ARI (only slightly greater than for the current-climate ARI maps shown in Appendix Figure B.11 and Appendix Figure B.12). This follows the trend-curve in the Rockhampton airport FFDI-ARI determination (Appendix Figure B.1) where the difference between the 50 year ARI and 100 year ARI assessments are smaller than the uncertainty in the average predictor (as shown as the 95% confidence limits).

As with current-climate bushfire hazard, there is an increase in the extent of the higher bushfire hazard categories between the 50 and 100 year ARI hazard for each time period. For both 2050 and 2090 there is a range of increase of between 0 and 20 bushfire danger units (Appendix Figure B.18 and Appendix Figure B.19).

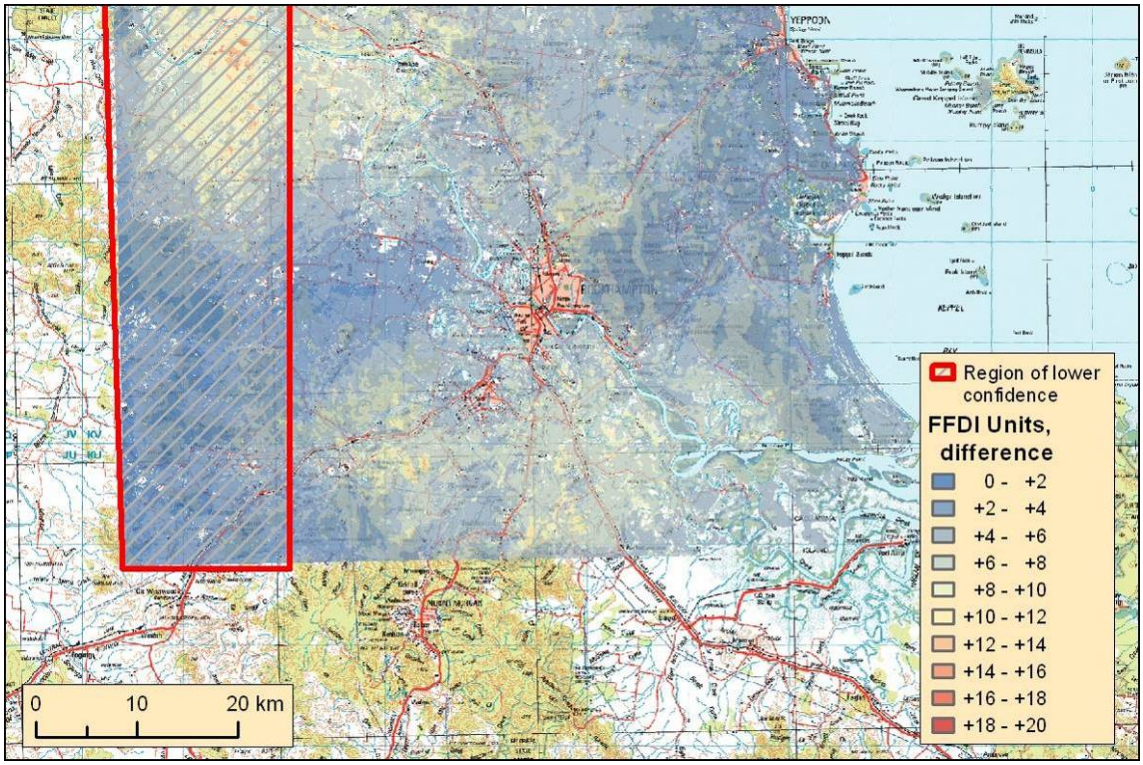

Appendix Figure B.18. Bushfire hazard difference – 2050 100 year ARI minus 2050 50 year ARI.

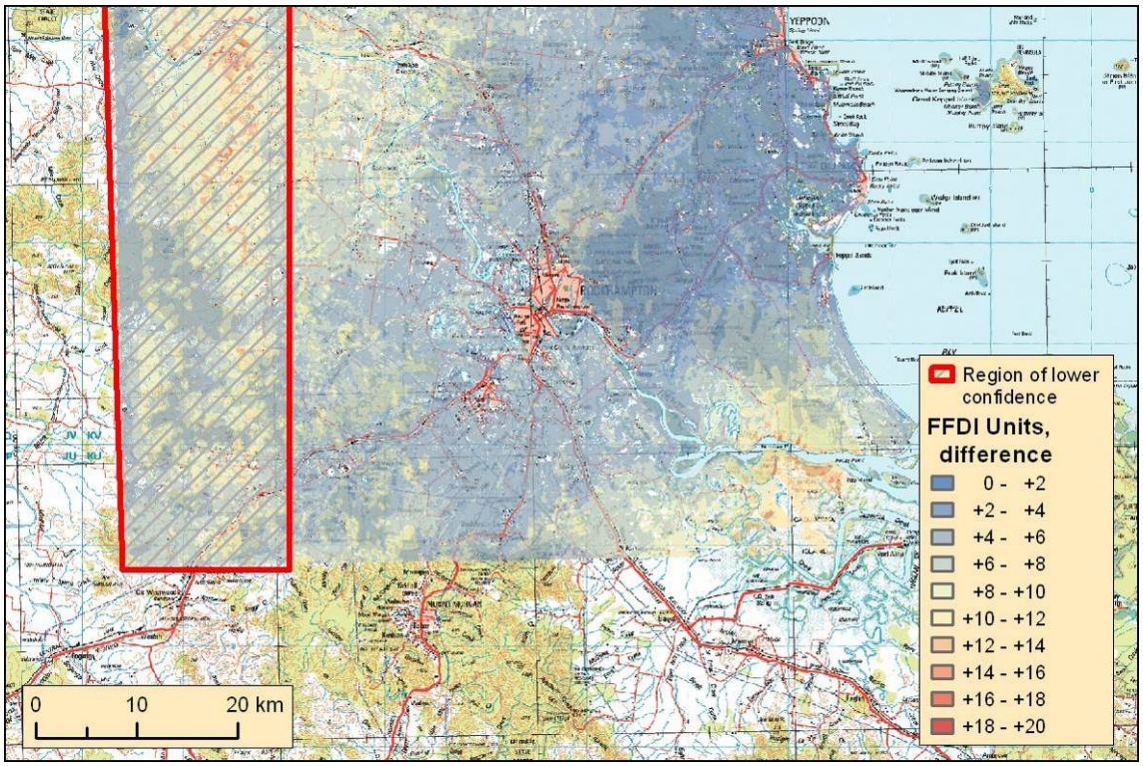

Appendix Figure B.19. Bushfire hazard difference – 2090 100 year ARI minus 2090 50 year ARI.

B.5.3 Future climate vs. current climate

Comparing the future-climate bushfire hazard with current-climate bushfire hazard results in the 2050 comparison (Appendix Figure B.20 and Appendix Figure B.21) with negative through to positive change in both the 50 and 100 year ARI bushfire hazard. The swirl pattern to the west and south-west of the figures is caused by the downscaling of the spatial resolution (bilinear interpolation) from the courser GCM scaling results.

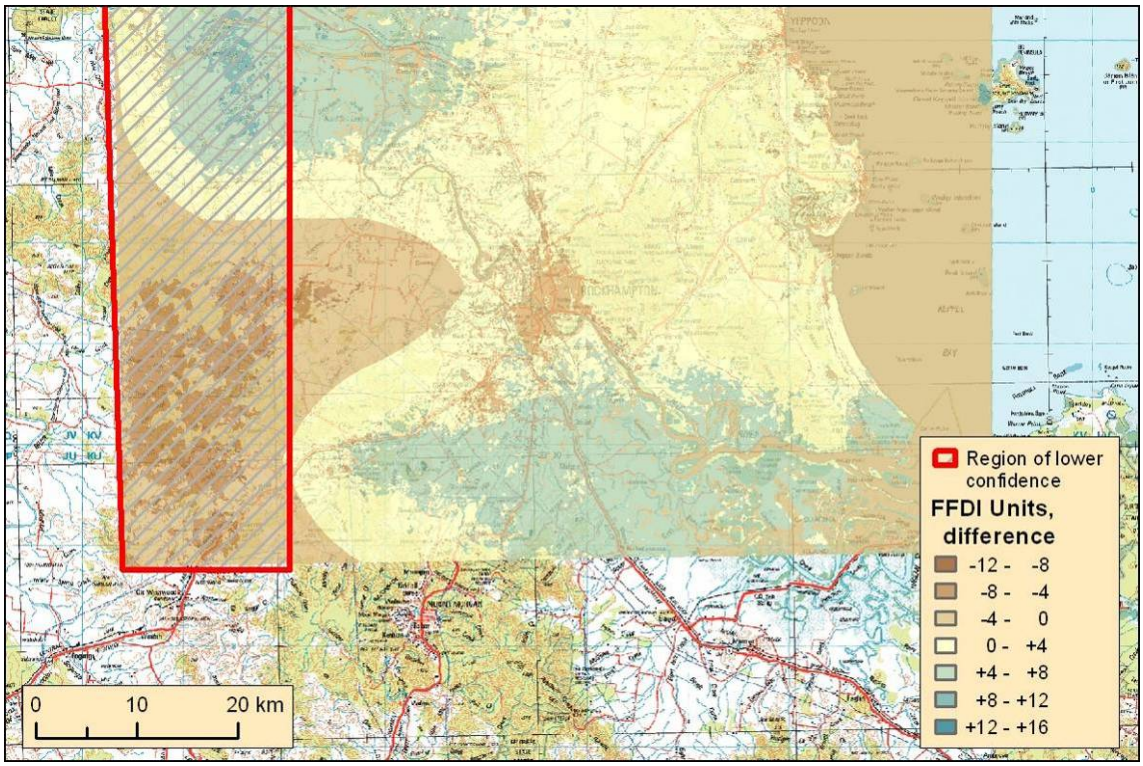

Appendix Figure B.20. Bushfire hazard difference – 2050 50 year ARI minus current-climate 50 year ARI.

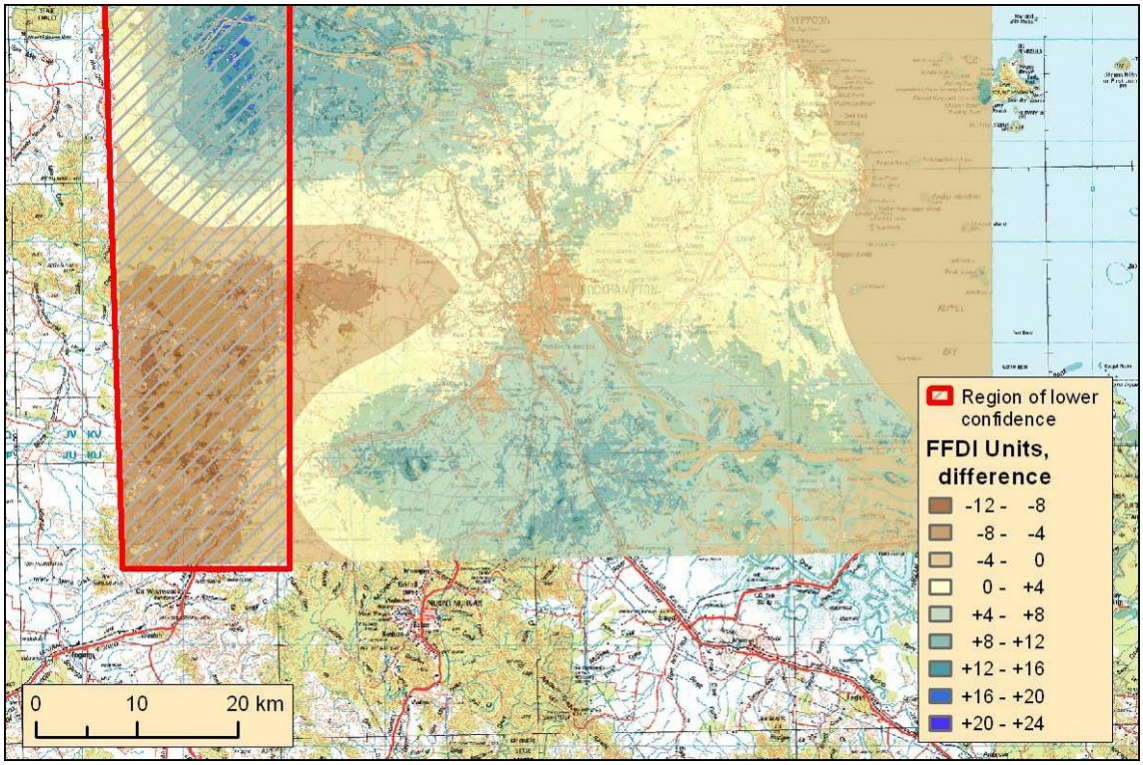

Appendix Figure B.21. Bushfire hazard difference – 2050 100 year ARI minus current-climate 100 year ARI.

This swirl pattern is not present in the 2090 comparison to current climate (Appendix Figure B.22 and Appendix Figure B.23) where the change is all positive.

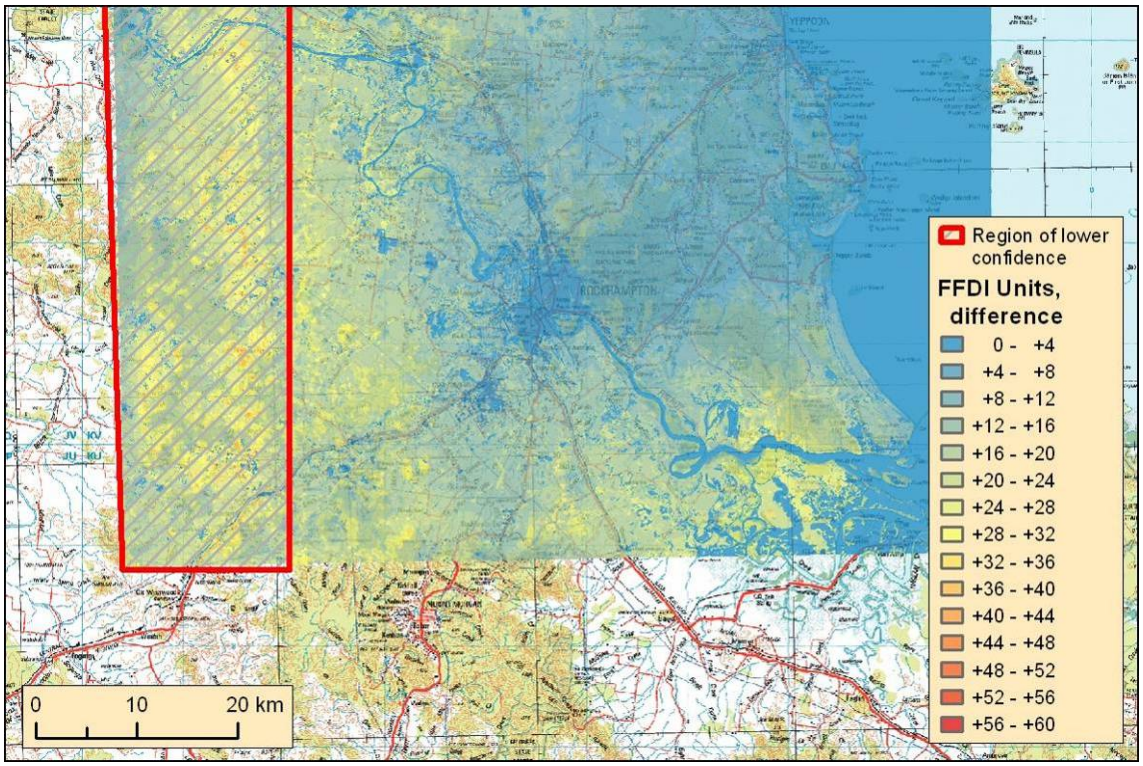

Appendix Figure B.22. Bushfire hazard difference – 2090 50 year ARI minus current-climate 50 year ARI.

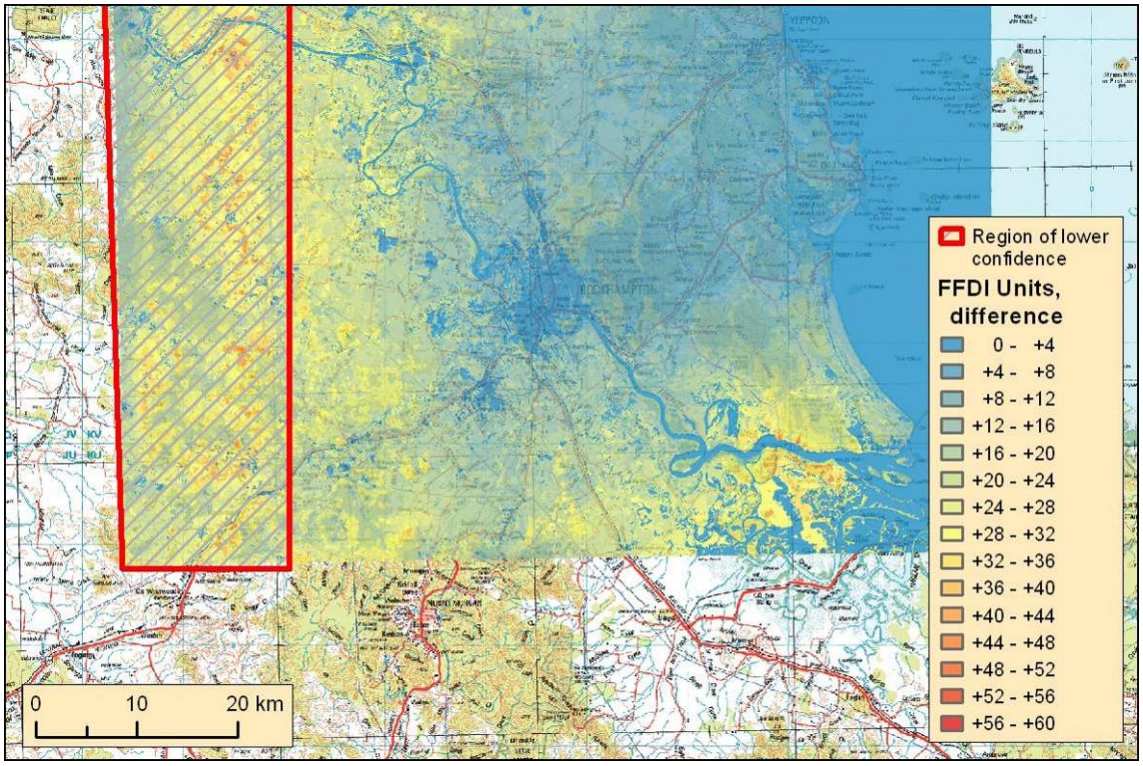

Appendix Figure B.23. Bushfire hazard difference – 2090 100 year ARI minus current-climate 100 year ARI.

The increase of FFDI for future climate is chiefly driven by the impact of climate change on the temperature. Little change was found in either the relative humidity or the wind speed compared to current-climate conditions. The vegetation and its condition are maintained at “current climate” status for the whole length of the simulations (see later for discussion of assumptions). The changes in the projected fire danger rating relative to current climate conditions were determined using the modelled data for temperature, relative humidity and wind speed for Rockhampton Airport. The results are summarised in Appendix Table B.5. The number of ‘Very High’ fire danger days generally increases -24 to +35% by 2050 and -44 to +92% by 2090 (A2 GHG scenario). For ‘Severe’ and ‘Extreme’ days the increase is -18 to +43% and -100 to +600% respectively for 2050 and -33 to +243% and +200 to +600% respectively for 2090.

Appendix Table B.5. No. of days per decade at Rockhampton Airport when the fire danger rating (based on FFDI) exceeds Very High, Severe and Extreme thresholds. Three climate change simulations (SIM1=ECHAM, SIM2=GFDL & SIM3=MIROC) employing the A2 emissions scenario are considered.

Period	VERY HIGH (FFDI > 25)			SEVERE (FFDI > 50)			EXTREME (FFDI > 75)		
Current Climate (Observed)	92			5			0.5		
	SIM1	SIM2	SIM3	SIM1	SIM2	SIM3	SIM1	SIM2	SIM3
Current Climate (Modelled)	68	52	89	4.25	3.5	4.5	0.25	0.5	0.25
2050 (A2 scenario)	72	70	68	3.5	5.0	5.0	1.5	0	0.5
2090 (A2 scenario)	116	100	50	6.0	8.5	3.0	1.5	1.0	0.5

B.6 Further Modelling

This initial modelling has the WRF weather variables at 270 m resolution and the vegetation at 30 m resolution. To improve the horizontal resolution of the simulations, to provide greater refinement in the final “Bushfire Hazard” maps, either or both the following techniques could be employed:

- Introduce modifiers to scale the wind down to 30 m resolution
- Undertake finer horizontal resolution modelling by utilising a tiled-grid approach within WRF.

The numerical weather modelling covered a smaller area than the case study region. New weather simulations could be run covering the whole case study area and the bushfire hazard map could be produced for the whole case study region.

Directional characteristics of historical severe fires (with regards to fire spread) could be exploited to inform the setback distance (currently 100 m buffer in all directions) and direction.

B.7 Assumptions – Current & Future Climate

In the numerical modelling that was the basis for this study, land cover (composition and extent) has been maintained at the same level for the whole simulation period (1971-2100), and does not vary with season or respond to year-to-year rainfall variability (i.e. vegetation considered as a static layer in all three models utilised). Significant episodic events such as tropical cyclones and tropical depressions, are known to cause significant vegetation growth and regeneration in the months following their passage through a region, but this does not influence either the vegetative growth or the drought factor used in the FFDI calculations. Finally, the impact of climate change on the vegetation, land use and land cover is not considered in this study. This may affect the results of this study in various ways. Not only is the bushfire hazard sensitive to changes in fuel, but changes in land cover and land-use directly affect the climate through impacts on energy and water balances of the surface (e.g. Feddema *et al.,* 2005; Cotton and Pielke, 2007; Ge *et al.,* 2007; Mahmood *et al.,* 2010). To improve reliability of results, future-climate models may need to incorporate a full range of ecosystem dynamics caused by urbanisation, agriculture, deforestation and episodic disturbances such as fires (Running, 2008).

This page is intentionally blank

Appendix C Storm Tide

Contents

Figures

Tables

C.1 Method

C.1.1 Current Climate

C.1.1.1 Storm tide modelling

The storm tide data was sourced from the National Storm Tide Database which, at the time of this study, was being developed by the University of Western Australia as part of the Haigh *et al.* (2012) study for the ACE CRC. The aim of this study was to estimate present day extreme total water level exceedance probabilities for Australia's coastline. The extreme water level considered was a combination of MSL, astronomical tide and storm surge generated by both extra-tropical and tropical storm events. The modelling did not include the effects of wave setup or run-up and due to the coarse modelling grid, 10 km, the resulting ARI water heights are suited to the application at the open coast and not within estuaries (Haigh, pers comm.). The hydrodynamic model was forced with global tidal model and global meteorological fields, validated against 30 tide gauges with long records. The nearest validation gauges to Rockhampton were Mackay and Bundaberg, each being in the order of 300 km to the north and south respectively of Rockhampton.

The model results consist of points adjacent to the coastline (231 in the LGA and 45 in the study area) with attributes at each point defining storm-tide water level heights (MSL + tide + surge) for ARIs from 0.1 through to 10 000 years. Data was provided for extra-tropical and tropical storm events. The points on the Rockhampton Regional Council LGA coastline are shown in Appendix Figure C.1.

The national storm-tide modelling was undertaken concurrently with this study. At the time of carrying out the Rockhampton analysis the modelling was complete for the extra-tropical events, however the tropical storm tide modelling was incomplete; 5000 years of synthetic cyclone events had been processed with a further 5000 years yet to be completed.

Due to the large number of storm-tide data points off the Rockhampton Regional Council coastline, and the difficulty in analysing and visualising all 45 inundation depths for the study area, cluster analysis was carried out to identify statistically similar regions. This resulted in five distinct areas being identified within the Rockhampton Regional Council LGA. Area 4 and Area 5 (Appendix Figure C.1) were within the study area; these were previously referred in the summary report (Storm tide section p23) as Area A and B respectively.

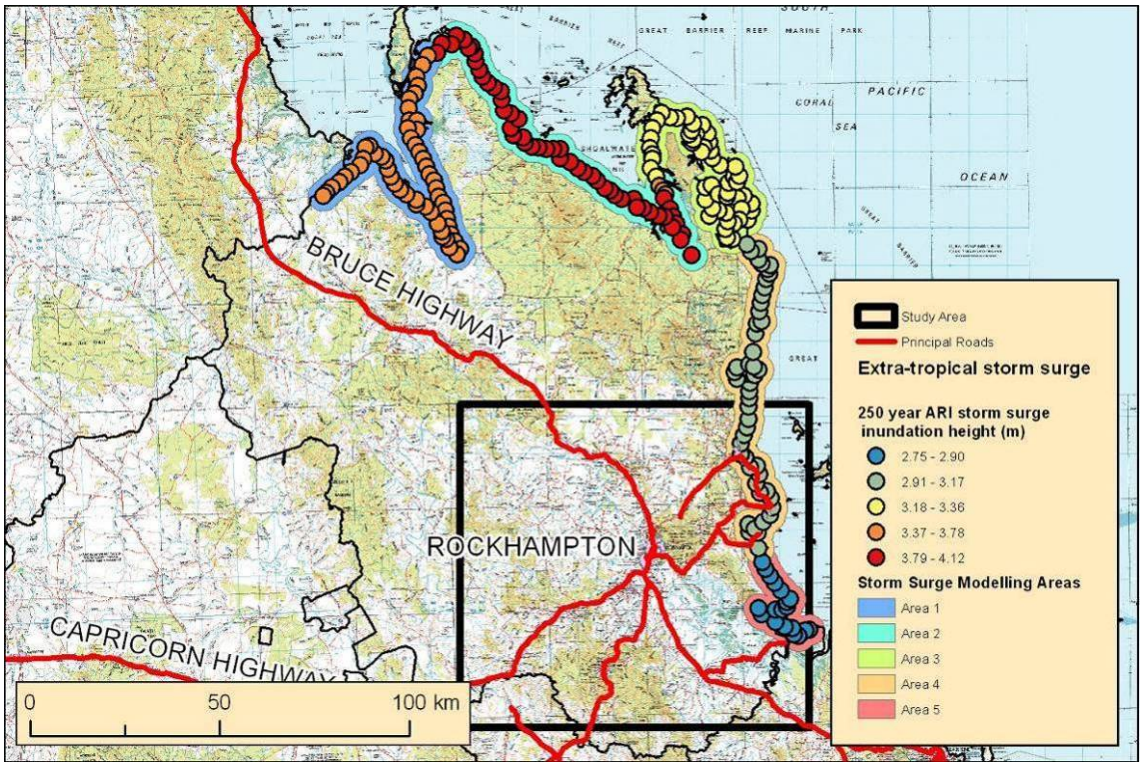

Appendix Figure C.1. Storm tide modelling results for Rockhampton (250 year ARI inundation depth (m))

C.1.1.2 Cluster analysis

Pattern investigation of the storm tide data indentified five cluster areas within the Rockhampton Regional Council LGA (Appendix Figure C.2). Fortunately, the automatically allocated ID number (ObjectID) had been completed sequentially along the coastline so that spatially adjacent points have an adjacent ID number. The ObjectID therefore supported graphical investigation of spatial and attribute relationships via a scatter plot matrix (ObjectID vs. ARI water level heights) that confirmed clusters of water level heights for broadly every 100 km of coastline. The scatterplot matrices identify five distinct clusters as shown in Appendix Figure C.2 for the extra-tropical 250 year ARI inundation results. Appendix Figure C.3 shows the tropical cyclone storm tide 250 year ARI inundation points.

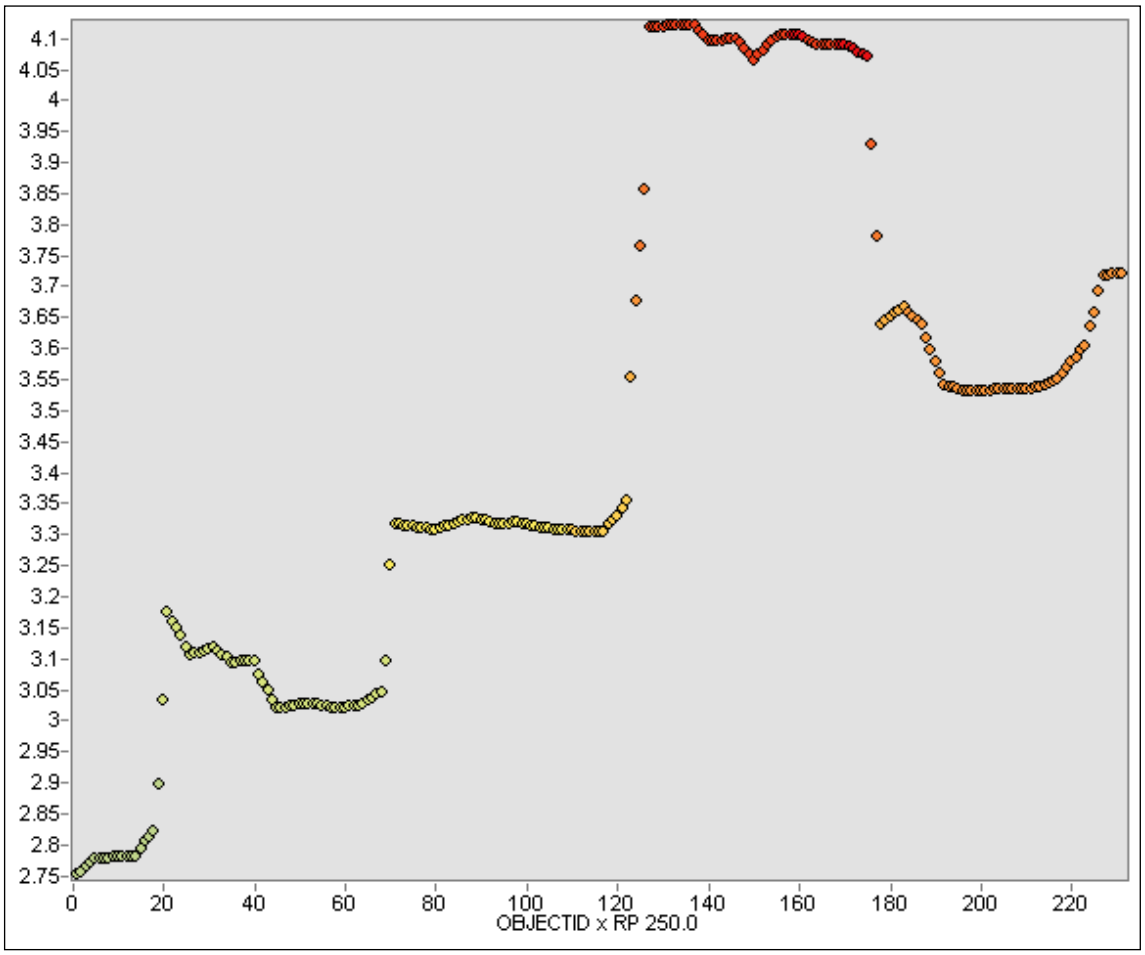

Appendix Figure C.2. Extra-Tropical Storm tide scatterplot matrix (250 year ARI). The X-axis is the ID field. The Y-axis is inundation depth above MSL (m).

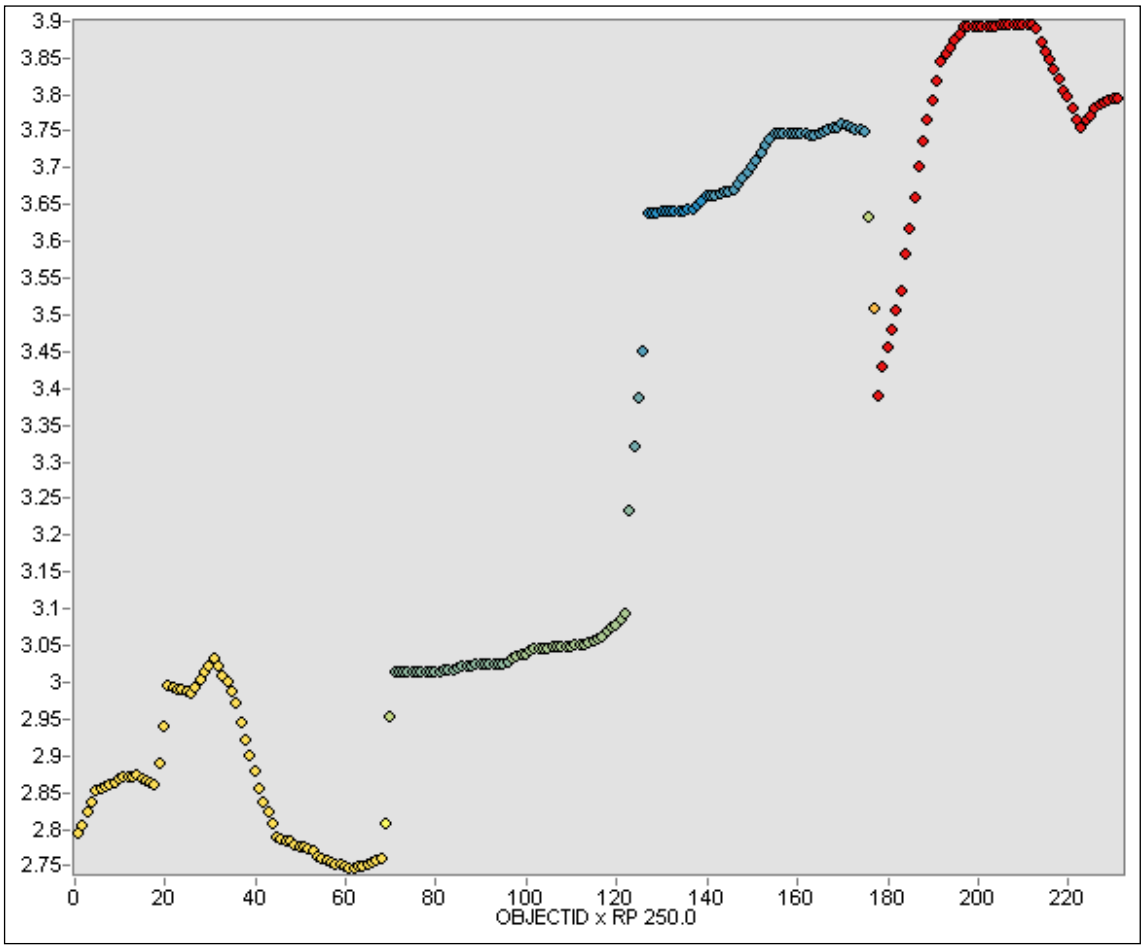

Appendix Figure C.3. Tropical Cyclone Storm tide scatterplot matrix (250 year ARI). The X-axis is the ID field. The Y-axis is inundation depth above MSL (m).

For each area and for extra-tropical and tropical events the mean, minimum, maximum and standard deviation were calculated. These are presented in the following figures (Appendix Figure C.4 to Appendix Figure C.7). The mean, minimum and maximum are plotted on the left Y-axis and the standard deviation is plotted on the right Y-axis.

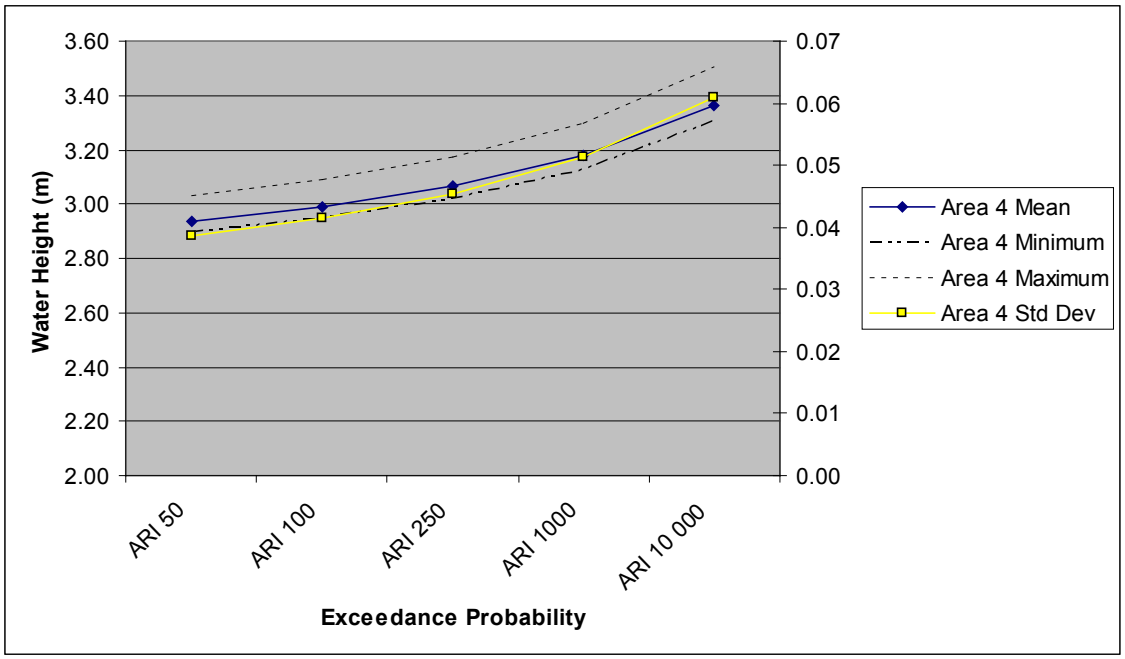

Appendix Figure C.4. Area 4 statistics – extra-tropical storm events.

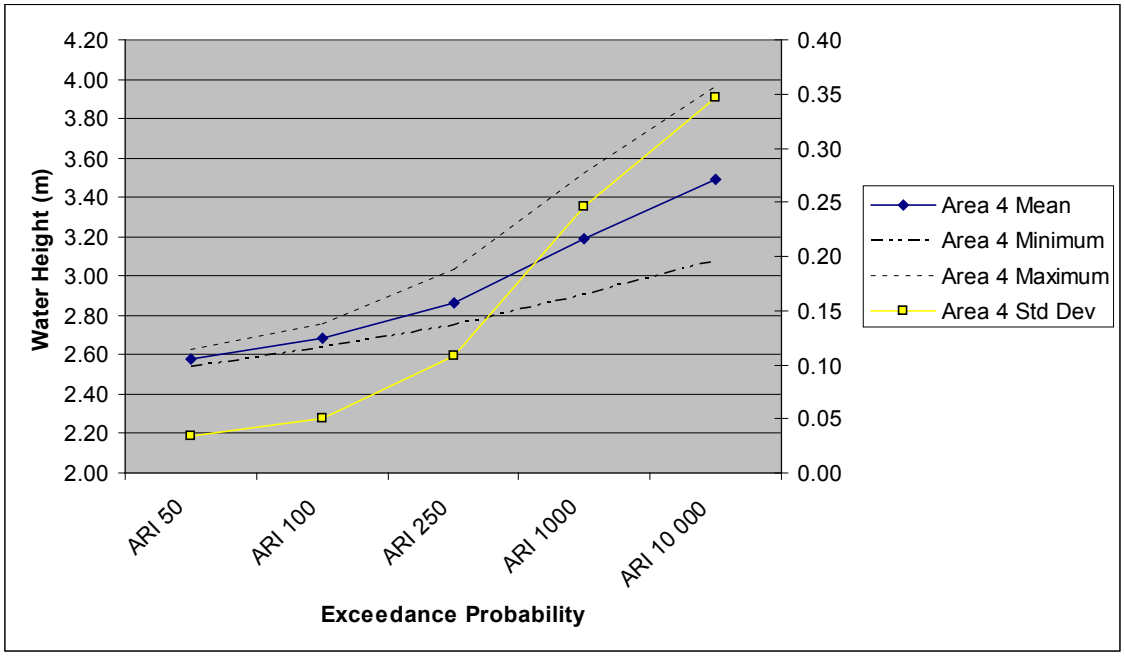

Appendix Figure C.5. Area 4 statistics – tropical storm events

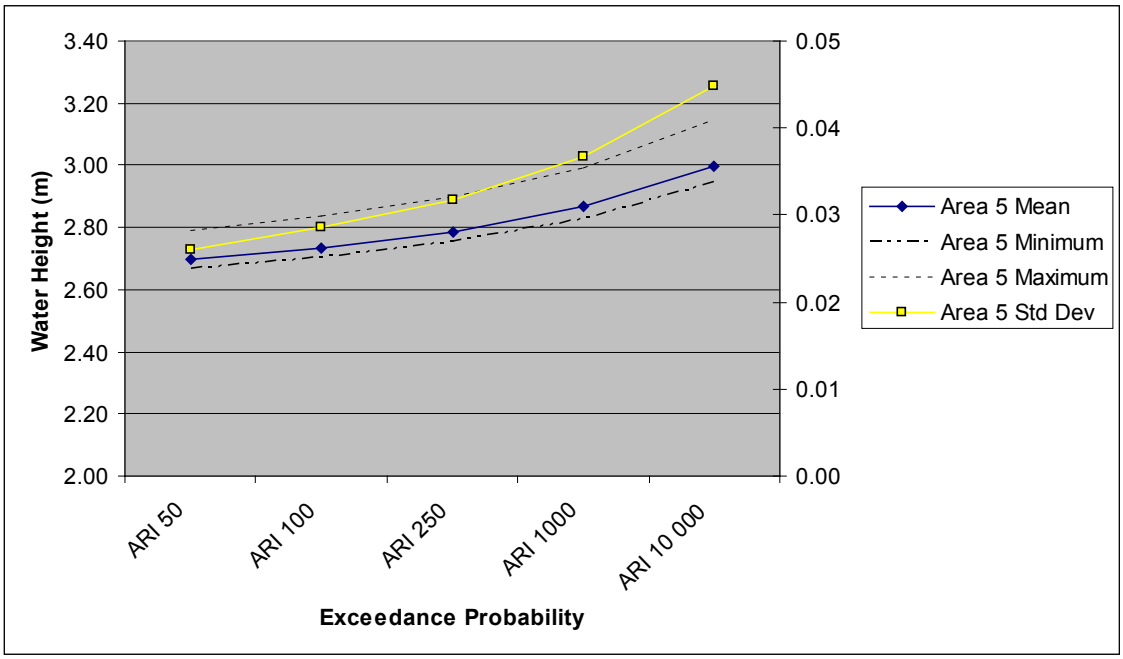

Appendix Figure C.6. Area 5 statistics – extra-tropical storm events.

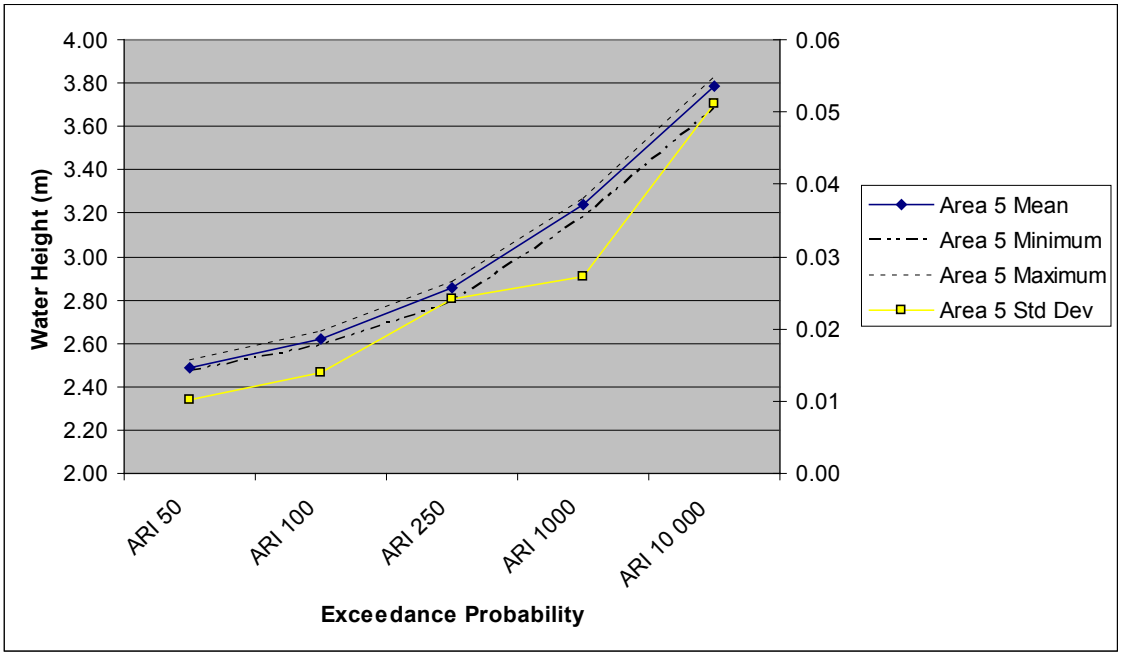

Appendix Figure C.7. Area 5 statistics –tropical storm events.

Within areas four and five the mean water level height for the ARI50, ARI100, ARI250, ARI1000 and ARI10 000) were used to identify the inundation extent on a high resolution (LiDAR[27] derived) DEM. The LiDAR surveys were:

- Gladstone, acquired 12/6/2009 to 3/7/2009
- Capricorn South, acquired 8/9/2009 to 19/10/2009
- Sunwater, acquired 6/10/2008 to 14/10/2008.

The data has a horizontal resolution of 1 m and a vertical accuracy of 0.15 m with a 67% confidence interval.

Inundation associated with the modelled water level heights was modelled using the 'bath-tub' method (Eastman, 1993). The application of this method considered the 'still-water' inundation level and not the increase in water height due to wave setup or wave run-up on the inundation extent as this was not factored into the Haigh *et al.* (2012) study. The spatial queries were carried out using a python geoprocessing script to identify elevation raster cell values being equal to or less than the storm tide water heights. For each ARI the hazard map shows the inundation extent for the mean storm-tide water height. The results have been clipped to within 4 km of the coastline in order to limit overestimation of inundation within estuaries. The full extent of the inundation will be provided to the Rockhampton Regional Council as they may prove useful in comparing the results of this method to any localised hydrodynamic storm-tide modelling undertaken in the future.

The mean inundation levels for Areas 4 and 5 are shown in Appendix Table C.1

Appendix Table C.1. Mean storm tide inundation water heights (m above AHD)

Sea-Level	Surge Type	Area	50 year ARI	100 year ARI	250 year ARI	1000 year ARI	10 000 year ARI
0 m (current climate)	Extra-Tropical	Area 4	2.93	2.99	3.07	3.18	3.36
0 m (current climate)	Extra-Tropical	Area 5	2.70	2.74	2.79	2.87	3.00
0 m (current climate)	Tropical	Area 4	2.58	2.68	2.86	3.19	3.49
0 m (current climate	Tropical	Area 5	2.49	2.62	2.85	3.24	3.79

C.1.2 Future Climate

C.1.2.1 Storm tide modelling

The ACE CRC study (Haigh *et al.,* 2012) did not undertake any future-climate modelling. Therefore, the sea-level rise scenarios, as described in the sea-level rise section (p133), were combined with the current-climate storm-tide assessment (Appendix Table C.1), to model future-climate storm-tide hazard (Appendix Table C.2). This method has also been applied by the ACE CRC within the Canute

[27] Light Detection and Ranging

Sea Level Calculator[28] which provides a user interface to identify combined current-climate storm tide and sea-level rise around Australia for extra-tropical storms only.

Spatial queries were completed, as described in the current-climate storm-tide modelling section, for each of the water heights shown in Appendix Table C.2.

Appendix Table C.2. Storm tide plus sea-level rise scenario water heights (m AHD).

Sea-Level Rise	Surge Type	Area	50 year ARI	100 year ARI	250 year ARI	1000 year ARI	10 000 year ARI
+ 0.3 m (QLD 2050)	Extra-Tropical	Area 4	3.23	3.29	3.37	3.48	3.66
+ 0.3 m (QLD 2050)	Extra-Tropical	Area 5	3.00	3.04	3.09	3.17	3.30
+ 0.3 m (QLD 2050)	Tropical	Area 4	2.88	2.98	3.16	3.49	3.79
+ 0.3 m (QLD 2050)	Tropical	Area 5	2.79	2.92	3.15	3.54	4.09
+ 0.5 m (QLD 2070)	Extra-Tropical	Area 4	3.43	3.49	3.57	3.68	3.86
+ 0.5 m (QLD 2070)	Extra-Tropical	Area 5	3.20	3.24	3.29	3.37	3.50
+ 0.5 m (QLD 2070)	Tropical	Area 4	3.08	3.18	3.36	3.69	3.99
+ 0.5 m (QLD 2070)	Tropical	Area 5	2.99	3.12	3.35	3.74	4.29
+ 0.8 m (QLD 2100)	Extra-Tropical	Area 4	3.73	3.79	3.87	3.98	4.16
+ 0.8 m (QLD 2100)	Extra-Tropical	Area 5	3.50	3.54	3.59	3.67	3.80
+ 0.8 m (QLD 2100)	Tropical	Area 4	3.38	3.48	3.66	3.99	4.29
+ 0.8 m (QLD 2100)	Tropical	Area 5	3.29	3.42	3.65	4.04	4.59
+ 1.1 m (FED 2100)	Extra-Tropical	Area 4	4.03	4.09	4.17	4.28	4.46
+ 1.1 m (FED 2100)	Extra-Tropical	Area 5	3.80	3.84	3.89	3.97	4.10
+ 1.1 m (FED 2100)	Tropical	Area 4	3.68	3.78	3.96	4.29	4.59
+ 1.1 m (FED 2100)	Tropical	Area 5	3.59	3.72	3.95	4.34	4.89

[28] http://canute2.sealevelrise.info/slr/Important%20Information

C.2 Results

C.2.1 Current Climate

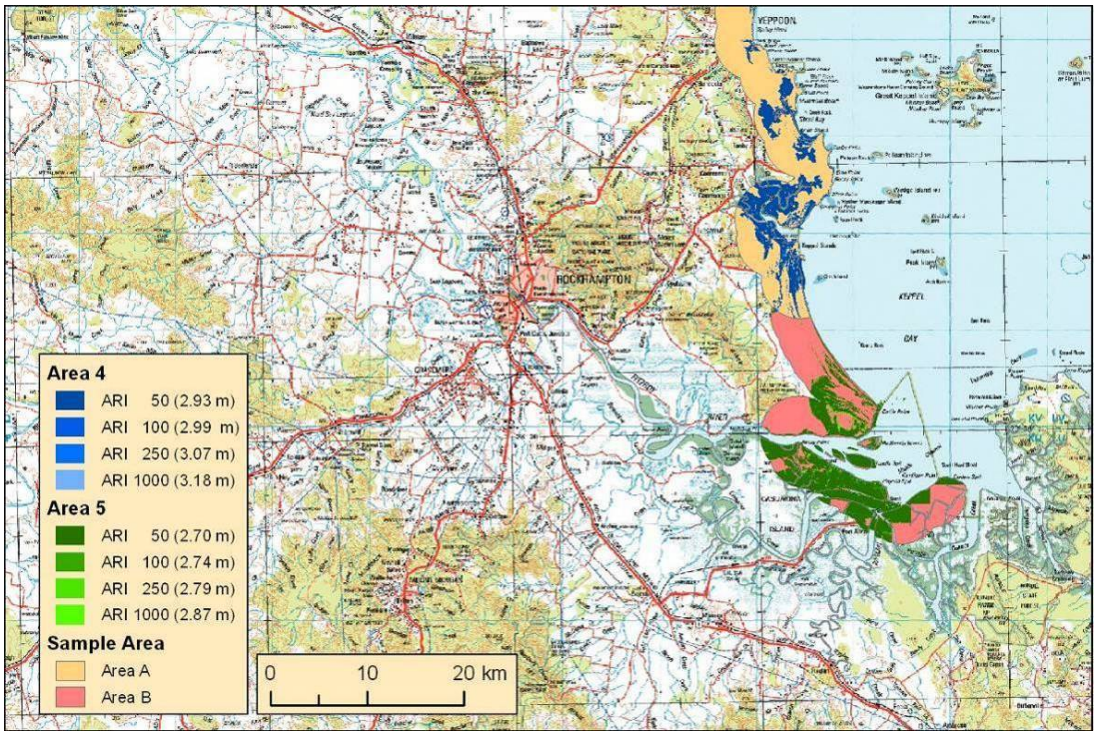

Appendix Figure C.8. Extra-tropical storm tide inundation.

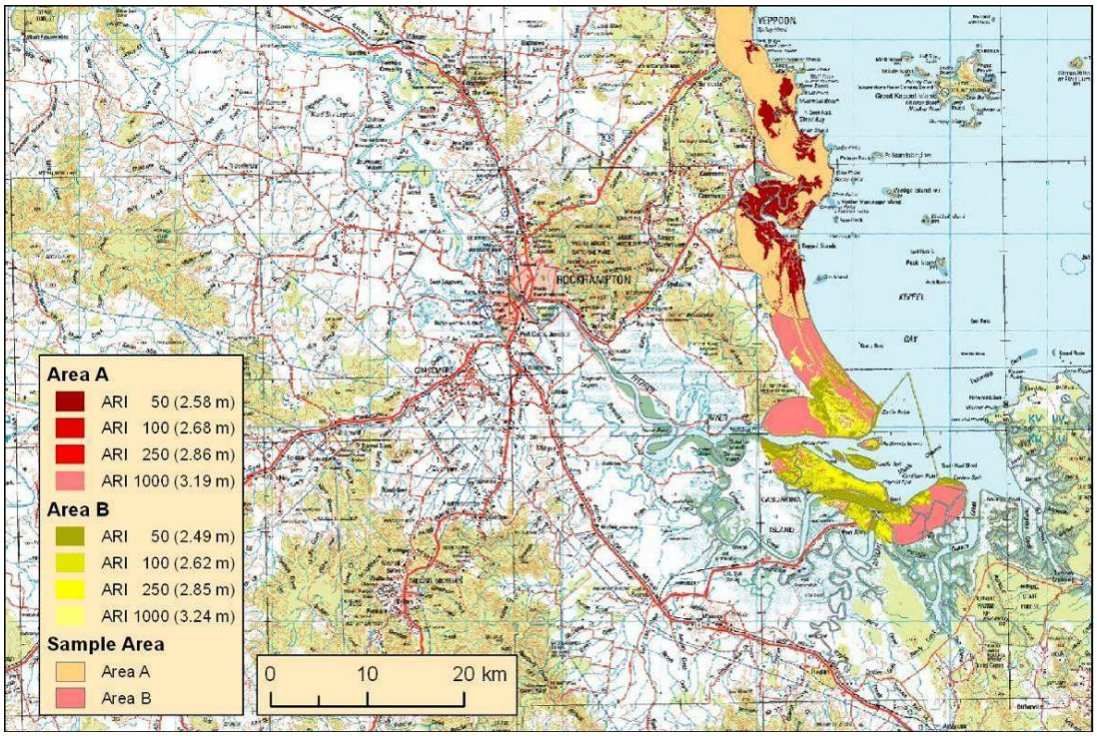

Appendix Figure C.9. Tropical cyclone storm tide inundation.

C.2.2 Future Climate

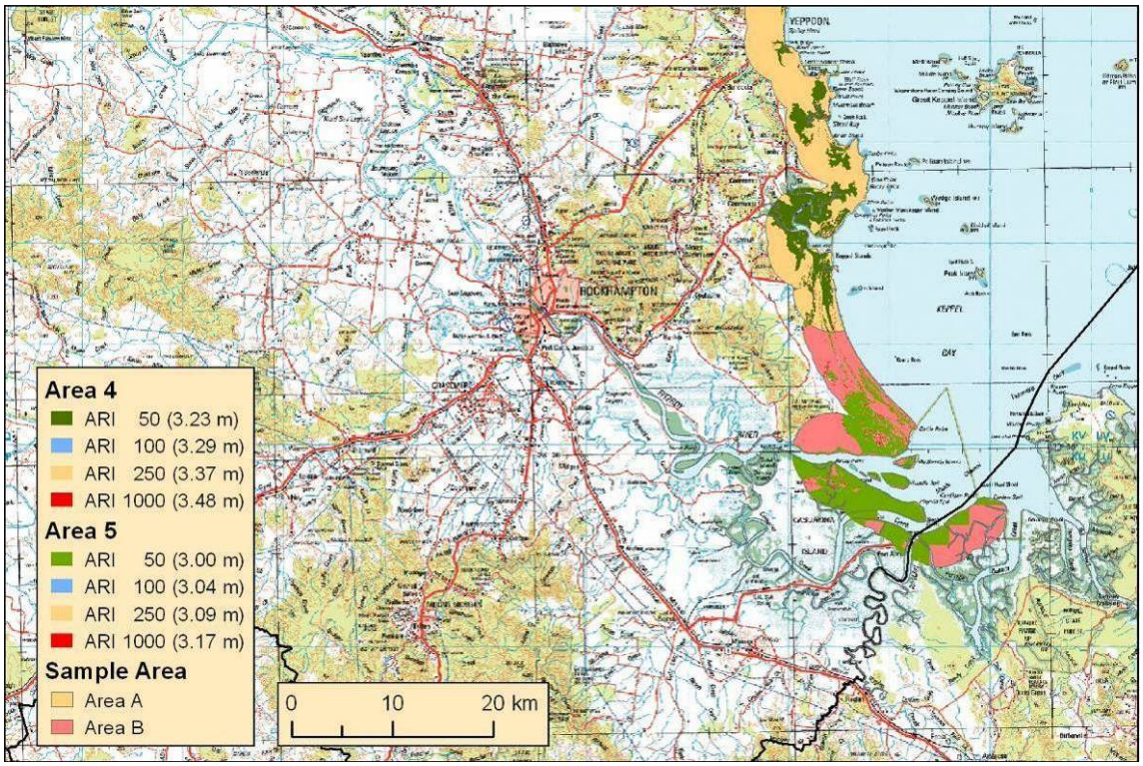

Appendix Figure C.10. 2050 sea-level rise (+0.3 m) combined with extra-tropical storm tide inundation.

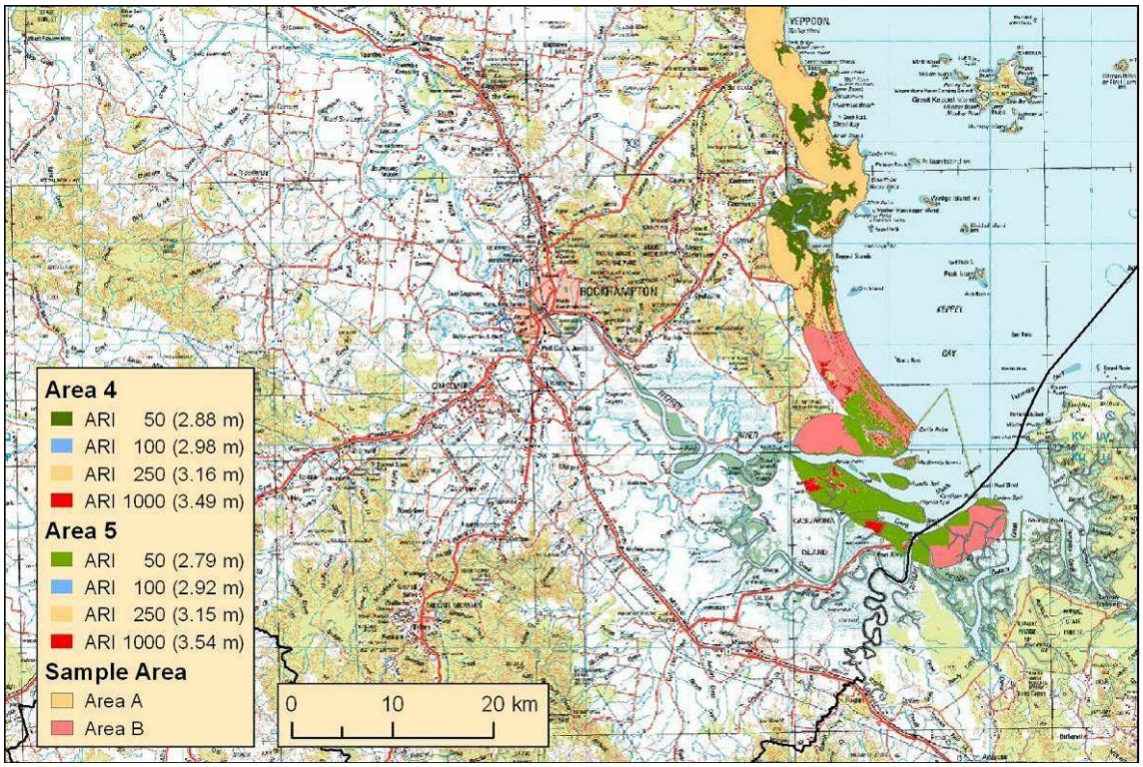

Appendix Figure C.11. 2050 sea-level rise (+0.3 m) combined with tropical storm tide inundation.

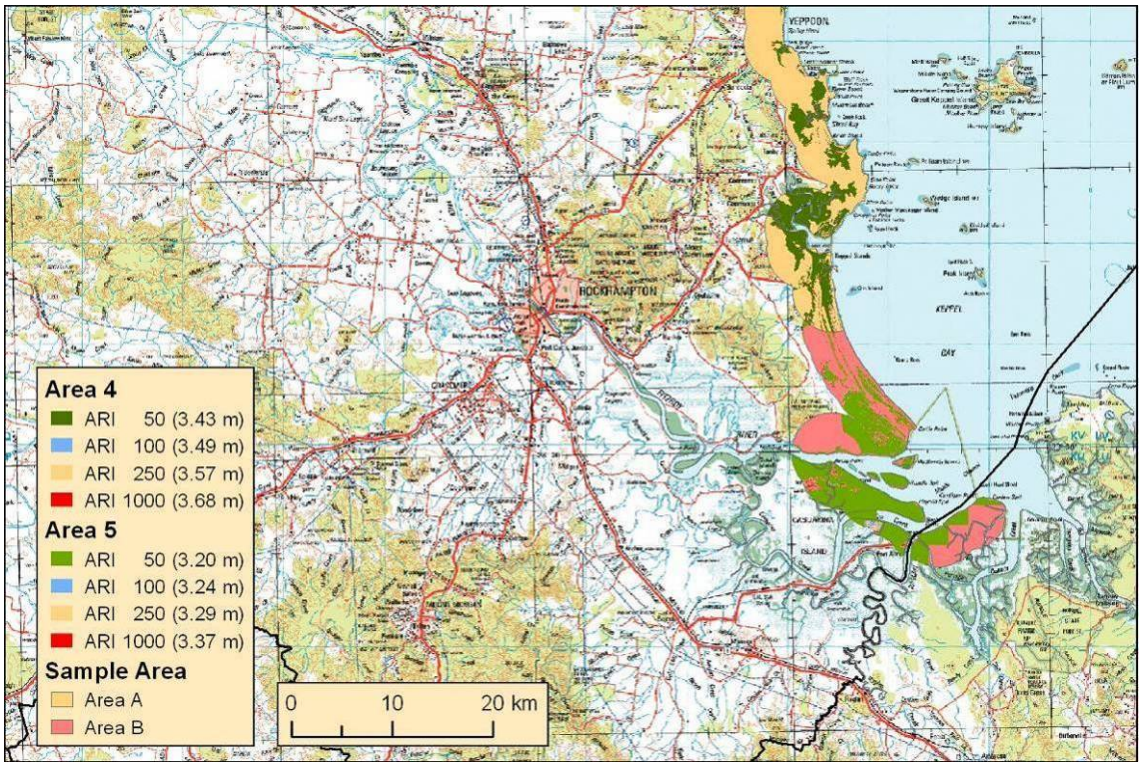

Appendix Figure C.12. 2070 sea-level rise (+0.5 m) combined with extra-tropical storm tide inundation.

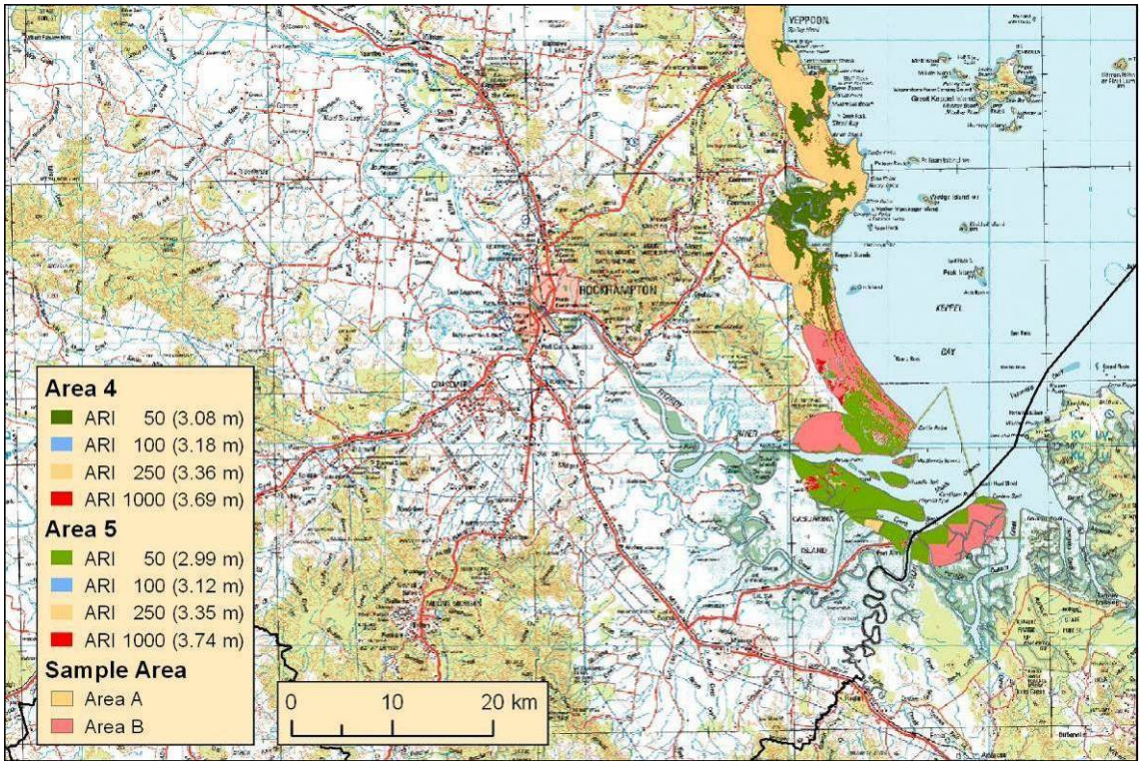

Appendix Figure C.13. 2070 sea-level rise (+0.5 m) combined with tropical storm tide inundation.

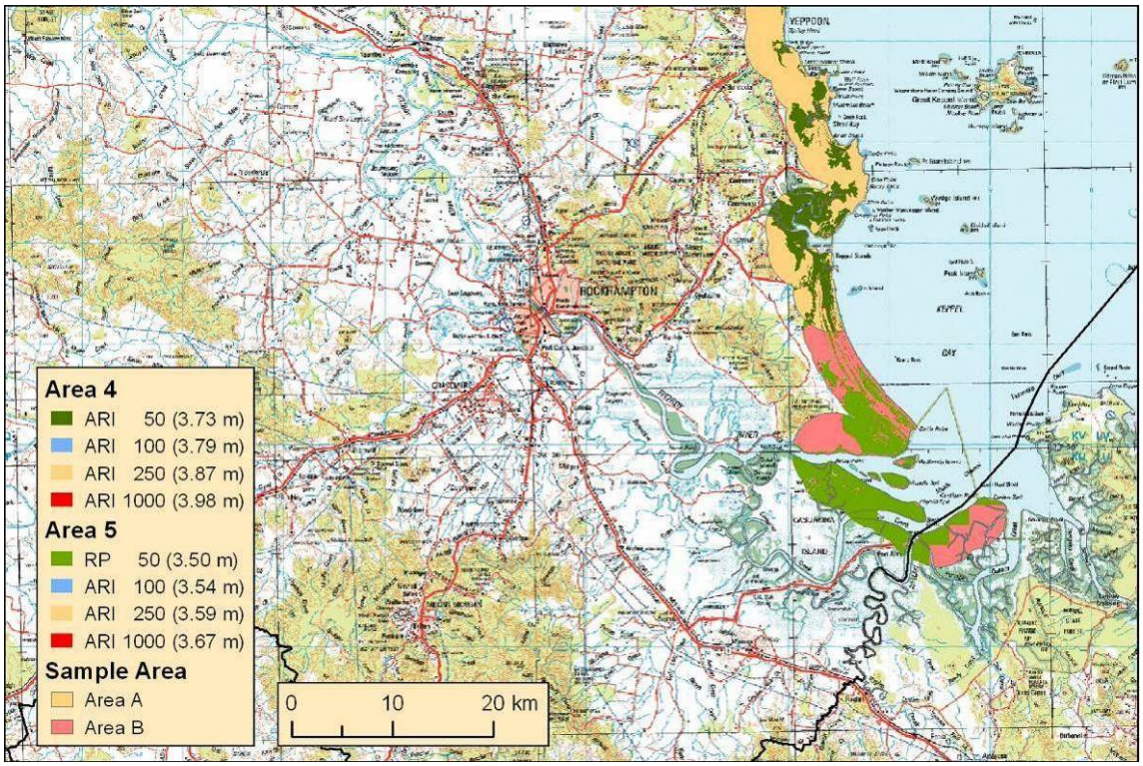

Appendix Figure C.14. 2100 sea-level rise (+0.8 m) combined with extra-tropical storm tide inundation.

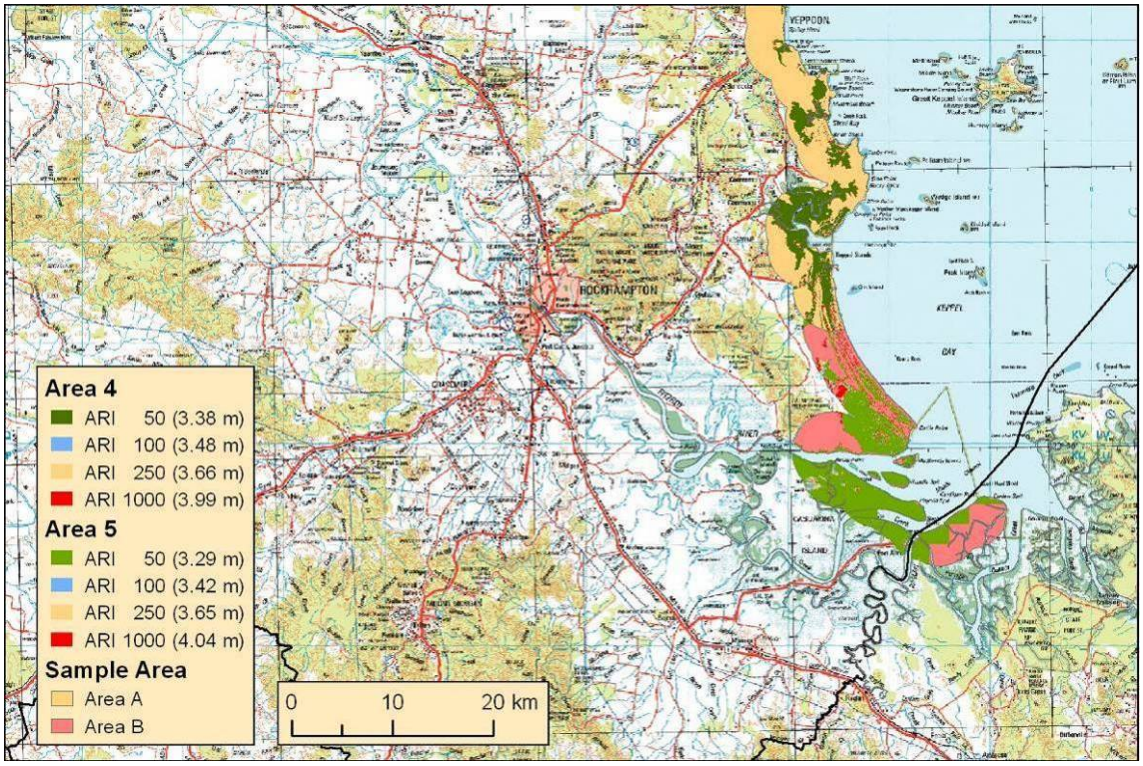

Appendix Figure C.15. 2100 sea-level rise (+0.8 m) combined with tropical storm tide inundation.

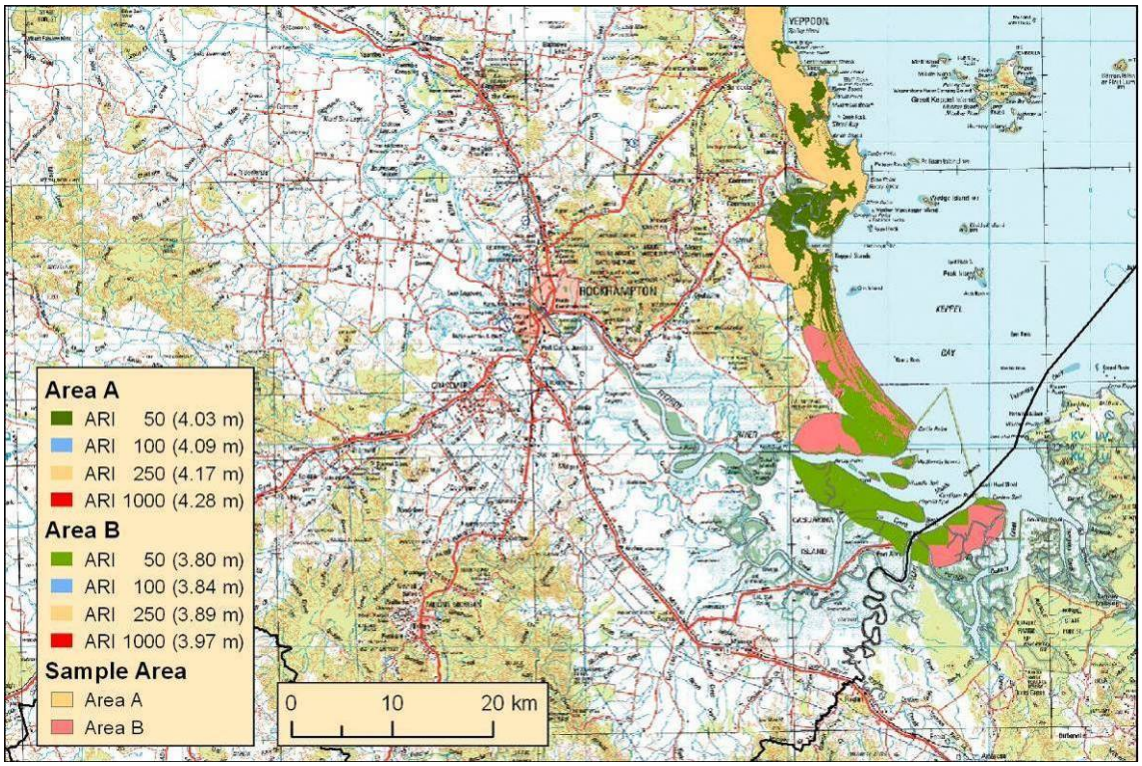

Appendix Figure C.16. 2100 sea-level rise (+1.1 m) combined with extra-tropical storm tide inundation.

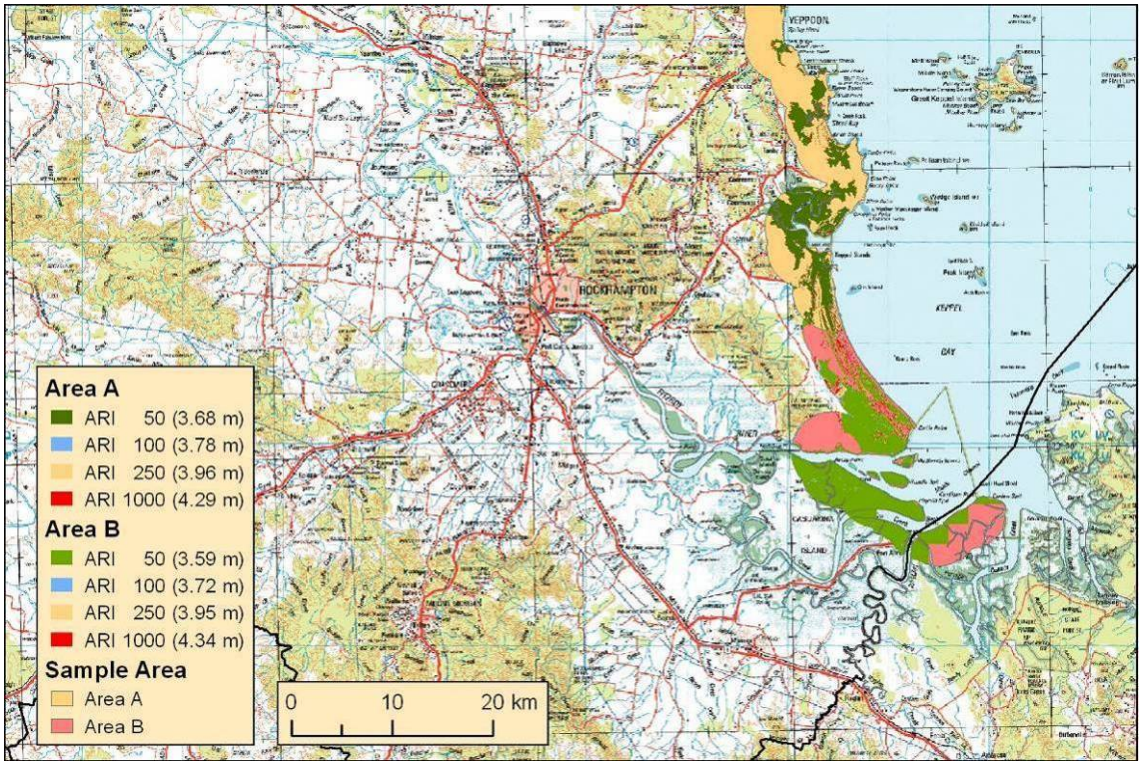

Appendix Figure C.17. 2100 sea-level rise (+1.1 m) combined with tropical storm tide inundation.

C.3 Discussion

C.3.1 Current Climate

Analysis of the current-climate area inundated revealed that there is only a relatively small increase in extent (+1% to +3%) with increasing inundation heights with ARI for the extra-tropical storm tide. There is a larger extent increase (+5% to +6%) for tropical storm tide in Area 4. The impact is largest for tropical cyclone storm tide for Area 5 with a range of +13% to +50%. This is caused by:

- the relatively low height of the ARI 50 event (2.49 m) for Area 5 tropical cyclone storm tide inundation
- the topography is relatively flat in Area 5, as compared with Area 4, due to the mouth and floodplain of the Fitzroy River
- the inundation height increment between adjacent ARIs is larger for tropical cyclone storm tide (+0.1 to +0.39 m) as compared with extra-tropical storm tide (+0.06 to +0.11 m).

The comparison is shown graphically in Appendix Figure C.18. Only with the recent availability of high-resolution DEMs, derived from LiDAR, has such small inundation height variation been able to be tested with accuracy (+/- 0.15 m).

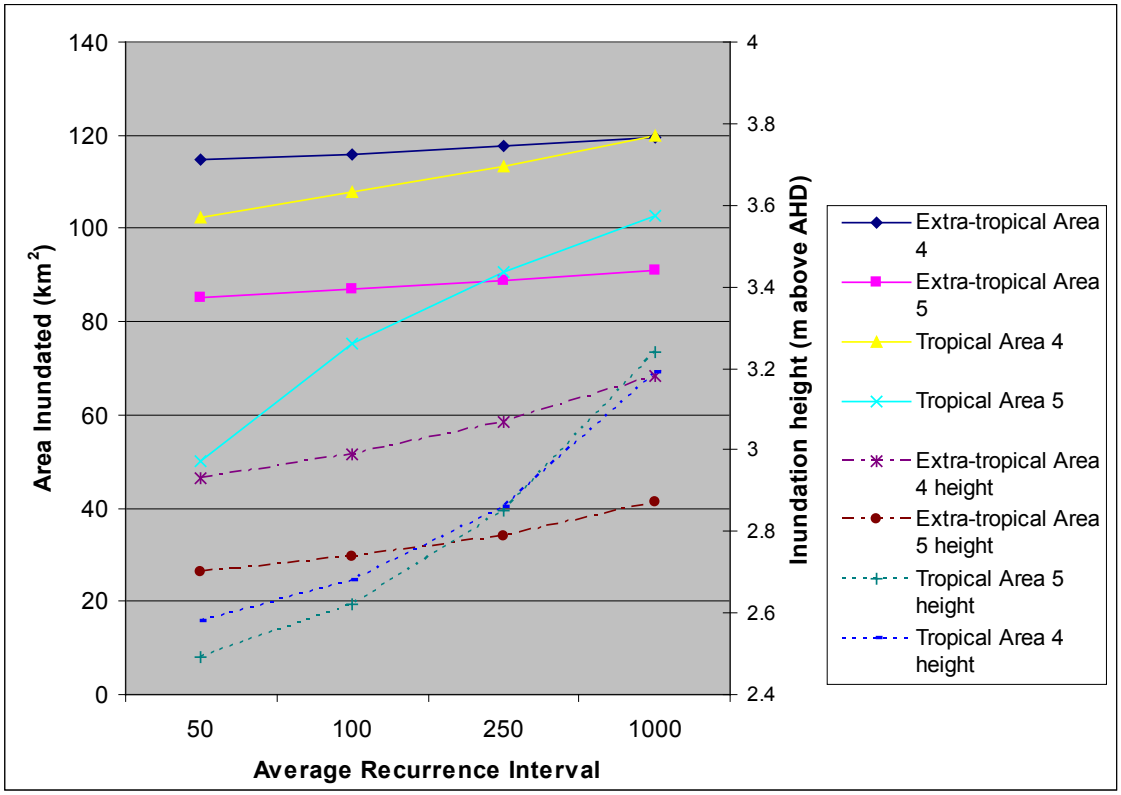

Appendix Figure C.18. Current-climate storm tide inundation area (tropical and extra-tropical). Area is plotted against the primary Y-axis and inundation height is plotted against the secondary Y-axis.

C.3.1.1 Limitations

Limitations within the method used include the:

- tropical cyclone simulation was not complete at the time of the inundation analysis
- averaging of the inundation heights to group inundation areas
- tide used in the storm tide modelling is different to that of the sea-level rise analysis (See the Sea-level Rise section, p31)
- bath-tub method does not consider hydrodynamic forcing, nor topographic barriers
- Rockhampton MSL differs from AHD[29].
- MSL varies at Rockhampton by ~ 0.3 m with greatest cycle in Jan/Feb/March, see Haigh *et al.*, 2012.

At the time of the analysis, the tropical cyclone simulation had been completed for 5000 of the 10 000 years. Results of the completed tropical cyclone simulation may change the ARI inundation heights used in this study. However, this is unlikely to have a significant impact of the ARI values below 500 years.

The statistical method used to identify a single inundation height for similarly exposed spatially related areas (clusters) results in an average inundation height per cluster. As can be seen for each ARI inundation extent in Appendix Figure C.2 and Appendix Figure C.3 each cluster area contains a range of inundation heights including those that smoothly link cluster areas that may not be well represented by the mean value for the cluster. These outlying points will affect the resulting average inundation height values for the cluster and they may warrant specific attention to the immediate area they represent. This investigation, however, needs to also consider the uncertainty in the storm tide modelling, as discussed further below, to determine if further analysis is required.

As the ACE CRC study was a probabilistic study, the inundation heights include a tide level from a modelled tidal sequence. These tides were modelled with a check against validation sites around Australia for the year 1995; Mackay and Bundaberg were the closest validation sites (Haigh *et al.,* 2012). The root mean square error for combined MSL, tide and surge modelled vs. observations were 0.45 m and 0.14 m for Mackay and Bundaberg respectively. The year 1995 was selected for the high record completeness. Without having the results of the tidal modelling for Rockhampton, the Maritime Safety Queensland data show that for 2012 Rockhampton has a tidal range peak of 2.66 m (AHD) and -1.57 m (AHD) being Mean High Water Springs and Mean Low Water Springs[30] respectively. In comparison the sea-level rise analysis in this study draws solely upon the Highest Astronomical Tide level (3.9 m, AHD) which is a theoretical maximum high water level based on astronomical conditions.

The bath-tub inundation method does not consider the hydrodynamic forces (e.g. wave setup and wave run-up) when estimating inundation extent. For example, the hydrodynamics of the storm approaching the coastline varies depending on the angle of approach and inlet morphology. In addition, the storm tide data consisted of points every 2 km along the coastline which, whilst advised

[29] http://www.msq.qld.gov.au/~/media/msqinternet/msqfiles/home/tides/tidal%20planes/semidiurnal_planes_2012.pdf

[30] http://www.msq.qld.gov.au/~/media/msqinternet/msqfiles/home/tides/tidal%20planes/semidiurnal_planes_2012.pdf

as being accurate for the open coast, may not apply within estuaries or macro-tidal areas. Hydrodynamic modelling would more accurately resolve the extent to which the inundation extends overland and specifically within the Fitzroy river, where the forces may be amplified or attenuated depending on the approach of the storm with respect to Curtis Island for example.

Rockhampton is between two storm tide modelling validation points; approximately 300 km from each: Mackay and Bundaberg: 0.45 m and 0.14 m total RMSE respectively. Other uncertainty to consider is that of the DEM (+/-0.15 m) and the range of inundation heights that are considered in calculating the mean water height for each cluster.

C.3.2 Future Climate

Considering both storm tide areas and the four sea-level rise scenarios none of these water heights exceed the HAT + 1.1 m (5 m total) shown in the sea-level rise section.

The areal inundation extent increases with increasing inundation heights. When comparing neighbouring scenarios (e.g. current climate to the next scenario in time, QLD2050) the largest exposure area increase occurs when comparing the current-climate inundation area to that of the QLD2050 (+0.3 m) scenario (Appendix Figure C.19). The two largest increases are in Area 5: the tropical cyclone ARI50 (+101%) and the ARI100 (+27%) scenarios. This large increase in inundation extent is a function of the initial low inundation height within current climate (2.49 m and 2.79 m AHD respectively) and the fact that Area 5 encompasses the Fitzroy River mouth which is wide, flat and low-lying as compared to the topography of Area 4. Similar heights in Area 4 for tropical cyclone ARI50 and ARI100 (2.58 m and 2.68 m AHD respectively) only increase 16% and 9% respectively with the 0.3 m increase in inundation height for QLD2050 over current-climate storm-tide inundation. For the remainder of the scenario comparisons, the percentage increase and the range of increase is much more modest, although the Area 5 average increase is always greater than that for Area 4. Again, this can be attributed to the broad low-lying topography in Area 5 as compared with that of Area 4.

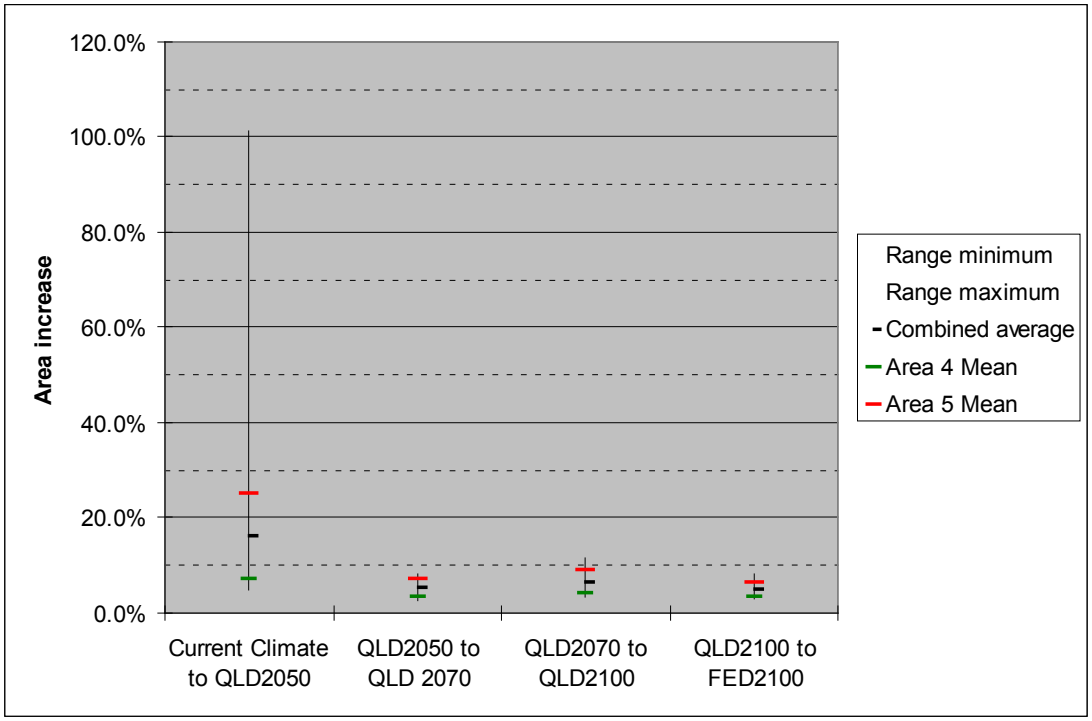

Appendix Figure C.19. Area inundation extent comparison. The vertical black line shows the percentage range of increase.

The hazard maps and digital spatial data provided with this report support more detailed analysis which identifies the following:

- Wetlands, lakes and some buildings are exposed to storm tide inundation in both current-climate and the 2100 future-climate scenario
- Yeppoon-Emu Park Road is exposed to storm tide hazard in the current climate. This can very nearly cut the road to the north of Emu Park. The road is cut by storm tide inundation in the 2100 future-climate scenario
- Keppel Sands Road is exposed to the impacts of storm tide in the 2100 future-climate scenario
- Bajool-Port Alma Road is exposed to storm tide inundation in current climate. It is increasingly exposed in the future climate with the banks of salt evaporators also being over-topped in the 2100 future-climate scenario.

C.3.2.1 Limitations

The limitations that apply to the current-climate storm-tide analysis similarly apply to future climate with the addition of the frequency and intensity changes that may occur in the future due to climate change.

Future-climate storm tide modelling is an area for potential further study as in this study sea-level rise has been combined with current-climate storm-tide hazard. As described in Appendix 3 of the "ClimateQ: towards a greener Queensland" (DERM, 2009), studies suggest a reduction in frequency of tropical cyclone events (e.g. Abbs *et al.,* 2006) and an increase in the number of Category 3 – 5 tropical cyclones on the east Australian coastline (Walsh *et al.,* 2004, Leslie *et al.,* 2007 and Abbs *et al.,* 2006). As more severe tropical storms are predicted to become more frequent the associated storm surge may also increase in frequency (i.e. occur more often) and this is not considered when only combining current-climate storm tide exceedance probability water heights and sea-level rise.

This page is intentionally blank

Appendix D Coastal Erosion

Contents

Figures

Tables

D.1 Introduction

For the purpose of this study, coastal erosion is defined as “shoreline recession due to sea erosion causing a permanent loss of land” (DERM, 2012a). This study does not consider the temporary erosion associated with storm events, after which the beach or section of coastline may recover naturally.

Keppel Bay was the subject of a series of major studies under the Cooperative Research Centre for Coastal Zone, Estuary and Waterway Management (Coastal CRC). The main objective of this work was to determine the spatial distribution and accumulation history of sediments in Keppel Bay derived from the Fitzroy River.

D.1.1 Regional setting

Keppel Bay represents the coastal margin of the Fitzroy River basin, the second largest modern sedimentary basin in Australia. The study area lies on the Tropic of Capricorn and is bounded to the north by Great Keppel Island and to the south by Curtis Island (Appendix Figure D.1). The 144 000 km^2 catchment of the Fitzroy River is topographically and geologically diverse, comprising over 100 different rock types within the Thompson Fold Belt, the New England Fold Belt, the Bowen Basin, the Surat Basin, and several other minor formations (Douglas *et al.,* 2005; Willmott *et al.,* 1984). The catchment was extensively vegetated with Brigalow scrub (Acacia harpophylla) before several phases of land clearing during the 19th and 20th century. Land use in the catchment is dominated by agriculture and coal mining.

D.1.2 Climate and oceanography

Due to the Australasian monsoon, the region experiences highly seasonal rainfall and prevailing easterly winds (Appendix Figure D.3). Rainfall is predominantly in the summer and temperatures range between a summer maximum of 32 °C (January) and a winter minimum of 9 °C (July). Large-volume flood events in the Fitzroy basin are produced by intense but short-lived rainfall events linked to summer monsoonal or cyclonic depressions. These floods inundate large areas of the floodplain and take considerable time to discharge through the Fitzroy River system into Keppel Bay (Devlin *et al.,* 2001; Kelly and Wong, 1996). The tides within Keppel Bay are semi-diurnal, and feature a spring tidal range of 5 m (macrotidal), with a neap tidal range of approximately half this (Hekel, 1980). The oceanography along the adjacent continental shelf is dominated by the southward flowing East Australian Current (EAC). Using sea surface drifters, Woodhead (1970) showed that the EAC is partly deflected into the Capricorn Channel forming a clockwise gyre (Appendix Figure D.3). A time-series dataset of NOAA-9 AVHRR satellite imagery has shown that the EAC follows the 200 m contour until it reaches the Capricorn Channel (Kleypas and Burrage, 1994). Annual variation in regional oceanographic conditions result in the EAC either following the slope contour westward along the shelf, or flowing directly south until it hits the shelf break near Fraser Island (Appendix Figure D.3). During periods of southward flow, the current tends to bifurcate, producing a southern current that continues along the coast and a northern component that becomes a cyclonic eddy within the Capricorn Channel. Satellite imagery also shows much cooler waters occur along the shelf edge and possibly the result of upwelling events that bring cooler water from depth onto the shelf, coolest in Hervey Bay. This cold upwelling water is considered to be important source of nutrients to the southern Great Barrier Reef and coastal region. The cool, nutrient-rich water extends as far north as Cape Clinton, and is probably transported by wind driven longshore currents. In addition, cold water

jets have been observed at Cape Clinton heading back into the Capricorn Channel (Kleypas and Burrage, 1994).

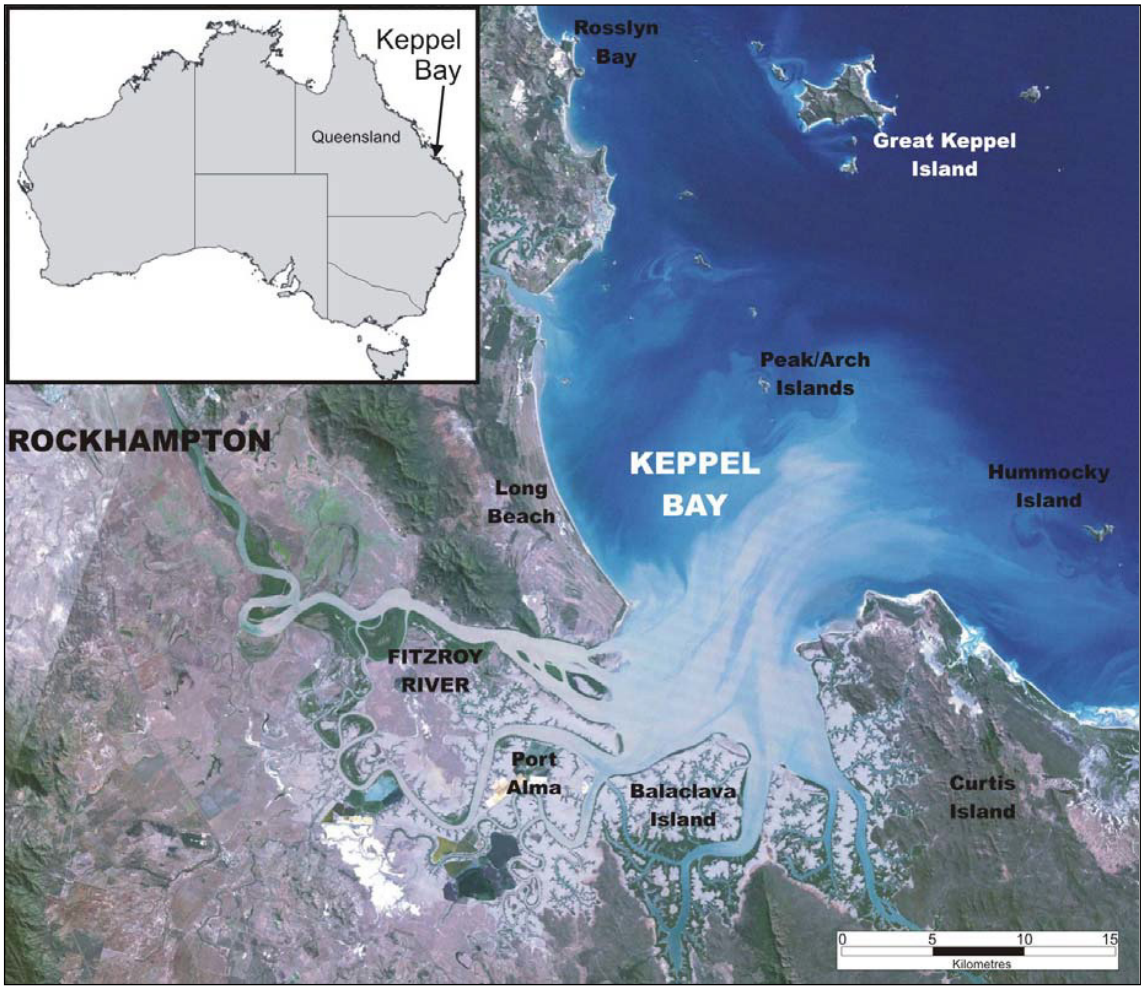

Appendix Figure D.1. Keppel Bay and the Fitzroy River on the coast of the south-east Queensland. The base map is a Landsat ETM+ image, acquired 24/5/2003, Copyright © Commonwealth of Australia, 2003 (Source: Ryan et al., 2009).

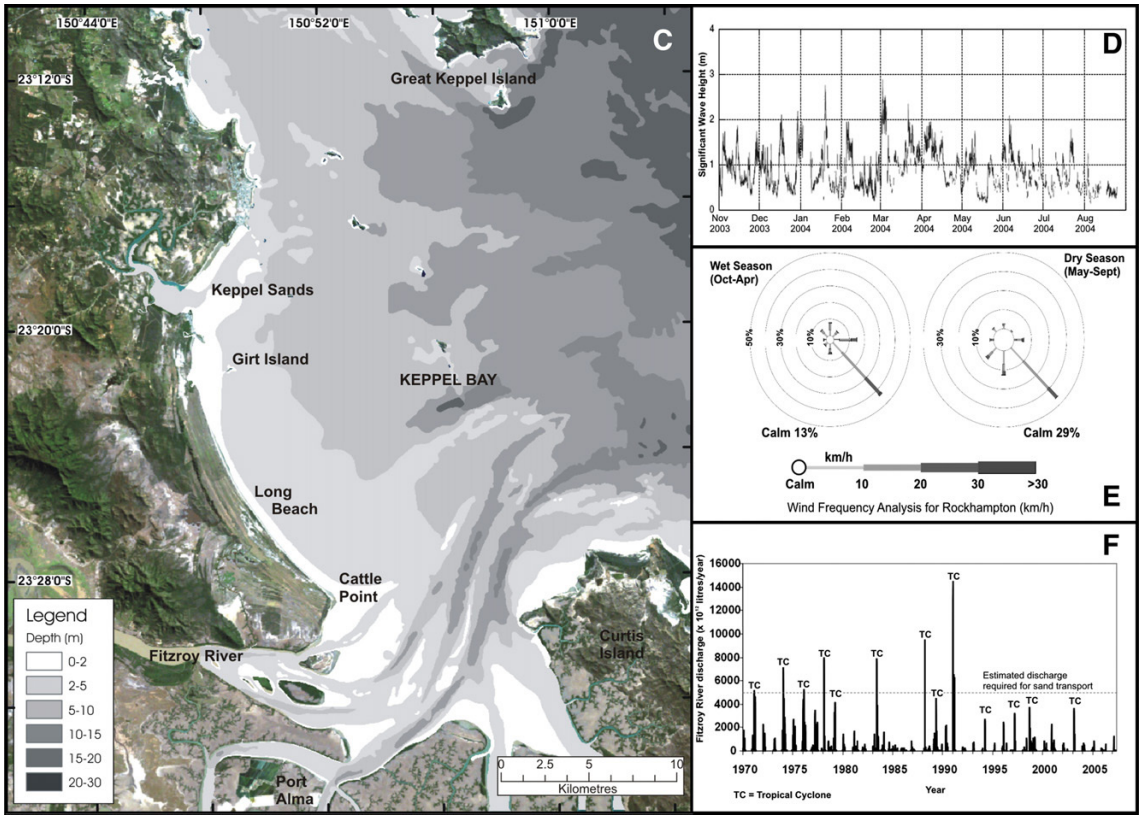

Appendix Figure D.2. The Fitzroy River estuary and Keppel Bay bathymetry. D.Wave heights recorded by a wave rider buoy in outer Keppel Bay (Queensland Environmental Protection Agency, 2005). E. Wind records for Rockhampton, 50 km W of Long Beach (Bureau of Meteorology). F. Fitzroy River discharge between 1970 and 2007. Also indicated is the discharge required for sand export to Keppel Bay (dashed line), and flood events produced by tropical cyclones (data from Queensland Department of Natural Resources and Water, Rockhampton) (source Brooke et al., 2008).

D.1.3 The Capricorn Channel and southern Great Barrier Reef

A major survey of the marine geology of the Capricorn Channel and region adjacent to Keppel Bay was undertaken by Marshall (1977), and identified high quartz and feldspar sediments in outer Keppel Bay and to the east of Great Keppel Island. These sediments were classified as terrigenous sands (in the north of Keppel Bay) and mixed marine and terrigenous sands (in the south of Keppel Bay).

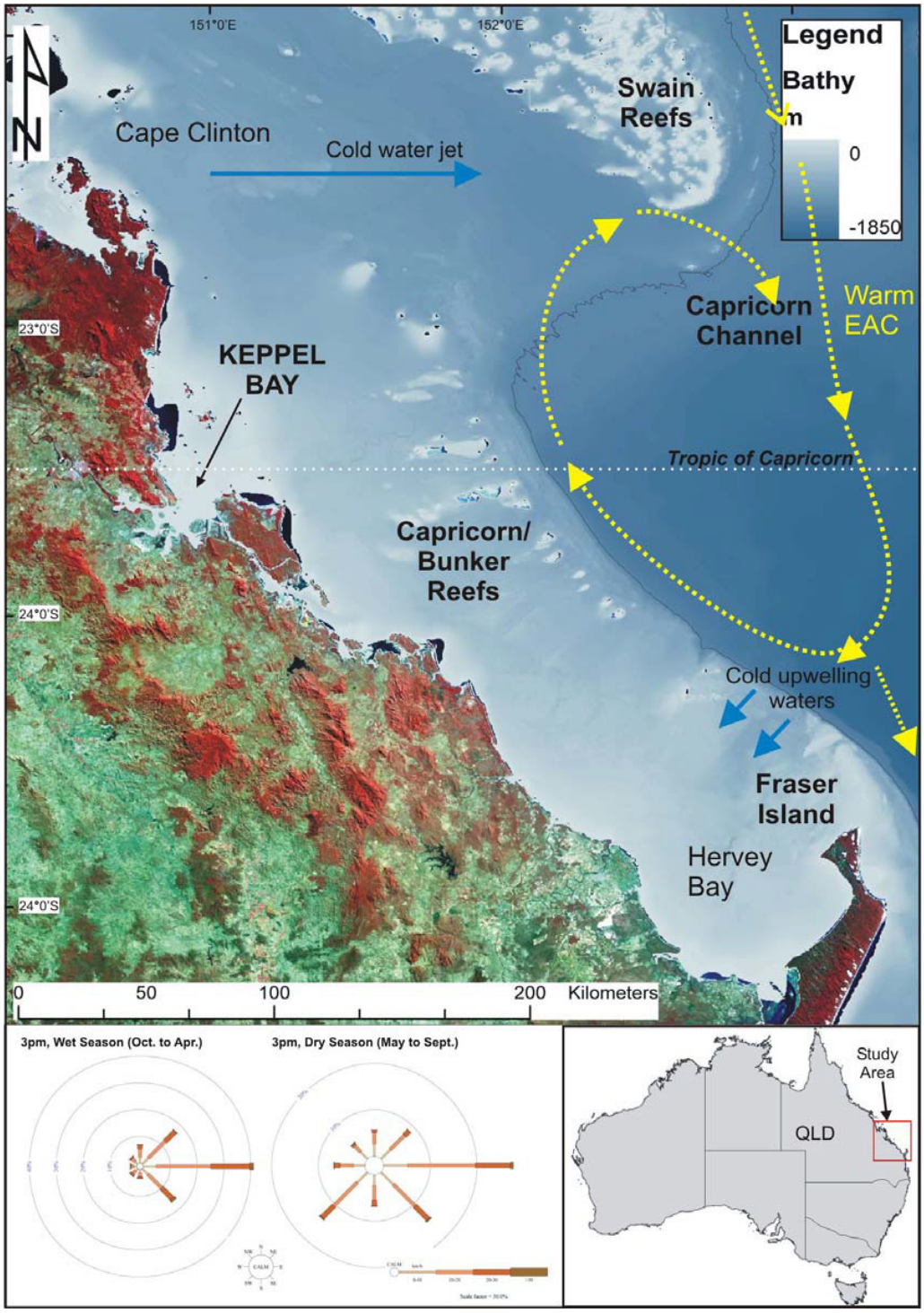

Appendix Figure D.3. Summary map of bathymetry, water masses and circulation in the study region, with the -120 m isobath indicated (Imagery: Landsat MSS, Copyright © Commonwealth of Australia). The unbroken black line indicates the 120 m isobath. Wind frequency analysis are provided for Rockhampton, 1939-2004, for the wet season (October to April, 3pm) and the dry season (May to September, 3pm; Bureau of Meteorology, June 2005). Bathymetry after Webster and Petkovic (2005) (source: Ryan et al., 2009).

Although the seabed of the Capricorn Channel is mainly flat, both symmetrical and asymmetrical sediment dunes comprising 90% quartz sand occur at a water depth of 60-80 m. These features were probably formed by tidal currents during a period of lower sea level (Marshall, 1977). Evidence of pre-Holocene shorelines with mangrove rootlets, a series of drowned reefal shoals and banks

extending northwest from the Capricorn Group of reefs, and ooids (16 800 cal. yrs BP) were also reported from depths of 100-120 m (Marshall and Davies, 1975; Yokoyama *et al.,* 2006). Maxwell channels cut to a base level of 64 m, corresponding to a Pleistocene low sea-level. These are probably the palaeochannels of the Mary, Burrum and Elliott Rivers (Marshall, 1977). Marshall (1977) also suggested that during the glacial lowstand, the Fitzroy River meandered northeast across the shelf before being diverted down the Capricorn Channel.

D.1.4 Geomorphology and bathymetry of Keppel Bay

Keppel Bay is a semi-protected oceanic embayment located south of the widest part of the Queensland continental shelf (Marshall, 1977; Searle, 1978). The Capricorn coastal area bordering Keppel Bay is a drowned landscape, with prominent rocky headlands that divide low-lying stretches of beach dunes and strandplains. A previous geological investigation of Keppel Bay by Searle (1978) using a 'boomer' seismic profiling system found evidence that significant quantities of sediment have accumulated in Keppel Bay since the late Tertiary. Evidence of the sub-aerial erosion of the Pleistocene surface was also noted. In addition, a relatively thick Holocene sediment wedge has been deposited adjacent to the Fitzroy River estuary, which becomes thinner to the north. Searle (1978) suggested that fine sediments originating from the Fitzroy River may be advected as far north as Corio Bay (20 km north of Yeppoon). The southern portion of the study area is bordered by the bedrock hills of Curtis Island and expansive low gradient salt flats, mangroves, and tidal creek networks in the Port Alma region (Appendix Figure D.4), which form the Casuarina Basin (Murray, 1980). Significant brine deposits occur below the extensive mudflats and supratidal lowlands near Port Alma, Casuarina Island, and Balaclava Island (Laycock, 1980; Flood and Walbran, 1986). Numerous smaller rocky islands exist within the bay, most notably Humpy, Pelican, Divided and Wedge Islands in the north, and Girt, Quartz, Arch, Peak and Hummocky Islands in the south and south-east. Keppel Bay is bordered to the west by Long Beach, an elongate beach and beachridge plain that extends northwards toward a series of rocky headlands.

D.1.5 Modern sediment Transport in Keppel Bay

Keppel Bay contains both coarse (bedload) sediment and a proportion of the fine fraction of material deposited by the Fitzroy River (suspended sediment and nutrient inputs into and out of Keppel Bay have been examined in Radke *et al.,* 2005). A comprehensive study of the modern sediments and hydrodynamics of the southern Queensland coast including Keppel Bay was undertaken by the Queensland Government between 1976 and 1978 (Beach Protection Authority, 1979). The study found that large volumes (approximately 450 000 m^3 yr^{-1} - median grain size 150 µm) of quartzose sand eroded from the Fitzroy River catchment are transported into Keppel Bay during flood events. This sediment is reworked northwards and onshore by advection which is the result of the combined effects of local waves and tidal currents on seabed sediments. Cyclones can induce short periods of shoreline erosion from which the coast quickly recovers under normal atmospheric and marine conditions. Extensive beach-ridge deposits indicate there has been a long-term positive sediment supply to the bay from the Fitzroy River (Brooke *et al.,* 2008).

The distribution of modern sediments in Keppel Bay indicates that river sediment is deposited by the Fitzroy River in the mouth of the estuary and in the southern section of the bay. The coarser sediment is subsequently reworked by advection to the north and onshore, where it accumulates in dunes and beach deposits (Appendix Figure D.4).

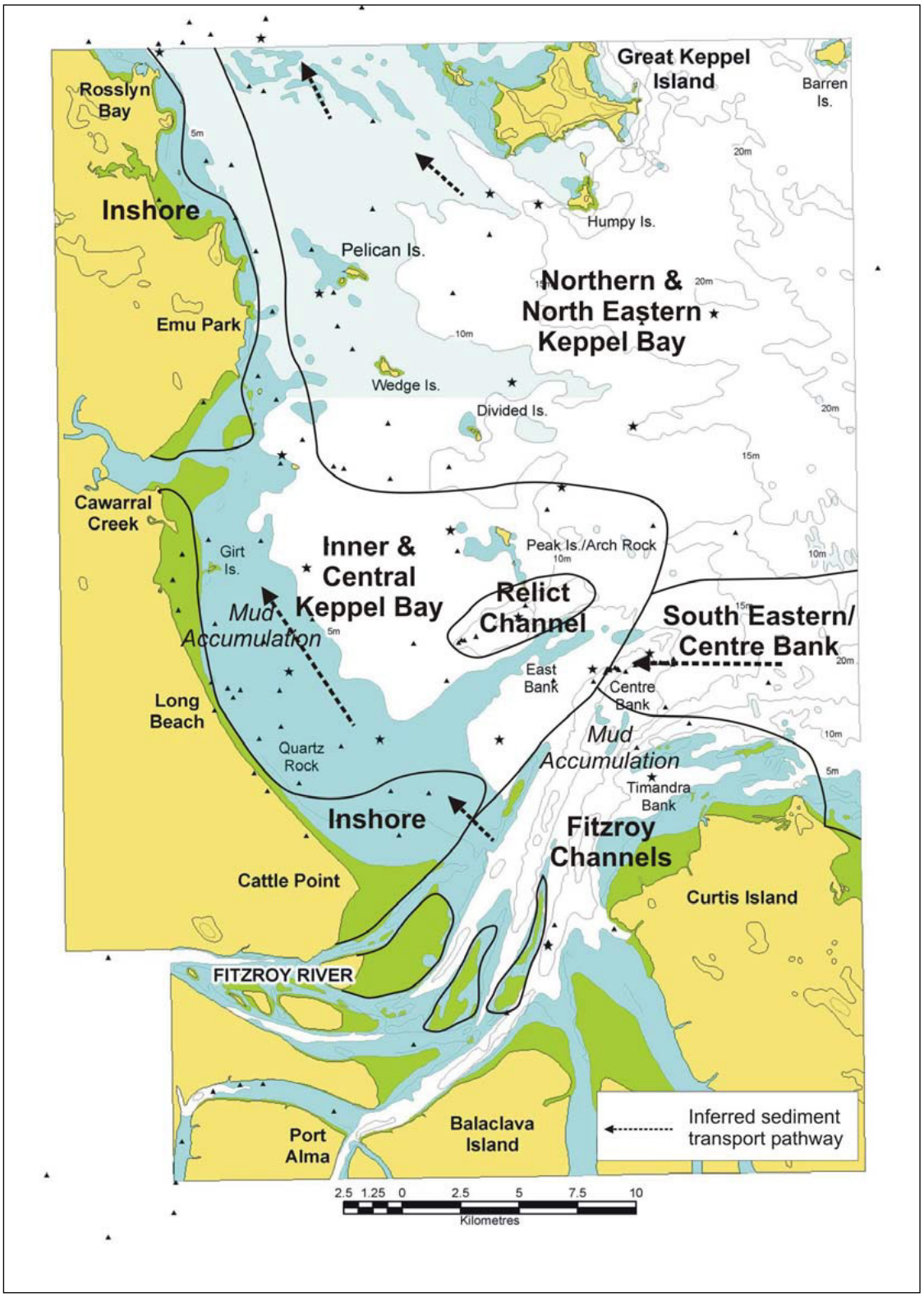

Appendix Figure D.4. Map of sediment facies and depositional regions in Keppel Bay, showing sediment transport pathways and areas of fine sediment accumulation.

D.2 Method

D.2.1 Current Climate

D.2.1.1 Spatial analysis

The current-climate erosion spatial extents (overlays) were determined using the Queensland Coastal Hazards Guideline (QCHG; DERM, 2012a). The guideline requires erosion prone area widths to accommodate both short-term and long-term erosion for a specific planning period. The current-climate erosion overlays reported here refer to short-term erosion prone areas only.

The extent of short-term erosion is determined by identifying the areas of the open coast already experiencing some degree of erosion, i.e. the presence of a sea wall or protective engineering structure, and areas where the dunes are substantially reduced by wave action. The erosion prone area is defined as the area bounded by the seaward limit of Queensland waters – Highest Astronomical Tide (HAT) and on land adjacent to coastal waters as:

- a line measured 40 m landwards of the plan position of HAT except where approved revetments (e.g. sea walls) exist in which case the line is measured 10 metres landwards of the upper seaward edge of the revetment, irrespective of the presence of outcropping bedrock.

The guideline makes further provision for the assessment of the erosion hazard based on the potential impact of a "design" storm[31]. Whilst not considered for current climate, these provisions were incorporated into the future-climate erosion overlays.

To assist in the identification of the existing erosion prone areas two series of historical aerial photography (captured on 05/1961 and 06/1964) were visually compared with the 2010 image mosaic of the Rockhampton coastline. This comparison enabled the identification of sections of the coastline that experience coastal recession or accretion during this time period. A current coastline was then digitised from the 2010 aerial photography and buffers applied to eroding sections of coast to represent the areal extent of coastal erosion hazard under current climate as described in the point above.

D.2.2 Future Climate

The future-climate erosion hazard was determined using the QCHG. The guideline requires erosion prone area widths to accommodate both short and long term erosion for a specific planning period, for the purpose of this study 100 years.

Short-term erosion refers to the erosion of sediment from the shore profile by wave action associated with extreme weather events, e.g. tropical cyclone or severe storm activity. Fair-weather beach processes between erosive storm events produce conditions for the onshore transport of eroded sediments leading to beach recovery. Beach recovery may take many years to occur, depending on storm frequency. Long-term erosion refers to erosion of beach sediments due to coastal processes

[31] A storm whose and probability of occurrence and magnitude, in this case storm tide water height and duration, does not exceed the parameters established by the Queensland Coastal Hazard Guidelines. In this case, a storm event of a severity that only occurs on average once in 100 years.

(e.g. alongshore drift) operating over decades, and interruptions to the natural sediment transport by anthropogenic structures, e.g. groynes and seawalls.

The formula adopted by DERM in the QCHG for the calculation of the erosion prone area width is as follows:

$$E = [(N \times R) + C + S] \times (1 + F) + D \quad \text{(Equation 2)}$$

Where:

- E = erosion prone area width (metres)
- N = planning period (years)
- R = rate of long-term erosion (metres per year)
- C = short-term erosion from the 'design' storm or cyclone (metres)
- S = erosion due to sea-level rise (metres)
- F = factor of safety (0.4 has been adopted)
- D = dune scarp component to allow for slumping of the erosion scarp (metres).

The QCHG suggests that values of R, C, S and D be determined for individual beaches based on existing data and site specific modelling or profile response. The choice of values for N and F, as well as the specifications of the storm used to determine C, are based subjective decisions that rely on accepted practices. Further guidance on quantifying these parameters is provided in the QCHG (p6 – 11, 2012a).

The future-climate coastal erosion overlays presented here have been calculated through applying the DERM (2012a) formula presented above (DERM, 2012a) which defines the Erosion Prone Area from either of two methods:

1. Erosion-prone areas include areas subject to inundation by the Highest Astronomical Tides (HAT) by the year 2100 or at risk from sea erosion.
2. On land adjacent to tidal water, the landward boundary of the erosion prone area shall be defined by whichever of the following methods gives the greater erosion prone area width:
    a. a line measured 40 metres landward of the plan position of the present day HAT level except where approved revetments exist in which case the line is measured 10 metres landward of the upper seaward edge of the revetment, irrespective of the presence of outcropping bedrock;
    b. a line located by the linear distance calculated, shown in Appendix Table D.1, and measured, unless specified otherwise, inland from:
        i. the seaward toe of the frontal dune (the seaward toe of the frontal dune is normally approximated by the seaward limit of terrestrial vegetation or, where this cannot be determined, the level of present day HAT); or
        ii. a straight line drawn across the mouth of a waterway between the alignment of the seaward toe of the frontal dune on either side of the mouth
    c. the plan position of the level of HAT plus 0.8 m vertical elevation for sea-level rise by 2100.

The extent of the erosion prone area where it is defined by "HAT plus 0.8 m" is considered to be the HAT coastline at 2100, and includes sea-level rise to that time. This was defined by DERM (2012a) as "the area of land inundated to the level HAT of the nearest adjacent open coast or river tide gauge

plus 0.8 m vertical elevation". However this is not based on any site specific assessments of the current HAT coastline, as the present day attenuation of inland HAT level due to flow constraints may not persist to 2100 due to potential coastline response to sea-level rise over the next 90 years. For further explanation see the Coastal Hazard Guideline (DERM, 2012a).

Appendix Table D.1. Erosion prone areas widths for each segment of coast in Rockhampton Regional Council study area[32].

Erosion prone area segment number	Segment start longitude (degrees)	Segment start latitude (degrees)	Erosion prone area width (metres)
RoR001	150.94512	-23.55251	400 m
RoR002	150.86402	-23.47200	Transition from 300 m to 135 m
RoR003	150.81990	-23.42384	135 m
RoR004	150.79689	-23.36910	240 m
RoR005	150.79174	-23.34885	140 m
RoR006	150.79190	-23.33522	0 m
RoR007	150.79835	-23.33773	100 m (Possible bedrock)
RoR008	150.79818	-23.33610	0 m
RoR009	150.79525	-23.33539	100 m
RoR010	150.79308	-23.33130	Transition from 100 m to 70 m
RoR011	150.79309	-23.32499	0 m
RoR012	150.79073	-23.32186	400 m
RoR013	150.79246	-23.30795	250 m
RoR014	150.80035	-23.29834	400 m
RoR015	150.81117	-23.28709	0 m
RoR016	150.81390	-23.28787	125 m
RoR017	150.82010	-23.27926	Transition from 125 m to 40 m
RoR018	150.82274	-23.27850	40 m (Possible bedrock)
RoR019	150.82470	-23.27921	65 m (Possible bedrock)
RoR020	150.82444	-23.27831	135 m
RoR021	150.82482	-23.27472	0 m
RoR022	150.82566	-23.27321	40 m (Possible bedrock)
RoR023	150.82670	-23.26927	0 m
RoR024	150.82792	-23.26734	140 m
RoR025	150.82927	-23.25885	0 m
RoR026	150.82908	-23.25491	160 m
RoR027	150.82592	-23.23959	0 m

[32] Source: http://www.ehp.qld.gov.au/coastal/development/assessment/pdf/ror1a.pdf)

Erosion prone area segment number	Segment start longitude (degrees)	Segment start latitude (degrees)	Erosion prone area width (metres)
RoR028	150.82599	-23.23794	160 m (Possible bedrock)
RoR029	150.81951	-23.22388	0 m
RoR030	150.81687	-23.22189	140 m
RoR031	150.80031	-23.22810	400 m
RoR032	150.79731	-23.22587	140 m (measured from old creek bank)
RoR033	150.79619	-23.22196	215 m
RoR034	150.78919	-23.20690	140 m
RoR035	150.78907	-23.19924	0 m
RoR036	150.79193	-23.19609	140 m
RoR037	150.79460	-23.18446	0 m
RoR038	150.79384	-23.17862	120 m
RoR039	150.79268	-23.16407	0 m
RoR040	150.78351	-23.16571	140 m (Possible bedrock)
RoR041	150.77921	-23.16587	0 m
RoR042	150.77636	-23.16529	150 m
RoR043	150.76400	-23.14554	0 m
RoR044	150.76137	-23.14281	150 m
RoR045	150.75912	-23.14025	0 m
RoR046	150.75487	-23.13891	40 m (Possible bedrock)
RoR047	150.75192	-23.13668	125 m
RoR048	150.74961	-23.12833	0 m
RoR049	150.74978	-23.12592	135 m
RoR050	150.75139	-23.10809	185 m
RoR051	150.75121	-23.10570	235 m

D.2.2.1 Spatial Analysis

The future-climate erosion hazard was developed by creating spatial data (points) from the latitude and longitude data for each of erosion-prone area segment boundaries as shown in Appendix Table D.1. The boundary points were co-located on the current coastline digitised for the current-climate erosion overlays. The segment of coastline between the two erosion-prone area boundaries points was then buffered landward by the erosion prone area width (in metres) calculated by DERM (2012a) to create the polygon showing the aerial extent of the future-climate erosion hazard.

D.3 Results

D.3.1 Current Climate

The coastal erosion hazard is shown in Appendix Figure D.5 and Appendix Figure D.6, and has also been presented as an A3 overview map sheet. The overview map sheet only displays the coastline that is vulnerable and does not identify the extent of coastal erosion. This data has been symbolised with a greater line width so as to be visible when viewed at the standard map extent. The recession extent is either 10 m or 40 m, as described above, and this is provided within the large scale hazard maps.

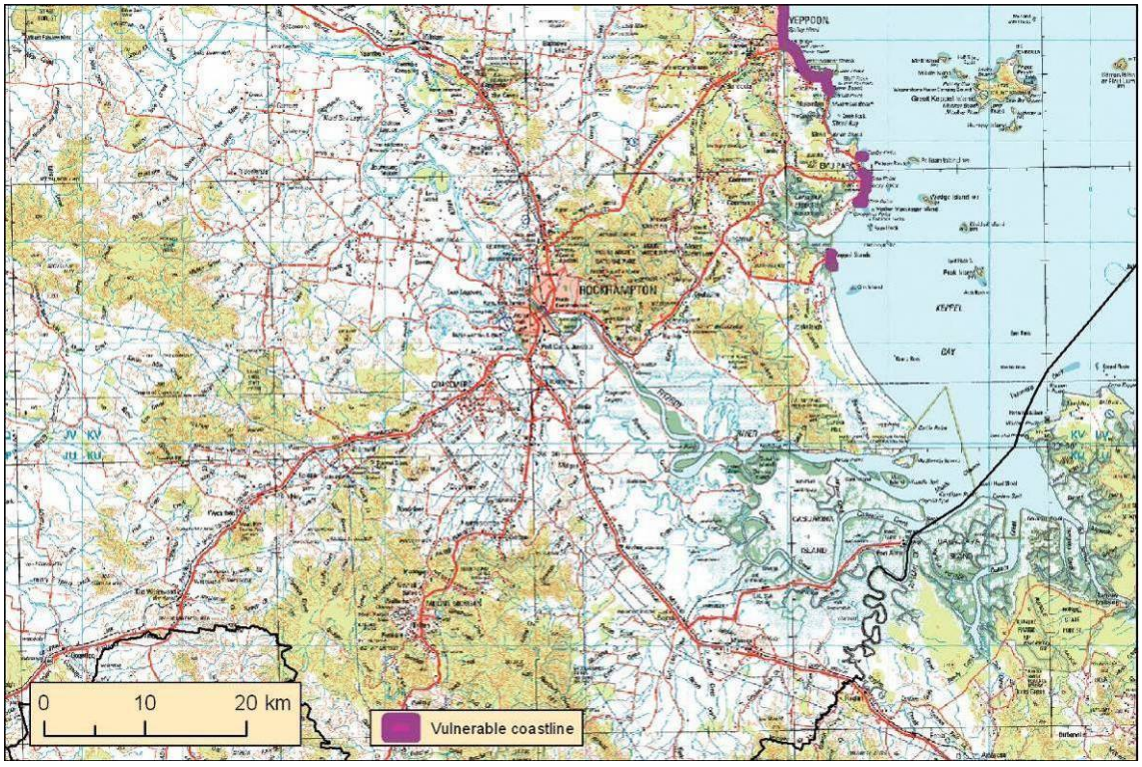

Appendix Figure D.5. Current climate coastal erosion exposed coastline

D.3.2 Future Climate

Appendix Figure D.6. Future-climate (2100) coastal erosion exposed coastline.

D.4 Discussion

D.4.1 Current Climate

The current-climate vulnerability to coastal erosion is largely confined to the sections of coastline including:

- East facing and directly open to the prevailing wave climate, e.g. Rocky Point Beach and the northern section Long Beach
- The southern sections of the predominantly E to ENE facing beaches due to wave refraction by the southern headlands concentrating the wave energy, e.g. Tanby Point. This is a natural phenomenon and will continue under current climate
- Beaches where there has been significant anthropogenic activity resulting the loss of sediment from the beach system resulting in erosion, and often leading to the construction of hard engineering structures to prevent further losses. For example, southern section of Farnborough Beach.

As the recent sediment study identified (Ryan *et al.,* 2009) there is very little additional sediment being delivered to the Rockhampton beaches north of Keppel Bay under the present wave climate. Most of the sediment being transported northwards from the Fitzroy River discharge is being transported via the deeper offshore pathways (Ryan *et al.,* 2009). Under present conditions, there is very little sediment available to naturally renourish the currently eroding beaches. Therefore, where there is an existing coastal erosion hazard under current climate, this is likely to continue at similar rates.

The “erosion prone area” guidelines in the QCHG are currently the best available to the Rockhampton Regional Council on which to base planning decisions.

D.4.2 Future Climate

There have been very few studies of the macrotidal beaches in the southern and central part of Queensland (e.g. Brooke *et al.*, 2008; Webster and Ford, 2008); of those undertaken even fewer have attempted to model them (Masselink, 1993; Masselink and Short, 1993; Masselink and Hegge, 1995). As a consequence there is considerable uncertainty around how the beaches within the Rockhampton Regional Council area are responding under current-climate conditions and even greater uncertainty about the morphodynamic response of these beaches to the impacts of climate change.

The lack of fundamental data, both observational (e.g. near-shore wave climate and storm-tide run-up levels) and instrumental (e.g. bathymetry), in the Rockhampton Regional Council local government area along with an absence of any suitable morphodynamic models to predict shoreline change on these meso- to macro-tidal beaches (Della Pozza, pers comm.) was a significant limitation to this study. Insufficient data exists to gain an understanding of the current beach behaviour from which to predict or forecast beach behaviour under future climate.

In recognition of these data and modelling gaps, the Queensland government’s erosion-prone area width estimates used in this study to generate future-climate coastal erosion overlays are the best available but are to be considered as indicative only.

This page is intentionally blank

Appendix E Sea-level Rise

Contents

Figures

E.1 Method

The sea-level rise analysis was completed through the addition of sea-level rise heights to the 2012 Highest Astronomical Tide (HAT: 3.9 m) value at Rockhampton[33]. HAT is defined by the Australian Hydrographic Service as "…The highest level of water which can be predicted to occur under any combination of astronomical conditions"[34].

The four sea-level rise scenarios are:

- + 0.3 m (QLD 2050)
- + 0.5 m (QLD 2070)
- + 0.8 m (QLD 2100)
- + 1.1 m (FED 2100)

The three Queensland scenarios (2050, 2070 and 2100) are identified within the Queensland Coastal Plan[35]. The Federal scenario (+1.1 m by 2100) was identified by CSIRO from the Intergovernmental Panel on Climate Change's 4th Assessment Report and subsequent research[36]. This 1.1 m scenario considers the "high-end" risk including the effects of warming trends on ice sheet dynamics.

E.1.1 Spatial analysis

Utilising the high resolution, 1 m resolution raster, Digital Elevation Model (DEM) spatial queries were completed to identify bare-earth elevation values that were equal to or less than the scenario value. In the example of the QLD 2050 scenario, the elevation is identified where it is equal to or less than 4.2 m (3.9 m (HAT) + 0.3 m) above the Australian Height Datum (AHD).

E.2 Results

As the hazard map shows (Appendix Figure E.1), there is significant inundation from a HAT event. The Yeppoon Road and the Scenic Highway, South of Yeppoon, is inundated by a HAT scenario. With the progressive addition of sea-level rise heights, the area inundated increases between 3.8% and 6.7%. The greatest extension to the inundation extent from the addition of SLR scenarios is on the floodplain downstream of Rockhampton.

[33] http://www.msq.qld.gov.au/~/media/msqinternet/msqfiles/home/tides/tidal%20planes/semidiurnal_planes_2012.pdf Levels quoted to Lowest Astronomical Tide therefore HAT (6.42 m) minus AHD (2.52 m) is 3.9 m. Source :Semidiurnal Tidal Planes, Queensland Tide Tables 2012, Maritime Safety Queensland, September 2011

[34] http://www.hydro.gov.au/aboutus/glossary.htm

[35] http://www.ehp.qld.gov.au/coastalplan/pdf/qcp-web.pdf

[36] http://www.ozcoasts.gov.au/climate/sd_visual.jsp

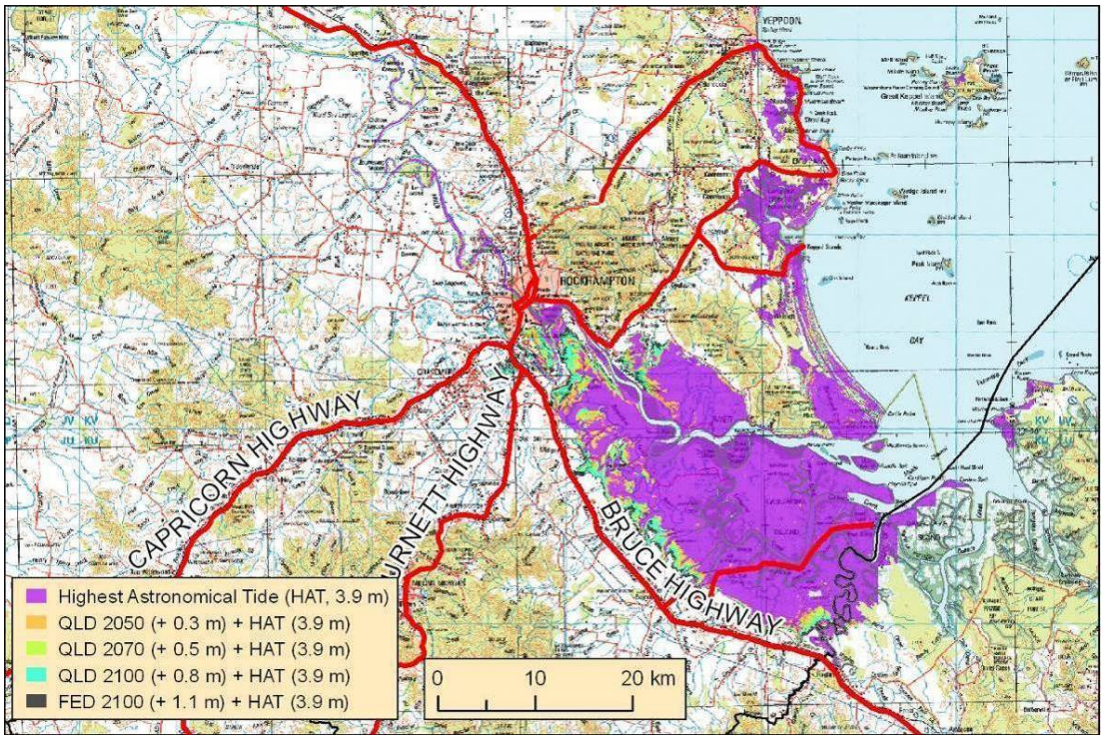

Appendix Figure E.1. Sea-level rise inundation extent

Within the Fitzroy river region, with the progressive addition of sea-level rise to HAT, it can be seen that the inundation extends on the south-western extent of the floodplain towards the Bruce Highway. In proximity to the city of Rockhampton, the Bruce Highway is shown as being exposed to the south of the Capricorn Highway intersection; however, this area of inundation is isolated from the main body of water. This phenomenon is also apparent upriver of Rockhampton in the Fitzroy river channel where there are disconnected areas of HAT and SLR + HAT inundation due to depth variations in the river channel.

E.3 Discussion and Limitations

As the exposure of the Bruce Highway indicates, this method identifies all elevation lower than the scenario height. This will tend to overestimate inundation where there are low elevations separated by areas of higher elevation, e.g. flood levies and dam walls.

The high-resolution DEM has a vertical accuracy of +/-0.15 m. At the completion of the project, the inundation data will be provided to the Rockhampton Regional Council with the inclusion of the uncertainty inundation extents. The uncertainty inundation extent represents another spatial query where the inundation value is altered through the addition or subtraction of 0.15 m. For the QLD 2050 scenario there will be three resulting raster datasets:

- Scenario + Uncertainty (4.2 + 0.15 m)
- Scenario (4.2 m)
- Scenario – Uncertainty (4.2 – 0.15 m)

The inundation analysis was constrained to areas covered by the DEM. This constraint is shown in the A3 sea-level rise hazard map as a dark blue border.

This page is intentionally blank

Appendix F Hazard Maps

A series of maps for each hazard and scenario has been produced. The map sheet is presented at the 1:50 000 scale and has been designed to be printed at an A3 paper size. Appendix Figure F.1 shows an example map sheet.

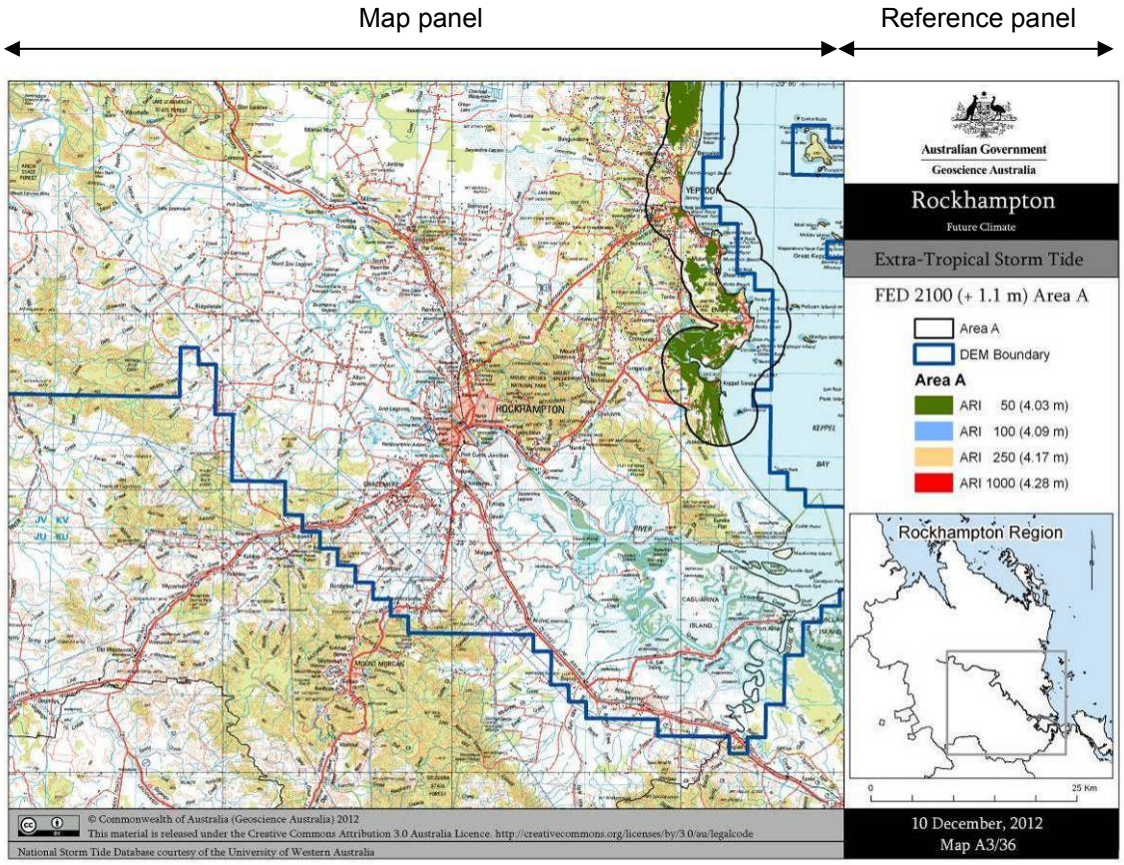

Appendix Figure F.1. Example hazard map.

F.1 Current Climate Hazard Maps

Map Reference	Map content
A3/0	50 year ARI TC Wind Hazard
A3/1	100 year ARI TC Wind Hazard
A3/2	250 year ARI TC Wind Hazard
A3/3	500 year ARI TC Wind Hazard
A3/4	1000 year ARI TC Wind Hazard
A3/5	Extra-tropical Storm Tide Hazard (50 - 1000 year ARI)
A3/6	Tropical Storm Tide Hazard (50 - 1000 year ARI)
A3/7	AS3969 Bushfire Constraints
A3/8	Bushfire Vegetation Classification
A3/9	50 year ARI Bushfire Danger Rating
A3/10	100 year ARI Bushfire Danger Rating
A3/11	Coastal Erosion - small scale
A3/11-1	Coastal Erosion - large scale
A3/11-2	Coastal Erosion - large scale
A3/11-3	Coastal Erosion - large scale
A3/11-4	Coastal Erosion - large scale
A3/11-5	Coastal Erosion - large scale
A3/11-6	Coastal Erosion - large scale
A3/11-7	Coastal Erosion - large scale
A3/11-8	Coastal Erosion - large scale

F.2 Future-Climate Hazard Maps

Map Reference	Map content
A3/12	2055 - 50 year ARI TC Wind Hazard
A3/13	2055 - 100 year ARI TC Wind Hazard
A3/14	2055 - 250 year ARI TC Wind Hazard
A3/15	2055 - 1000 year ARI TC Wind Hazard
A3/16	2090 - 50 year ARI TC Wind Hazard
A3/17	2090 - 100 year ARI TC Wind Hazard
A3/18	2090 - 250 year ARI TC Wind Hazard
A3/19	2090 - 1000 year ARI TC Wind Hazard
A3/20	2050 - 50 year ARI Bushfire Hazard
A3/21	2050 - 100 year ARI Bushfire Hazard

Map Reference	Map content
A3/22	2090 - 50 year ARI Bushfire Hazard
A3/23	2090 - 100 year ARI Bushfire Hazard
A3/24	2050 - Extra-tropical Storm Tide Hazard - Area 4[37]
A3/25	2050 - Extra-tropical Storm Tide Hazard - Area 5
A3/26	2050 - Tropical Storm Tide Hazard - Area 4
A3/27	2050 - Tropical Storm Tide Hazard - Area 5
A3/28	2070 - Extra-tropical Storm Tide Hazard - Area 4
A3/29	2070 - Extra-tropical Storm Tide Hazard - Area 5
A3/30	2070 - Tropical Storm Tide Hazard - Area 4
A3/31	2070 - Tropical Storm Tide Hazard - Area 5
A3/32	2100 - Extra-tropical Storm Tide Hazard - Area 4
A3/33	2100 - Extra-tropical Storm Tide Hazard - Area 5
A3/34	2100 - Tropical Storm Tide Hazard - Area 4
A3/35	2100 - Tropical Storm Tide Hazard - Area 5
A3/36	2100 - Extra-tropical Storm Tide Hazard - Area 4
A3/37	2100 - Extra-tropical Storm Tide Hazard - Area 5
A3/38	2100 - Tropical Storm Tide Hazard - Area 4
A3/39	2100 - Tropical Storm Tide Hazard - Area 5
A3/40	Sea-level Rise Hazard
A3/41	2100 Coastal Erosion Hazard - small scale
A3/41-1	2100 Coastal Erosion Hazard - large scale
A3/41-2	2100 Coastal Erosion Hazard - large scale
A3/41-3	2100 Coastal Erosion Hazard - large scale
A3/41-4	2100 Coastal Erosion Hazard - large scale
A3/41-5	2100 Coastal Erosion Hazard - large scale
A3/41-6	2100 Coastal Erosion Hazard - large scale
A3/41-7	2100 Coastal Erosion Hazard - large scale
A3/41-8	2100 Coastal Erosion Hazard - large scale
A3/41-9	2100 Coastal Erosion Hazard - large scale
A3/41-10	2100 Coastal Erosion Hazard - large scale
A3/41-11	2100 Coastal Erosion Hazard - large scale
A3/41-12	2100 Coastal Erosion Hazard - large scale
A3/41-13	2100 Coastal Erosion Hazard - large scale
A3/41-14	2100 Coastal Erosion Hazard - large scale

[37] Area 4 and 5 are referred to as Area A and B respectively in the Storm Tide Summary Section.

Map Reference	Map content
A3/41-15	2100 Coastal Erosion Hazard - large scale
A3/41-16	2100 Coastal Erosion Hazard - large scale
A3/41-17	2100 Coastal Erosion Hazard - large scale
A3/41-18	2100 Coastal Erosion Hazard - large scale
A3/41-19	2100 Coastal Erosion Hazard - large scale
A3/41-20	2100 Coastal Erosion Hazard - large scale
A3/41-21	2100 Coastal Erosion Hazard - large scale
A3/41-22	2100 Coastal Erosion Hazard - large scale
A3/41-23	2100 Coastal Erosion Hazard - large scale
A3/41-24	2100 Coastal Erosion Hazard - large scale
A3/41-25	2100 Coastal Erosion Hazard - large scale
A3/41-26	2100 Coastal Erosion Hazard - large scale
A3/41-27	2100 Coastal Erosion Hazard - large scale
A3/41-28	2100 Coastal Erosion Hazard - large scale
A3/41-29	2100 Coastal Erosion Hazard - large scale
A3/41-30	2100 Coastal Erosion Hazard - large scale
A3/41-31	2100 Coastal Erosion Hazard - large scale
A3/41-32	2100 Coastal Erosion Hazard - large scale
A3/41-33	2100 Coastal Erosion Hazard - large scale
A3/41-34	2100 Coastal Erosion Hazard - large scale
A3/41-35	2100 Coastal Erosion Hazard - large scale
A3/41-36	2100 Coastal Erosion Hazard - large scale